UNIVERSITI SAINS MALAYSIA

Laporan Akhir Projek Penyelidikan Jangka Pendek

Development of Si/SiOX Core-Shell Structured Nanowire and SiOX Nanowire for Nanoelectronic Device Applications

By

Assoc. Prof. Ir. Dr. Cheong Kuan Yew
Assoc. Prof. Dr. Zainovia Lockman

2012

UNIVERSITI SAINS MALAYSIA

UNIVERSITY RESEARCH GRANT FINAL REPORT
Geran Penyelidikan Universiti Laporan Akhir

A.	**PARTICULARS OF RESEARCH** / *MAKLUMAT PENYELIDIKAN:*
(i)	**Title of Research:** *Tajuk Penyelidikan:* **Development of Si/SiO$_x$ Core-Shell Structured Nanowire and SiO$_x$ Nanowire for Nanoelectronic Device Applications**
(ii)	**Account Number:** *Nombor Akaun: 1001 / PBAHAN / 814061*
B.	**PERSONAL PARTICULARS OF RESEARCHER** / *MAKLUMAT PENYELIDIK*
(i)	**Name of Research Leader:** *Nama Ketua Penyelidik:* Assoc. Prof . Ir .Dr. Cheong Kuan Yew
	Name of Co-Researcher *Nama Penyelidik Bersama:* Assoc. Prof. Dr. Zainovia Lockman
(ii)	**School/Institute/Centre/Unit :** *Pusat Pengajian /Institut/Pusat/Unit :* SCHOOL OF MATERIALS & MINERAL RESOURCES ENGINEERING
C.	**Research Platform (Please tick (/) the appropriate box):** *Pelantar Penyelidikan (Sila tanda (/) kotak berkenaan):*

RECEIVED
9 MAR 2012
UNIVERSITI SAINS MALAYSIA
ENTERP

- ☐ A. **Life Sciences** *Sains Hayat*
- ☐ B. **Fundamental** *Fundamental*
- ☑ C. **Engineering & Technology** *Kejuruteraan & Teknologi*
- ☐ D. **Social Transformation** *Transformasi Sosial*
- ☐ E. **Information & Communications Technology (ICT)** *Teknologi Maklumat & Komunikasi*
- ☐ F. **Clinical Sciences** *Sains Klinikal*
- ☐ G. **Biomedical & Health Sciences** *Bioperubatan Sains Kesihatan*

D. **Duration of this research :**
Tempoh masa penyelidikan ini :

***Duration :** 24 Months
Tempoh :

From : 15 Jan 2010
Dari:

To : 14 Jan 2012
Ke :

E.

ABSTRACT OF RESEARCH

(An abstract of between 100 and 200 words must be prepared in **Bahasa Malaysia and in English**. This abstract will be included in the Annual Report of the Research and Innovation Section at a later date as a means of presenting the project findings of the researcher/s to the University and the community at large)

Abstrak Penyelidikan

(Perlu disediakan di antara 100 - 200 perkataan di dalam **Bahasa Malaysia dan juga Bahasa Inggeris**.
Abstrak ini akan dimuatkan dalam Laporan Tahunan Bahagian Penyelidikan & Inovasi sebagai satu cara untuk menyampaikan dapatan projek tuan/puan kepada pihak Universiti & masyarakat luar).

ABSTRAK

Struktur-struktur nano berasaskan silikon telah berjaya dihasilkan oleh pertumbuhan atas substrat silikon secara langsung dengan menggunakan wafer silikon dan serbuk karbon aktif sebagai bahan mentah. Nanowayar SiO_x dan Si/SiO_x dihasilkan oleh gabungan pertumbuhan dengan bantuan karbon dan oksida melalui mekanisma wap-pepejal apabila masa pengoksidaan adalah 24 minit dan masa rendaman adalah1 jam. Nanowayar SiO_x disintesiskan pada suhu pertumbuhan 1200°C sementara nanowayar Si/SiO_x disintesiskan pada suhu pertumbuhan 1300°C. Apabila masa pengoksidaan kurang daripada 12 minit, hanya struktur nano SiC dihasilkan. Nanorod dan nanotiang dihasilkan pada masa rendaman 1 jam. Diameter dan jumlah struktur-struktur nano ini susut apabila masa pengoksidaan jatuh daripada 12 minit kepada 1 minit. Nanorod SiC dijumpai pada tengah substrat manakala nanotiang dijumpai pada tep substrat silikon. Strukturnya tukar kepada nanowayar SiC/SiO_2 apabila masa rendaman dinaikkan kepada 2 jam. Struktur-struktur nano baru seperti nanokabel dan nanosarang dihasilkan bergantung pada lokasi pertumbuhan atas substrat silikon. Diameter nanokabel dan nanosarang susut apabila jumlah serbuk karbon aktif bertambah. Pembentukan nanokabel dan nanosarang adalah disebabkan oleh kesan aerodinamik kerana perbezaan tekanan di dalam dan luar mangkuk pijar. Pertumbuhan struktur-struktur nano SiC ini adalah melalui mekanisma wap-pepejal.

ABSTRACT

Si-based nanostructures were successfully synthesized through the method of direct growth on silic
substrates using only silicon wafers and activated carbon powder as sources. SiOx and Si/SiOx cor
nanowires were produced through combination of carbon-assisted growth and oxide-assisted growt
vapour-solid mechanism when the oxidation time was 24 minutes at a soaking time of 1 hour. SiO
were formed at 1200°C while Si/SiOx core-shell nanowires were formed at 1300°C. When the oxi
was reduced to below 12 minutes, SiC nanostructures were mainly formed. SiC nanorods and nano
were formed at a soaking time of 1 hour, with decreasing diameter and amount with decreasing oxi
from 12 minutes to 1 minute. SiC nanorods were formed at the center while SiC nanocolumns wer
the side of silicon substrates. The structure changed from SiC nanorods and nanocolumns to SiC/Si
shell nanowires when the soaking time was increased from 1 hour to 2 hours. New nanostructures
core-shell nanocables and nanowebs were formed depending on the growth locations on the silicon
when the activated carbon powder was added. The nanocables and nanowebs decreased in diameter
increasing amount of activated carbon powder. The formation of these nanocables and nanocables
of aerodynamic effects due to the pressure difference inside and outside of the crucible. The growt
SiC nanostructures was correlated to the vapour-solid mechanism.

F. **SUMMARY OF RESEARCH FINDINGS**
Ringkasan dapatan Projek Penyelidikan

Different Si-based nanostructures, namely Si/SiO$_x$ core-shell nanowires, SiO$_x$ nanowires, SiC nanorods, SiC nanocolumns, SiC/SiO$_2$ core-shell nanowires, SiC/SiO$_2$ core-shell nanocables and nanowebs, were successfully synthesized using direct growth on Si substrates depending on the oxidation time, amount of activated carbon powder and growth locations on the Si substrates.

SiO$_x$ and Si/SiO$_x$ core-shell nanowires were formed when the oxidation time was fixed at 24 min while exposed to 0.5 g activated carbon powder. SiO$_x$ nanowires were formed at the growth temperatures of 1200 °C whereas Si/SiO$_x$ core-shell nanowires were formed at growth temperatures of 1300 °C. As the soaking time increased from 1 h to 4 h, the Si/SiO$_x$ core-shell nanowires increased in amount and length, though the change in the diameters of the nanowires was not significant due to constraints by the oxide layer.

SiC nanorods and nanocolumns were successfully synthesized at 1300°C and at a soaking time of 1 hour while exposed to 0.5 g activated carbon powder. As the oxidation time was increased, an increase in the amount of nanorods and nanocolumns could be observed but ultimately led to agglomeration of these nanostructures into SiC clusters or SiC layers. SiC nanowires were also found only at an oxidation time of 2 min.

When the soaking time was increased from 1 hour to 2 hours while the experiment was fixed at an oxidation time of 2 min, a growth temperature of 1300°C and an activated carbon powder amount of 0.5 g, the products changed from SiC nanorods and nanocolumns to SiC/SiO$_2$ core-shell nanostructures in the form of clusters, nanowires, nanocables and nanowebs.

SiC/SiO$_2$ core-shell nanostructures in the form of clusters, nanowires, nanowebs and nanocables were formed along with side products of Si/SiO$_x$ or Si nanowires and SiC nanoparticles. When ACP was increased to 1.0 g ACP, the diameter of nanowires increased but then started to decrease with further increase to 1.5 g ACP. The fluctuation of the diameters with increasing ACP amount was due to the increasing vapor pressure of CO produced. Addition of ACP also resulted in the formation of nanowebs and nanocables.

The growth of all these Si-based nanostructures was correlated to vapor-solid mechanism though the reaction kinetics differed for each product formed. The difference in nanostructures formed at different growth locations was a result of the aerodynamic effects created by pressure difference between the inner crucible chamber and the outside environment, and increased reactant gas flow rate in the gap.

G.

COMPREHENSIVE TECHNICAL REPORT

Laporan Teknikal Lengkap

Applicants are required to prepare a comprehensive technical report explaining the project.
(This report must be attached separately)
Sila sediakan laporan teknikal lengkap yang menerangkan keseluruhan projek ini.
[Laporan ini mesti dikepilkan]

Please refer to the attached document.

List the key words that reflectour research:
Senaraikan kata kunci yang mencerminkan penyelidikan anda:

English	Bahasa Malaysia
Si-based nanostructures	Struktur nano berasaskan Si
Chemical vapor growth	Pertumbuhan secara pemeruapan kimia

H. **a) Results/Benefits of this research**
Hasil Penyelidikan

No. *Bil:*	**Category/Number:** *Kategori/ Bilangan:*	**Promised**	**Achieved**
1.	**Research Publications (Specify target journals)** *Penerbitan Penyelidikan (Nyatakan sasaran jurnal)*	4	7 (published) 1 (under review)
2.	**Human Capital Development**		
	a. Ph. D Students		
	b. Masters Students	**1**	**1 (writing up thesis)**
	c. Undergraduates (Final Year Project)		
	d. Research Officers		
	e. Research Assisstants		
	f. Other: Please specify		
3.	**Patents** *Paten*	0	1 (filed)
4.	**Specific / Potential Applications** *Spesifik/Potensi aplikasin*	1	1
5.	**Networking & Linkages** *Jaringan & Jalinan*	2	1 (University of Applied Regensburg, Germany)
6.	**Possible External Research Grants to be Acquired** *Jangkaan Geran Penyelidikan Luar Diperoleh*	1	0

- Kindly provide copies/evidence for Category 1 to 6.

b) Equipment used for this research.
Peralatan yang telah digunakan dalam penyelidikan ini.

Items *Perkara*	Approved Equipment	Approved Requested Equipment	Location
Specialized Equipment Peralatan khusus	No	No	NA
Facility Kemudahan	No	No	NA
Infrastructure Infrastruktur	No	No	NA

- Please attach appendix if necessary.

Hindawi Publishing Corporation
Journal of Nanomaterials
Volume 2009, Article ID 572865, 5 pages
doi:10.1155/2009/572865

Research Article

Growth Mechanism of Cubic-Silicon Carbide Nanowires

K. Y. Cheong and Z. Lockman

Electronic Materials Research Group, School of Materials and Mineral Resources Engineering, Engineering Campus, Universiti Sains Malaysia, Nibong Tebal, Penang 14300, Malaysia

Correspondence should be addressed to K. Y. Cheong, cheong@eng.usm.my

Received 12 August 2009; Accepted 13 December 2009

Recommended by Donglu Shi

Cubic-SiC nanowires were synthesized using activated carbon powder and Si substrate in vacuum at 1200–1350°C for 1–4 hours. The nanowires were grown according to the following proposed mechanisms: (1) diffusion of C/CO into Si substrate, (2) weakening of Si bond and atomic kick-out, (3) formation of Si-C in vapor phase, (4) formation of saturated SiC layer, (5) formation of pyramid-like SiC nanostructure, and (6) formation of SiC nanowires.

1. Introduction

SiC nanowires have gained interest in optoelectronics, high temperature, and high-power applications owing to their excellent chemical, physical, and electronic properties [1, 2]. Various methods have been used to grow SiC nanowires, which include laser ablation [3], chemical vapor deposition [4], carbothermal reduction [5], and thermal evaporation process [6]. To explain the formation of the nanowires, three different mechanisms have been proposed, which are vapor-liquid-solid (VLS) growth mechanism [6, 7], solid-liquid-solid (SLS) growth mechanism [8], and vapor-solid (VS) growth mechanism [9–12], depending on the configuration of growth/deposition condition and sources of raw materials. Most techniques involved VLS and SLS growth mechanisms, in which a metal catalyst droplet has been used as a nucleation site for adsorption of SiC vapor phase during the growing process of nanowires [6–8]. However, the nanowires are contaminated by metal residue that is originated from the catalyst [13]. Therefore, some studies have been performed without using any catalyst. Zhang et al. [14] have used silica xerogel and carbon nanoparticles as the source materials to deposit cubic-SiC nanowires on alumina substrate. They were using carbothermal reduction process that performed at Ar ambient. Using the similar set up, Gundiah et al. [5] have replaced the carbon nanoparticles and Ar gas flow with activated carbon and NH_3 or H_2 gas, respectively, to produce the same product. The source materials are initially decomposed, reacted and deposited on a substrate, and then nanowires are grown, without consuming any material from the substrate. The production of the cubic-SiC nanowires is according to VS mechanism. In this paper, an alternative route to produce cubic-SiC nanowires is being reported. The nanowires have been grown simultaneously from a Si substrate using an appropriate amount of activated carbon powder under medium vacuum and high temperature conditions. The growth mechanism of the nanowires is totally different from those reported in the literatures.

2. Experimental

The growth of SiC nanowires was performed in a vacuum furnace as schematically outlined in Figure 1. A one surface polished and precleaned n-type <100> oriented Si substrate was used as the Si source and was placed on top of a columniform graphite crucible that contained an appropriate amount of activated carbon powder (8.5 at % of O and 91.5 at % of C). The average particle size of the activated carbon powder obtained from a particle size analyzer was 13.55 μm. To hold the substrate firmly, a graphite block was placed on top of the substrate. The whole setup was placed in the middle of the vacuum furnace that had been evacuated down to 10 m Torr (1.333×10^{-9} GaP). The furnace was then

Physica E 42 (2010) 1338–1342

LSEVIER

Contents lists available at ScienceDirect

Physica E

journal homepage: www.elsevier.com/locate/physe

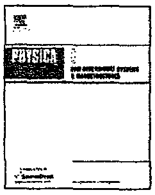

ormation and characterization of SiO_x nanowires and Si/SiO_x core-shell anowires via carbon-assisted growth

i L. Chiew, Kuan Y. Cheong*

niversiti Sains Malaysia, Engineering Campus, School of Materials and Mineral Resources Engineering, 14300 Nibong Tebal, Seberang Perai Selatan, Penang, Malaysia

RTICLE INFO

rticle history:
eceived 20 July 2009
eceived in revised form
November 2009
ccepted 9 November 2009
vailable online 17 November 2009

eywords:
ore-shell structure
anowire
rowth mechanism

ABSTRACT

Large amount of SiO_x nanowires and Si/SiO_x core-shell nanowires on silicon wafer had been synthesized through carbon-assisted growth. Carbon-assisted growth was employed in this study due to the lack of contamination from metallic catalysts and cheaper raw materials. The nanowires produced had length up to 100 μm and diameter ranging from 20 to 40 nm. In this study, increasing the growth temperature (1100, 1200 and 1300 °C) caused a change in the morphology of the nanowires from SiO_x to Si/SiO_x core-shell structures while increasing the soaking time of the heating profile (1, 2 and 4 h) increased the length of nanowires.

. Introduction

Nanostructures have been gaining worldwide interest due to heir small sizes that enable higher functionality in a given space nd their peculiar and fascinating properties, which make them pplicable in mesoscopic research, development of nanodevices nd potential application of large surface area structures [1]. anowires, which are one form of one-dimensional nanostruc- ures, have been used as versatile building blocks in the niniaturization of electronic and optoelectronic devices [2].

In this study, silicon oxide (SiO_x) nanowires and Si/SiO_x core- hell nanowires were produced. Silicon-based nanowires have ttracted much attention for their interesting semiconducting, nechanical and optical properties, which enable them to be used s one-dimensional quantum transistors, composites, blue–green ight-emitting diodes [3,4], optical sensor [5] as well as biological narkers and sensors [6,7]. Consequently, a great deal of effort has een made in fabricating Si-based nanowires, which include SiO_x nd the Si/SiO_x core-shell structure. Several methods have been sed to synthesize these Si-based nanowires, including laser blation [8], sol–gel [9], thermal evaporation [3], carbothermal eduction [10,11], physical evaporation [12], rapid thermal nnealing [13], chemical vapor deposition [14] and thermal xidation route [15], oxide assisted growth (OAG) [16,17] and hermal sublimation [18].

There had been reports using similar methods as used in our tudy [13,15,19,20]. Through improvisation of these methods, our method offers greater benefits in terms of lower growth temperature, shorter growth period, use of common raw materials with the absence of metal catalyst and higher purity of product. Previous study by Gundiah et al. [19] produced Si/SiO_x core-shell nanowires using Si (1 0 0) wafer sputtered with carbon with growth temperature of 1350 °C for 3 h in an atmosphere of Ar/H_2 mixture. However, in our study, the Si wafer was not directly exposed to the carbon source but placed inside a crucible to avoid contamination of the product. The temperature involved in our study was also lower if compared to Gundiah et al. and only involved Ar gas as compared to Ar/H_2 mixture. Chen and Ruoff produced SiO_x nanowires and nanocoils by using a pre-oxidized silicon wafer of oxide thickness 230 nm without any additional chemicals in an atmosphere of Ar gas during temperature ramp up and down cycles and in Ar/H_2 mixture during soaking stage with temperatures ranging from 900 to 1200 °C for periods of time ranging between 10 min and 5 h [20]. Although the method used by Lai et al. [13] also involved the growth of SiO_2 nanowires using an oxide layer on Si (1 0 0) substrate, it required the presence of Pt catalyst to grow the nanowires while in our study it was not required. The presence of metal catalyst at the tip of nanowires might affect the mechanical properties of nanowire devices. For the method used by Hu et al. [15], although their steps were simple, which only involved two-step heating of oxidized silicon wafer, it took a long time of 5.5 h to grow the nanowires. Our study was able to produce nanowires in a shorter time as compared to them. Thus, a simple and effective method was developed in our study. In this study, a simple route had been used to produce large amount of high purity SiO_x and Si/SiO_x nanowires in Ar gas at high temperature using common starting materials (oxidized silicon wafer and activated carbon powder).

---

* Corresponding author. Tel.: +60 4 5995259; fax: +60 4 5941011.
E-mail address: cheong@eng.usm.my (K.Y. Cheong).

386-9477/$ - see front matter © 2009 Elsevier B.V. All rights reserved.
oi:10.1016/j.physe.2009.11.021

Journal of Alloys and Compounds 481 (2009) 345–348

Contents lists available at ScienceDirect

Journal of Alloys and Compounds

journal homepage: www.elsevier.com/locate/jallcom

Effects of temperature and crucible height on the synthesis of 6H-SiC nanowires and nanoneedles

K.Y. Cheong*, Z. Lockman

School of Materials & Mineral Resources Engineering, Engineering Campus, Universiti Sains Malaysia, 14300 Nibong Tebal, Penang, Malaysia

A R T I C L E I N F O

Article history:
Received 21 November 2008
Received in revised form 25 February 2009
Accepted 25 February 2009
Available online 13 March 2009

Keywords:
Nanostructures
X-ray diffraction

A B S T R A C T

6H-SiC has been produced via catalyst-free chemical vapor growth method using Si wafer and activated carbon powder as the respective Si and C sources. The effects of heating temperature (1250, 1300, and 1350 °C) and crucible height (9, 13, and 16 cm) on the formation of nanowires and nanoneedles have been systematically investigated. Scanning and transmission electron microscopy, X-ray diffraction (XRD), Raman and photoluminescence (PL) spectroscopy have been employed in this study. The reasons for the transformation of nanoneedles to nanowires have also been proposed.

1. Introduction

One-dimensional SiC nanowires have received considerable attraction owing to their excellent optical, electrical, mechanical and thermal properties [1]. They are suitable for high temperature, frequency, and power applications [2]. These applications include nanosensors and nanoscale electro-devices [3]. Unique properties of SiC nanowires also make them useful as building blocks in the development of optoelectronics, biomedical engineering [4], and nanoelectromechanical systems [5]. Besides, the superior properties of SiC are prerequisites in building devices capable of generating stable emission electron current. This enables SiC nanowires to be used in field emission display [6]. SiC nanowires are also of great interest for applications in nanocomposites [7–10]. They are used as reinforcements in ceramic matrix composites.

Up to now, various techniques have been used to synthesize SiC nanowires, such chemical vapor deposition, carbothermal reduction, direct heating method, laser ablation, thermal evaporation, etc. [11–18]. However, most of these approaches are complex due to the multistep operation in the process. Besides, the usage of metal catalyst is required to control critical nucleation and subsequent elongation step of the nanowires. In early work demonstrated by Wenger et al., [9] showed that homogeneous nanowires diameter can be controlled by the sized of catalyst droplet. Similarly, SiC nanoneedles have been synthesized via catalyst assisted thermal evaporation technique [19,20]. However, the usage of metal catalyst can lead to the present of impurities. It may hinder the application of these materials due to the purity issues of the product. Approximately 200 polytypes of bulk SiC have been reported [21] but most of the SiC nanostructures demonstrate a 3C phase [11–14,22]. Only limited reports were showing 2H- [23] and R-SiC [24] nanowires. In order to synthesize a high purity SiC nanostructure, catalyst-free chemical vapor growth method [24] has been used in this work to produce 6H-SiC nanowires or nanoneedles. The formation of these nanostructures is strongly depending on heating temperature and crucible height and it has been reported in this paper.

2. Experimental details

Silicon (Si) wafers were used as the substrates to grow SiC nanostructures, either in the form of nanowires or nanoneedles, while activated carbon powder was used as raw materials for the carbon source. Before the synthesis, Si wafer were cleaned using RCA cleaning procedure. Then, a pre-determined and fix amount of activated carbon powder (1.0027 g) (8.5 at% of O and 91.5 at% of C) supplied by a local manufacturer was placed inside a columniform graphite crucible. The crucible had a bore diameter of 3 cm and wall thickness of 1 cm. The volume moment diameter of the activated carbon powder used was 13.55 μm. Next, the Si wafer was placed on top of the crucible and covered with a graphite block that acted as a weight to hold the wafer in its place. The whole setup was then put into the center of a vacuum furnace (Fig. 1). The furnace was then pumped down to 10^{-3} mTorr and heated to 1250, 1300, or 1350 °C at a heating rate of 15 °C/min. After achieving the temperature, Ar gas was pump into the furnace at a flow rate of 150 ml/min. and the heating process was maintained for 4 h before it was cooled down to room temperature (15 °C/min). In this experiment, three crucible heights (9, 13, and 16 cm), which were having the same bore diameter and wall thickness, were used. Since the height of the contained activated carbon (approximately 0.4 cm) was relatively low if compared with the height of the crucibles and, therefore, the influence of this height in the formation of nanostructures was insignificant. The synthesized products grew on the Si substrate were then characterized using field-emission scanning electron microscope (FESEM, ZEISS SUPRA™ 35VP) with an energy dispersive X-ray detector (EDAX), transmission electron microscope (TEM, Philips Tecnai 20), X-ray diffraction (XRD) system (PANalytical X'pert PRO MRD PW3040), Raman and photoluminescence (PL) spectroscopy system (Jobin Yvon HR 800 UV).

---

* Corresponding author. Tel.: +60 4 599 5259; fax: +60 4 594 1011.
E-mail address: cheong@eng.usm.my (K.Y. Cheong).

0925-8388/$ – see front matter © 2009 Elsevier B.V. All rights reserved.
doi:10.1016/j.jallcom.2009.02.128

7

Advances of SiO_x and Si/SiO_x Core-Shell Nanowires

Kuan Yew Cheong and Yi Ling Chiew
School of Materials & Mineral Resources Engineering, Engineering Campus,
Universiti Sains Malaysia,
14300 Nibong Tebal, Seberang Perai Selatan, Penang,
Malaysia

Introduction

notechnology can be defined as the design, construction and utilization of functional
terials with at least one of the dimension measured is in nano-scale to exploit the new
perties and phenomena developed at that scale. These nanomaterials exhibit new and
proved physical, chemical and biological properties, phenomena and processes due to the
iation of wavelike properties of electrons inside matter as the size of matter is reduced
l the electrons are confined.

nowires, one of the one-dimensional nanostructures, are wire-like structure that has
meter less than 100 nm. Single crystal nanowires grow along a specific axial direction
ugh their side surfaces may not be well defined. The cross-section of the nanowires may
ier be round, hexagonal or polyhedron depending on the crystallography of the material
ber & Wang, 2007). The length of nanowires can vary from few hundred of nanometers
nicrometer and even millimeters.

his chapter, we review advances of SiO_x nanowires and Si/SiO_x core-shell nanowires.
owires, which are one form of one-dimensional nanostructures, have been used as
atile building blocks in the miniaturization of electronic and optoelectronic devices (Li
l., 2005). Various materials have been synthesized in the form of nanowires, such as
on, germanium, gallium nitride, gallium arsenide, and silicon carbide (Spanier, 2006).
s, it is important to understand properties, applications and synthesis methods of the
wires so as to be able to produce nanowires with well-controlled properties and
nsions to be incorporated into electronic devices. Here in this review, properties,
ications and how SiO_x nanowires and Si/SiO_x core-shell nanowires are made are
ssed in the following sections. Section 2 gives a brief discussion on the SiO_x nanowires.
on 3 discusses the properties that enable SiO_x nanowires to be successfully used in
ent applications. Section 4 gives a short review on the potential applications of SiO_x
wires. Section 5 reviews the different methods used to synthesize the nanowires,
also includes their phenomena, techniques and mechanism. Section 6 gives a brief
ssion on Si/SiO_x core-shell nanowires. Section 7 discusses the important properties of
$)_x$ core-shell nanowires that are linked to their potential applications. Section 8
vs the different methods used to synthesize the core-shell nanowires. Finally, section 9
des by a short summary.

Source: Nanowires Science and Technology, Book edited by: Nicoleta Lupu,
ISBN 978-953-7619-89-3, pp. 402, February 2010, INTECH, Croatia, downloaded from SCIYO.COM

2. SiO_x nanowires

Silicon oxide (SiO_x) nanowires have been reported to be amorphous, where there is no long-range order of positions of the atoms (Sood et al., 2006). SiO_x may exist in different ratio of silicon and oxygen. The atomic ratio of silicon and oxygen in SiO_x has the x value between 1 and 2 (Zhang et al., 1999). Different methods had been used to synthesize SiO_x nanowires though the ratio of Si:O differed from one another but they remained in the range of $1 \le x \le 2$. Table 1 lists down the values of x of the SiO_x nanowires produced using different methods.

Methods	*References*	*x value in* SiO_x
Laser Ablation	Aharonovich et al. (2008)	$1<x<2$
Chemical Vapor Deposition	Ni et al. (2006)	2
	Zheng et al. (2002)	2
	Zhang et al. (2006)	1.3
	Jiang et al. (2005)	1.2
	Yang et al. (2007)	1.8 - 2.1
Sol-Gel Processing	Liang et al. (2000)	1.4
Rapid Thermal Annealing	Lai et al. (2008)	1.2
Ion Implantation	Sood et al. (2006)	$1<x<2$
Carbon-Assisted Growth	Zhu et al. (1998)	$1<x<2$
	Saulig-Wenger (2003)	2
Thermal Oxidation Route	Hu et al. (2003)	2

Table 1. List of Si:O ratio of the silicon oxide nanowires produced using different methods.

3. Properties of SiO_x nanowires

Since dimensionality alters the properties of a structure as the dimension decreases, it is then important to understand the properties of SiO_x nanostructures so as to enable the exploitation of these materials for new applications. Some of these properties are summarized in the Table 2.

Properties	*Value*
Young's Modulus	57 - 93 GPa
Electrical	Varies according to number of Si-O bonds (changes from metallic to insulating as number of bonds increase)
Fermi level	-3 eV to -7 eV (more positive as number of Si-O chain increases)
PL band energies	1.9 - 4.3 eV

Table 2. Properties of SiO_x nanowires (Wei et al., 2006, Jin et al., 2008, Ni et al., 2006 and Bilalbegović, 2006).

3.1 Optical properties of SiO_x nanowires

Various SiO_2 glasses and nanowires have different photoluminesence (PL) energy peaks ranging from 1.9 to 4.3 eV according to Wei et al. (2006). From the study performed by Jin et

Development of Si/SiO$_x$ Core-Shell Structured Nanowire and SiO$_x$ Nanowire for Nanoelectronic Device Applications

A Final Research Report
Submitted to

Research Creativity and Management Office
Universiti Sains Malaysia

RECEIVED
-9 MAR 2012
UNIVERSITI SAINS MALAYSIA
ENTERP

by

Assoc. Prof. Ir. Dr. Cheong Kuan Yew (Principle Researcher)
Assoc. Prof. Dr. Zainovia Lockman

In the fulfillment of the requirements of

Research University (Individual) Grant of Universiti Sains Malaysia
(Grant No: 814061)

February 2012

ACKNOWLEDGEMENT

I would like to take this opportunity to express my appreciation and sincere gratitude to all those who have devoted their time in making this project a success. My heartiest thank to my postgraduate student, Chiew Yi Ling, who have contributed to the success of this project.

I would like to extend my most sincere gratitude to all staffs in USM that give me valuable assistance for completion this project. Last but no least, I would like to acknowledge the support and facilities given by the School of Materials & Mineral Resources Engineering, USM and the financial support provided by USM Short Term Grant (6035269).

ASSOC. PROF. IR. DR. CHEONG KUAN YEW
ASSOC. PROF. DR. ZAINOVIA LOCKMAN

TABLE OF CONTENTS

ACKNOWLEDGEMENT ii

LIST OF TABLES v

LIST OF FIGURES vi

RESEARCH OUTCOMES ix

ABSTRAK xi

ABSTRACT xii

CHAPTER 1 INTRODUCTION 1

- 1.1 Introduction 1
- 1.2 Problem Statement 2
- 1.3 Research Objectives 3
- 1.4 Scope of Project 4

CHAPTER 2 LITERATURE REVIEW 5

- 2.1 Introduction 5
- 2.2 Si-Based Nanostructures 5
  - 2.2.1 Nanostructures 5
  - 2.2.2 Silicon Carbide (SiC) 6
  - 2.2.2 Silica (SiO_2) 10
  - 2.2.3 Synthesis of Si-Based Nanostructures 12
- 2.3 Direct Growth of Si-Based Nanostructures on Si Substrate 13
  - 2.3.1 Effect of Starting Materials 14
  - 2.3.2 Effect of Growth Temperature 17
  - 2.3.4 Effect of Furnace Atmosphere 20
  - 2.3.5 Effect of Cooling Rate 22

CHAPTER 3 MATERIALS AND METHODOLOGY 24

3.1 Introduction 24

3.2 Chemical Vapor Growth (CVG) on Si Wafers 25

3.2.1 Chemicals and Reagents 26

3.2.2 Wafer Preparation 26

3.2.3 Thermal Oxidation of Silicon Wafer 27

3.2.4 Growth of Nanostructures in Vacuum Sintering Furnace 28

3.3 Characterization 30

3.4.1 Field-Emission Scanning Electron Microscope (FESEM) 30

3.4.2 Energy-Filtered Transmission Electron Microscope (EFTEM) 31

3.4.3 High-Resolution Transmission Electron Microscope (HRTEM) 32

3.4.4 X-ray Diffraction (XRD) 33

CHAPTER 4 RESULTS AND DISCUSSION 34

4.1 Introduction 34

4.2 Chemical Vapour Growth (CVG) on Si Substrates 35

4.2.1 Effect of growth temperature with constant soaking time 35

4.2.2 Effect of soaking time with constant growth temperature 38

4.2.3 Effect of Oxidation Time 42

4.2.4 Effect of Soaking Time in Vacuum Sintering Furnace 46

4.2.5 Effect of Activated Carbon Powder Amount 50

4.2.6 Growth Mechanism 59

CHAPTER 5 CONCLUSION 70

5.1 Conclusion 70

5.2 Recommendations for Future Work 72

REFERENCES 73

APPENDICES 82

LIST OF TABLES

Pages

Table 2.1: Properties for different polytypes of SiC and SiC nanowires at room temperature. 8

Table 2.2: Properties of SiO_2 nanowires at room temperature. 11

Table 2.3: Comparison of several synthesis methods of Si-based nanostructures (Zhou et al., 2008). 12

Table 3.1: Specifications of the chemicals and reagents used in CVG on Si wafers. 26

Table 3.2: Experimental parameters used in CVG on Si wafers. 29

Table 4.1: Summary of nanostructures formed on Si wafer depending on the amount of ACP and the location on Si wafer. 51

LIST OF FIGURES

Pages

Figure 2.1: Tetrahedral bonding of a C atom with its four nearest Si atoms. 7

Figure 2.2: Stacking sequence of double layers of 3C, 4H, 6H and 15R-SiC (Sudarshan, 2006). 8

Figure 2.3: Tetrahedral bonding of a Si atom with its four nearest O atoms. 11

Figure 3.1: Flow chart of the experimental methodologies in CVG. 25

Figure 3.2: Heating profile for thermal oxidation. 28

Figure 3.3: Experimental setup in the vacuum sintering furnace. 29

Figure 3.4: Heating profile in vacuum sintering furnace. 30

Figure 4.1: (a) A FESEM image showing that no nanowires were formed on the silicon wafer at a growth temperature of 1100 °C. (b) A FESEM image of the aligned SiO_x nanowires formed on silicon wafer at a growth temperature of 1200 °C. (Inset) A FESEM image of the nanowires formed surrounding the activated carbon powder particles on the wafer surface. (c) A FESEM image of nanowires with length up to several micrometers long on the wafer surface at a growth temperature of 1300 °C. 36

Figure 4.2: (a) A lattice image from HRTEM of the amorphous SiO_x nanowires formed at 1200 °C. (Upper inset) SAED pattern of a SiO_x nanowire showing amorphous nature. (Lower inset) A typical TEM image of the single-layer SiO_x nanowires. (b) A typical TEM image of the Si/SiO_x core-shell nanowires formed at 1300 °C. (c) A lattice image from HRTEM of a Si/SiO_x core-shell nanowire. (Inset) SAED pattern of a Si/SiO_x nanowire. 37

Figure 4.3: TEM images of the core-shell nanowires formed at growth temperature of 1300 °C for soaking time of (a) 1 h, (b) 2 h and (c) 4 h. Inset showing the SEM images of the nanowires at the respective soaking time. 39

Figure 4.4: Correlation of the diameter of core to the diameter of the nanowire (inclusive of the core and shell) at growth temperature of 1300 °C at different soaking times of 1 h, 2 h and 4 h. 41

Figure 4.5: FESEM images of the nanorods and nanocolumns formed at the centre and the sides of silicon substrate when heated at 1300°C for 1 hour under different oxidation time of 1 min, 2 min, 8 min and 12 min. 43

Figure 4.6: EDS results of the nanorods at the centre of silicon wafer under different oxidation times of (a) 1 min, (b) 2 min, (c) 8 min and (d) 12 min. 44

Figure 4.7: EDS results of the nanorods at the side of silicon wafer under different oxidation times of (a) 1 min, (b) 2 min, (c) 8 min and (d) 12 min. 44

Figure 4.8: An EFTEM image of the nanostructures formed on a silicon wafer at the oxidation time of 2 min. 45

Figure 4.9: FESEM micrographs of nanostructures formed at the centre of Si substrate under different soaking time of (a) 1 hour (Inset showing higher magnification micrograph of the nanostructures) and (b) 2 hours. 47

Figure 4.10: EDS results of the grains formed at the centre of Si substrate under a soaking time of 2 hours. 47

Figure 4.11: (a) and (b) shows the FESEM micrographs of nanocolumns formed at the side of Si substrate under a soaking time of 1 hour while (c) and (d) shows the FESEM micrographs of nanowires and nanowebs formed at the side of substrate under a soaking time of 2 hours. 48

Figure 4.12: EFTEM images of (a) nanorods or nanocolumns formed under soaking time of 1 hour and (b) core-shell nanowires formed under soaking time of 2 hours. 49

Figure 4.13: ESI results showing composition of nanowires formed under soaking time of 2 hours. 49

Figure 4.14: Location of nanostructures formed on the SiO2/Si wafer. 50
Figure 4.15: FESEM images of nanostructures formed at the centre under different ACP amount of (a) 0 g, (b) 0.5 g, (c) 1.0 g and (d) 1.5 g. 52

Figure 4.16: EDS results of the (a) unetched Si substrate surface and (b) voids formed on Si substrate at the centre. 52

Figure 4.17: FESEM images of nanostructures formed at the border under different ACP amount of (a) 0 g, (b) 0.5 g, (c) 1.0 g and (d) 1.5 g. 53

Figure 4.18: EDS results of the nanowebs at the borders at two different locations showing (a) only Si and O and (b) Si, O and C. 53

Figure 4.19: EFTEM images of nanostructures formed at the border under different ACP amount of (a) 0 g, (b) 0.5 g, (c) 1.0 g and (d) 1.5 g. 54

Figure 4.20: FESEM images of nanostructures formed at the side under different ACP amount of (a) 0 g, (b) 0.5 g, (c) 1.0 g and (d) 1.5 g (Inset showing higher magnification of the nanowire cluster formed in 1.5ACP). 55

Figure 4.21: EDS results of (a) and (b) randomly oriented nanowires when exposed to 0 g, 0.5 g and 1.0 g ACP as well as (c) and (d) the nanowire clusters formed when exposed to 1.5 g ACP at the sides of Si substrate. 56

Figure 4.22: EFTEM images of nanostructures formed at the side under different ACP amount of (a) 0 g, (b) 0.5 g, (c) 1.0 g and (d) 1.5 g (Circled shows the presence of stacking faults). 57

Figure 4.23: (a) ESI results of the core-shell nanowires at the side of wafer, (b) ESI results of the nanowebs at the border and (c) XRD spectrum of the samples. 58

RESEARCH OUTCOMES

PUBLICATIONS

1. Y.L. Chiew and K.Y. Cheong, 'Synthesis of SiC Nanostructures Through Chemical Vapor Growth Route," ***International Journal Materialwissenschaft Und Werkstofftechnik (Materials Science and Engineering Technology)*** (Wiley-VCH in Germany). – (IF = 0.3700)
2. Y.L. Chiew and K.Y. Cheong, " Effect of Amount of Activated Carbon Powder on the Synthesis of SiC/SiOx Nanostructures via Chemical Vapor Growth Method," **Physica E** (Elsevier)
3. Y.L. Chiew and K.Y. Cheong, "A review on the synthesis of SiC nanostructures from plant-based biomasses," ***Materials Science and Engineering B*** (Elsevier) Vol. 176, pp. 951-964, 2011. (doi.: 10.1016/j.msed.2011.05.037).
4. Y. L. Chiew and K. Y. Cheong, "Formation and characterization of SiO_x nanowires and Si/SiO_x core-shell nanowires via carbon-assisted growth," ***Physica E*** (Elsevier), Vol. 42, pp. 1338 – 1342, 2010. **(ISI Impact Factor =1.230)**
5. K. Y. Cheong and Z. Lockman, "Growth Mechanism of Cubic-Silicon Carbide Nanowires," ***Journal of Nanomaterials*** (Hindawi), Vol. 2009, doi: 10.1155/2009/572865 (5 pages). **(ISI Impact Factor = 0.688)**
6. K.Y. Cheong and Z. Lockman, "Effects of temperature and crucible height on the synthesis of 6H-SiC nanowires and nanoneedles," ***Journal of Alloys and Compounds*** (Elsevier), vol. 481, pp. 345-348, 2009.
7. K.Y. Cheong and Y. L. Chiew, Advances of SiO_x and Si/SiO_x core-shell Nanowires in "**Nanowires Science and Technology"** Edn: N. Lupu, ISBN 978-953-7619-89-3, INTECH, Croatia, pp. 131 – 150, 2010.
8. Y.L. Chiew and K.Y. Cheong, "Synthesis of SiC Nanostructure Through Chemical Vapor Growth Route," **5th International Conference on Advanced Computational Engineering and Experimenting (ACE-X 2011)**, 3 – 6 July 2011, Algarve, Portugal, pp. 170 - 171.

AWARDS

1. Awarded a Gold Medal in "Persidangan dan Ekspo Ciptaan Institut Pengajian Tinggi Antarabangsa 2011 (PECIPTA 2011), 13 – 15 September 2011, at Kuala Lumpur Convention Centre (KLCC), Malaysia, for an invention of Chemical Vapor Growth (CVG) of nanowires.

2. Awarded a Bronze Medal in The 9th Malaysia Technology Expo (MTE), 4-6 Feb 2010, at Putra World Trade Centre, Kuala Lumpur, Malaysia, for an invention of Chemical Vapor Growth (CVG) of nanowires.

PATENTS

1. **PI 2010003119** – K.Y. Cheong, Z. Lockman, and Y.L. Chiew, "A Process for Producing Silicon Carbide (SiC) Nanowires on a Silicon Substrate" (30 June 2010).
2. **PCT/MY2010/000169** - K.Y. Cheong, Z. Lockman, and Y.L. Chiew, "A Process for Producing Silicon Carbide (SiC) Nanowires on a Silicon Substrate" (9 September 2010).

PERKEMBANGAN NANOWAYAR Si/SiO$_x$ DAN SiO$_x$ UNTUK APLIKASI ALAT ELEKTRONIK NANO

ABSTRAK

Struktur-struktur nano berasaskan silikon telah berjaya dihasilkan oleh pertumbuhan atas substrat silikon secara langsung dengan menggunakan wafer silikon dan serbuk karbon aktif sebagai bahan mentah. Nanowayar SiO$_x$ dan Si/SiO$_x$ dihasilkan oleh gabungan pertumbuhan dengan bantuan karbon dan oksida melalui mekanisma wap-pepejal apabila masa pengoksidaan adalah 24 minit dan masa rendaman adalah1 jam. Nanowayar SiO$_x$ disintesiskan pada suhu pertumbuhan 1200°C sementara nanowayar Si/SiO$_x$ disintesiskan pada suhu pertumbuhan 1300°C. Apabila masa pengoksidaan kurang daripada 12 minit, hanya struktur nano SiC dihasilkan. Nanorod dan nanotiang dihasilkan pada masa rendaman 1 jam. Diameter dan jumlah struktur-struktur nano ini susut apabila masa pengoksidaan jatuh daripada 12 minit kepada 1 minit. Nanorod SiC dijumpai pada tengah substrat manakala nanotiang dijumpai pada tep substrat silikon. Strukturnya tukar kepada nanowayar SiC/SiO$_2$ apabila masa rendaman dinaikkan kepada 2 jam. Struktur-struktur nano baru seperti nanokabel dan nanosarang dihasilkan bergantung pada lokasi pertumbuhan atas substrat silikon. Diameter nanokabel dan nanosarang susut apabila jumlah serbuk karbon aktif bertambah. Pembentukan nanokabel dan nanosarang adalah disebabkan oleh kesan aerodinamik kerana perbezaan tekanan di dalam dan luar mangkuk pijar. Pertumbuhan struktur-struktur nano SiC ini adalah melalui mekanisma wap-pepejal.

DEVELOPMENT OF SI/SIO$_X$ CORE-SHELL STRUCTURED NANOWIRE AND SIO$_X$ NANOWIRE FOR NANOELECTRONIC DEVICE APPLICATIONS

ABSTRACT

Si-based nanostructures were successfully synthesized through the method of direct growth on silicon substrates using only silicon wafers and activated carbon powder as sources. SiO$_x$ and Si/SiO$_x$ core-shell nanowires were produced through combination of carbon-assisted growth and oxide-assisted growth via vapour-solid mechanism when the oxidation time was 24 minutes at a soaking time of 1 hour. SiO$_x$ nanowires were formed at 1200°C while Si/SiO$_x$ core-shell nanowires were formed at 1300°C. When the oxidation time was reduced to below 12 minutes, SiC nanostructures were mainly formed. SiC nanorods and nanocolumns were formed at a soaking time of 1 hour, with decreasing diameter and amount with decreasing oxidation time from 12 minutes to 1 minute. SiC nanorods were formed at the center while SiC nanocolumns were formed at the side of silicon substrates. The structure changed from SiC nanorods and nanocolumns to SiC/SiO$_2$ core-shell nanowires when the soaking time was increased from 1 hour to 2 hours. New nanostructures of SiC/SiO$_2$ core-shell nanocables and nanowebs were formed depending on the growth locations on the silicon substrates when the activated carbon powder was added. The nanocables and nanowebs decreased in diameter with increasing amount of activated carbon powder. The formation of these nanocables and nanocables was a result of aerodynamic effects due to the pressure difference inside and outside of the crucible. The growth of these SiC nanostructures was correlated to the vapour-solid mechanism.

CHAPTER 1

INTRODUCTION

1.1 Introduction

Nanostructures have been gaining worldwide interest due to their small sizes that enable higher functionality in a given space and their peculiar and fascinating properties, which make them applicable in mesoscopic research, the development of nanodevices, and the potential application of large surface area structures (Xia et al., 2003). Interest in low-dimensional systems especially one-dimensional (1D) structures, such as nanotubes, nanowires and nanorods have caused the development of a variety of material in nanoscale.

Nanowires, which are one form of one-dimensional nanostructures, have been used as versatile building blocks in the miniaturization of electronic and optoelectronic devices (Li et al., 2006). Various materials have been synthesized in the form of nanowires, such as silicon, germanium, gallium nitride, gallium arsenide, and silicon carbide (Spanier, 2006).

In this study, silicon-based nanostructures, which include SiO_x nanowires, Si/SiO_x core-shell nanowires, SiC nanorods, SiC nanocolumns, SiC/SiO_2 nanowires, SiC/SiO_2 nanocables and SiC/SiO_2 nanowebs, have been produced. Silicon-based nanostructures have attracted much attention for their interesting semiconducting properties, mechanical properties, optical properties and their potential applications in mesoscopic research and nanodevices, such as one-dimensional quantum transistors, composites, light-emitting diodes (Pan et al., 2001b), high temperature, high frequency, high power applications (Shen et al., 2003), nanosensors and nanoscale electro-devices (Wei et al., 2002), biomedical applications (Fan et al., 2006b) and nanoelectromechanical systems (NEMS) (Choi et al., 2004). Consequently, a great deal of effort has been made in fabricating Si-based nanostructures.

Several methods have been used to synthesize silicon-based nanostructures, including laser ablation (Yu et al., 1998, Seeger et al., 2000), sol–gel (Liang et al., 2000b, Meng et al., 2000), thermal evaporation (Wei et al., 2006), carbothermal reduction (Shi et al., 2000b, Wu et al., 2001), rapid thermal annealing (Lai et al., 2008), chemical vapour deposition (CVD) (Zhou et al., 1999a, Mamails et al., 2004a, Zhang et al., 2006) and thermal oxidation route (Hu et al., 2003). However, these methods are somewhat expensive and complicated (Zhang et al., 2000a). Inability to control chemistry in the synthesized nanostructures is also evident. The nanowires produced by some of the methods above are either covered with silica layer or contaminated with metal catalyst.

1.2 Problem Statement

Nanowires have been synthesized through a series of methods, ranging from nanolithographic techniques, such as electron beam or focused-ion beam (FIB) writing (Nagarajan et al., 2006) to chemical synthesis method consisting of chemical vapor deposition or thermal evaporation (Law et al., 2004). However, the advancement in this field is hindered due to difficulties arising from the aspects of the synthesis of these nanowires with well-controlled dimensions, morphology, phase purity and chemical composition. It was found from extensive reports that it is difficult to produce very long nanowires that can be easily integrated and manipulated post-synthesis through simple methods. Another challenge was the need to organize the nanostructures in aligned patterns, and in high densities for use in industrial applications (Xia et al., 2003).

For the case of the synthesis of Si-based nanostructures, many techniques have been used to synthesize them with each of these methods having their own advantages and disadvantages. One of the limiting factors that were considered was the toxicity of the chemicals used in the synthesis process. For example, in the standard vapor-liquid-solid (VLS) growth via a chemical vapor deposition (CVD) process (Sekhar et al., 2006), it required the use of toxic and dangerous gases such as silane. These chemicals used were also very expensive in the CVD process. There are also methods that require metal catalyst that would contaminate the nanowires formed, which used Au catalyst in a CVD process (Yao et al., 2005, Colli et al., 2006). The metal catalyst would act as impurities and degrade the mechanical properties of devices formed using these nanowires.

Thus, it is desirable that a simple and effective method can be developed so as to overcome the problems presented by the methods currently available to produce Si-based nanostructures.

1.3 Research Objectives

The objectives of this study are:-

1. To synthesize Si-based nanostructures by direct growth on silicon substrates.
2. To investigate the effects of growth temperature (1100°C – 1300°C) and soaking time (1 hour, 2 hours and 4 hours) when the oxidation time was fixed at 24 minutes and exposed to 0.5 g activated carbon powder.

3. To investigate the effects of oxidation time (1 min, 2 min, 8 min, 12 min and 24 min) on the Si-based nanostructure growth at 1300°C and a soaking time of 1 hour while exposed to 0.5 g activated carbon powder.
4. To investigate the effects of soaking time (1 and 2 hours) on the growth of Si-based nanostructures at oxidation time of 2 min and growth temperature of 1300°C while exposed to 0.5 g activated carbon powder.
5. To investigate the effects of the amount of activated carbon powder (0 g, 0.5 g, 1.0 g and 1.5 g) on the growth of Si-based nanostructures at 1300°C and oxidation time of 2 min.

1.4 Scope of Project

In this study, Si-based nanostructures were synthesized using a modified CVD approach, conducted in a vacuum sintering furnace. This synthesis method involved a silicon wafer first subjected to thermal oxidation for a certain period (1 min, 2 min, 8 min, 12 min and 24 min) to introduce a thin oxide layer, followed by heating under Ar flow at certain growth temperature (1100°C – 1300°C) for 1 to 2 hours while exposed to different amounts of activated carbon powder (0 g, 0.5 g, 1.0 g and 1.5 g). The nanostructures produced were then subjected to characterization by field-emission scanning electron microscope (FESEM, LEO GEMINI) equipped with an energy dispersive X-ray spectrometer (EDS, ZEISS SUPRA^{TM} 35VP), an energy-filtered transmission electron microscope (EFTEM, ZEISS LIBRA 120) equipped with an electron spectroscopic imaging (ESI), high-resolution transmission electron microscope (HRTEM, Philips Tecnai 20) and X-ray diffraction (XRD, Bruker D8).

CHAPTER 2

LITERATURE REVIEW

2.1 Introduction

In this chapter, a brief background on the structures, properties and general synthesis routes of Si-based nanostructures especially for silicon carbide (SiC) and silica (SiO_2) will be described. Since two synthesis routes of direct growth on Si substrates and pyrolysis of biomass have been used, previous studies similar to these methods will also be reviewed in terms of the processes and the effects of the different parameters in the following sections.

2.2 Si-Based Nanostructures

2.2.1 Nanostructures

A nanostructured material can be defined as a material whose composition is modulated over nanometer range from 1 nm to 100 nm. They can be classified into zero, one and two dimensionalities based on geometrical shapes (Cao, 2004).

Zero-dimensional (0D) nanostructures are materials in which all three dimensions are in nanometer scale such as nanoparticles, nanospheres and nanoclusters and they have been widely studied for their potential applications as multifunctional nanoparticle probe (Cao, 2004). One-dimensional (1D) nanostructures are materials in which two of their dimensions are in nanometer scale. Variety of names has been given to 1D nanostructures depending on their shapes and sizes such as whiskers, fibers, nanorods and nanowires. Nanowires and nanorods are actually similar to whiskers and fibers respectively. They only differ in terms of the diameters of the product. Whiskers and nanowires both have very high aspect ratio, i.e. ratio of length to diameter is more than 10 but the diameter range of whiskers is in the range of 100 nm to 10000 nm while the diameter range of nanowires is in the range of 1 nm to 100 nm (Narciso-Romero and Rodriguez-Reinoso, 1996, Weaver, 1989). Fibers and nanorods both have aspect ratio of less than 10 but the diameter range of fibers is in the range of 100 nm to 10000 nm while the diameter range of nanorods is in the range of 1 nm to 100 nm (Narciso-Romero and Rodriguez-Reinoso, 1996). 1D nanostructures are known to exhibit quantum confinement effect like 0D nanostructures but for 1D nanostructures, the charge carriers can only travel in one direction along the wire. Thus, making them useful as interconnects and critical devices in nano-electronic and nano-optoelectronic applications (Cao, 2004). Two-dimensional (2D) nanostructures are materials having nanometer dimension perpendicular to the layer plane such as thin film and nanoporous materials. The charge carriers in these 2D nanostructures are limited to the direction perpendicular to the layer and can move freely in the layer plane. These 2D nanostructures especially nanoporous materials have been studied for their applications in biosensors, nanophotonics and nano-electronic applications.

2.2.2 Silicon Carbide (SiC)

SiC was first discovered accidentally when a Swedish scientist, Jöhn Jacob Berzelius was trying to synthesize diamond in 1824 (Zimmermann, 19 December 2000). It was then largely manufactured when Cowless (1885) and Acheson (1892) found that the hard and stable compound was suitable for grinding and cutting purposes and Acheson developed an industrial method which involved carbothermal reduction of silica sand with green petroleum coke at temperature of 2400°C (Sudarshan, 2006).

SiC is a covalently-bonded IV-IV compound with alternating layers of silicon (Si) and carbon (C). The carbon atom is linked to three Si atoms in a tetrahedral structure within the bilayer and has a single bond linked to a Si atom in the layer below, as shown in Figure 2.1. The bond length of the nearest neighbour is approximately 1.89 Å and the closest distance between two atoms of the same species in the SiC lattice is approximately 3.08 Å (Zhou et al., 2008).

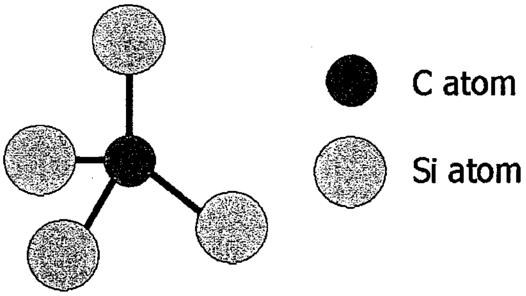

Figure 2.1: Tetrahedral bonding of a C atom with its four nearest Si atoms.

SiC has almost 200 different polytypes due to its different periodic stacking faults as a result of alternate layer arrangement. The most common polytypes are cubic 3C, hexagonal 4H and 6H, as well as rhomboheral 15R, which are differentiated by the repeated stacking sequences of the biatom layers of SiC structure, as shown in Figure 2.2 (Sudarshan, 2006). A, B, C in the figure represent the position of the lattice site of SiC without changing the tetrahedral bonding of the Si-C bilayer. 3C-SiC is also referred as β-SiC whereas the other polytypes are referred as α-SiC. β-SiC can be considered as a low-temperature polytype since it is easier to nucleate and grow while α-SiC is considered as high-temperature polytype that needs relatively high temperatures to grow.

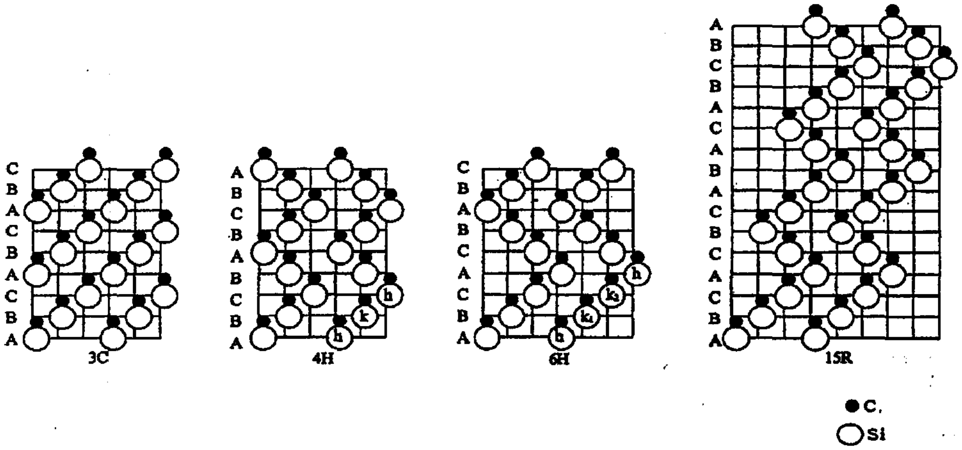

Figure 2.2: Stacking sequence of double layers of 3C, 4H, 6H and 15R-SiC (Sudarshan, 2006).

SiC materials are extremely hard, inert, have wide band gap, high breakdown field strength, high saturation electron drift velocity and depending on doping, the material can be made transparent to optical wavelengths. Table 2.1 shows some of the important properties at room temperature for different polytypes of bulk SiC as well as SiC nanowires (Wang et al., 2012, Chen et al., 2010, Fan et al., 2006a, Powell and Rowland, 2002, Ryu et al., 2005, Shen et al., 2006, Wong et al., 1997, Yan et al., 2006, Zhou et al., 2006a).

Table 2.1: Properties for different polytypes of SiC and SiC nanowires at room temperature.

Properties	**3C-SiC (bulk)**	**4H-SiC (bulk)**	**6H-SiC (bulk)**	**3C-SiC nanowires (depending on diameter, D)**
Carrier Concentration (cm^{-3})	~1000 (Zhou et al., 2006a)	~10^{-7}	~10^{-5}	0.82 - 1.76 x 10^7 at V_{ds} = 0.01 and 0.05V (Zhou et al., 2006a)
Energy Gap (eV)	2.4 (Yan et al., 2006)	3.2 (Powell and Rowland, 2002)	3.0 (Powell and Rowland, 2002)	4.42 - 3.31 eV for D = 0.61 - 0.92 nm (Yan et al., 2006)
Carrier Mobility (cm^2/V.s)	1.5	3.2	3.0	6.4 - 15.9 when V_{ds} = 0.01 - 0.05 V (Zhou et al., 2006a)
Turn On Field, E_{to}	N/A	N/A	N/A	4.0 (Ryu et al., 2005) For bamboo-like

($V\mu m^{-1}$)				nanowires, 10.1 at emission current of 10 μAm^{-1} (Shen et al., 2006) 5 and 8.5 at 10 μAm^{-1} and 10 mAm^{-1} (Fan et al., 2006a) 2.1 at current density of 10 μAm^{-2} (Chen et al., 2010)
Tensile Strength (GPa)	N/A	N/A	N/A	51.5 for D = 0.61 nm (Yan et al., 2006) 53.4 for D = 21.5 - 23.0 nm (Wong et al., 1997) 33.4 for D = ~5 nm (Wang et al., 2012) 12.4 for SiC/SiO_2 nanowires with D =5 nm with oxide thickness = 1 nm (Wang et al., 2012)

From Table 2.1, it can be observed that there is a change in the properties of SiC when its size is reduced to nanometer range. When materials are reduced to nanometer range, it allows the realization of miniaturized devices and systems while providing more functionalities, attainment of high surface area to volume and manifestation of new properties due to quantum confinement effect.

In some cases, the SiC nanostructures were observed to be covered with a layer of amorphous SiO_2 with thickness up to half of the diameter of the SiC cores (10 – 30 nm), forming SiC/SiO_2 core-shell nanostructures (Du et al., 2007, Kang et al., 2011, Kim et al., 2009, Liao et al., 2011, Lopez-Camacho et al., 2008, Niu and Wang, 2007a, Wang et al., 2007, Yang et al., 2009). The presence of an oxide layer had been reported to act as a protective layer against corrosion without affecting the mechanical properties, making them suitable for use as reinforcement in composites. The presence of the oxide layer was also found to enhance the electron emission properties. The improvement in the field emission properties of the core-shell structures, especially in nanowires as compared to conventional SiC nanowires was suggested to be a result of three reasons (Wang et al., 2007). Firstly, high density nanowires had more efficient electron emitting sites, leading to better field emission properties. The wide band-gap SiO_2 shell layer was reported to have a small electron affinity (0.6 – 0.8 eV) that could enhance the field emission of SiC emitters. Finally, the geometry of the core-shell nanowires with high aspect ratio also enhanced the field emission properties by improving the ability of the emitters in controlling the local electric field at the tips. However, there were also some disadvantages of the presence of the oxide shell. The thick oxide shell reduced the electronic conductivity between the nanowires and their contacting electrodes (Li et al., 2002). Aside from that, the different lattice structures of SiC and SiO_2 created thermal stress in the as-synthesized nanostructures due to uneven shrinkage (Li et al., 2002).

2.2.2 Silica (SiO_2)

Silica is an oxide of silicon with the formula with the chemical formula SiO_2. It is most commonly found in nature as sand or quartz. The basic building block of the silica molecule consists of a tetrahedral coordination of silica, whereby four oxygen atoms surrounds a central Si atom, as shown in Figure 2.3. The four oxygen atoms in the SiO_4 tetrahedral are shared with other tetrahedral in order to obtain a thermodynamically stable form of silica, yielding the net formula of SiO_2.

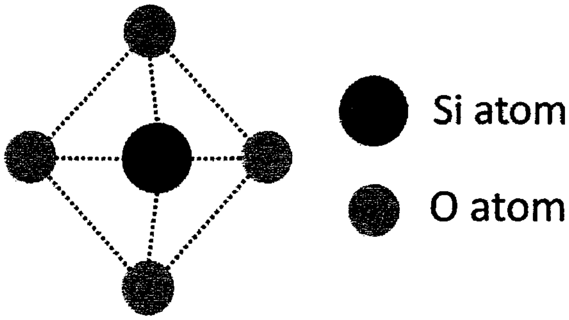

Figure 2.3: Tetrahedral bonding of a Si atom with its four nearest O atoms.

SiO_2 exist in amorphous form as well as in a number of crystalline forms. The crystalline forms involve tetrahedral SiO_4 units linked together by shared O_2 in different Si-O bond lengths and Si-O-Si angles, which result in various polymorphs with the common ones being α-quartz, β-quartz, tridymite and cristobalite. α-quartz is the only stable crystalline form under normal conditions and it is the SiO_2 form that is usually encountered. The difference between the crystalline and amorphous forms of SiO_2 arises in the connectivity of these SiO_4 tetrahedral units. The amorphous form consists of a non-repeating network of tetrahedra, where all oxygen atom corners connect two neighbouring tetrahedra.

Silica is best known for its hardness and inertness. In electronic field, bulk silica is also known as an electric insulator with high chemical stability but when the size is reduced to nanoscale, new properties manifest and the properties of the SiO_2 nanostructures are shown in Table 2.2 (Pang et al., 2011, Al-Ruqeishi et al., 2011, Bilalbegovic, 2006, Jin et al., 2008, Ni et al., 2006).

Table 2.2: Properties of SiO_2 nanowires at room temperature.

Properties	**Value**
Young's Modulus	57 - 93 GPa (Ni et al., 2006)
Electrical conductivity	Varies according to number of Si-O bonds (changes from metallic to insulating as number of bond increases) (Bilalbegovic, 2006)

Fermi level	-3 eV to -7 eV (more positive as number of Si-O chain increases) (Bilalbegovic, 2006)
PL band energies	1.9 – 4.3 eV (Jin et al., 2008, Al-Ruqeishi et al., 2011, Pang et al., 2011)

2.2.3 Synthesis of Si-Based Nanostructures

Due to the unique properties of Si-based nanostructures, many techniques, including top-down and bottom-up approaches, have been developed and applied in the synthesis of Si-based nanostructures (Vaseastha, 2005). The most common methods being chemical vapor deposition (CVD) (Yang et al., 2005, Yang et al., 2004, Ying et al., 2004, Mamails et al., 2004b, Chio et al., 2004, Zhang et al., 2001), thermal evaporation (Yang et al., 2008b, Zhou et al., 1999b, Li et al., 2003) and carbothermal reduction (Meng et al., 2000, Liang et al., 2000a, Xu et al., 2006). Although these methods are able to produce the nanostructures at lower temperatures and with smaller sizes, these methods have their own problems as compiled by Zhou et al. (2008) in Table 2.3.

Table 2.3: Comparison of several synthesis methods of Si-based nanostructures (Zhou et al., 2008).

Synthesized methods	**Yield**	**Cost**	**Temperature (°C)**	**Diameter (nm)**	**Catalyst**
Carbon-nanotube confined reaction	Low	Higher	1,400	20 – 25	No
Arc discharge	Higher	Low	3,000	20 – 60	Yes
Laser ablation	High	High	900	20 – 70	Yes
Sol-gel and carbothermal reduction	Higher	Lower	900	40 – 80	No
Chemical vapor deposition method	Higher	Higher	1,100	10 – 100	Yes
High-frequency induction heating	Higher	Lower	1,450	5 – 20	No

The methods listed in Table 2.3, aside from laser ablation and sol-gel method, all required high temperatures, which posed a problem in the commercialization of these methods in producing Si-based nanostructures as a result of the high cost incurred. Although laser ablation and sol-gel method could be performed at lower temperatures, the systems are complex and require expensive raw materials and these contributed to high production cost (Narciso-Romero and Rodriguez-Reinoso, 1996). Here, direct growth on Si substrate has been studied in the growth of Si-based nanostructures, namely direct growth on Si substrate and pyrolysis of biomass. Several techniques have been used in the direct growth route, which include CVD and carbothermal reduction.

2.3 Direct Growth of Si-Based Nanostructures on Si Substrate

The direct growth method involved the growth of Si-based nanostructures using only Si substrate on the Si substrate without using any external source except for carbon sources in the synthesis of SiC nanostructures. The ability to grow these nanostructures directly on Si substrate offered the possibility of direct integration of these nanostructures for electronic device building. This attracted various researches being performed on it. From previous works, it was found that different types of products were formed such as SiC nanorods or nanowires, core-shell SiC/SiO_2 nanowires, core-shell SiC/a-C nanowires, SiO_2 nanowires and carbon nanotubes using this method under different parameters. The effects of these parameters such as starting materials, growth temperature, catalyst, furnace atmosphere and cooling rate will be described in the following subsections.

2.3.1 Effect of Starting Materials

2.3.1.1 Si source

Si wafer is a good alternative in producing Si-based nanostructures as it acts as a Si source and simultaneously as a substrate in collecting the nanostructures without requiring additional Si sources. In addition, by controlling certain parameters, it is possible to control the growth location of nanostructures on the Si wafer, enabling selective patterning for electronic device building.

Introduction of a thin silicon oxide (SiO_x) layer on the Si substrate by either thermal oxidation (Jeong et al., 2008, Park et al., 2007) or thermal evaporation using SiO powder (Li et al., 2002) had been found to enhance the growth of Si-based nanostructures. Different thicknesses of the oxide layer would lead to different nanostructures formed. Thin layers of oxide (< 150 nm) were found to be beneficial for the growth of SiC nanostructures (Li et al., 2002) while thick layers of oxide (500 nm) were found to be more suitable for growth of SiO_2 nanostructures (Jeong et al., 2008). However, if the oxide layer was too thick (> 3 μm), it would inhibit the growth of Si-based nanostructures (Park et al., 2007). SiC nanowires were found growing on the bare Si substrate while no nanostructures were found in regions grown with 3 μm SiO_2.

Presence of defects had also been reported to have a large influence on the growth of Si-based nanostructures on the Si substrate. The defects were introduced on the Si substrate surface by mechanical scratching (Liao et al., 2011) or etching (Park et al., 2007). They acted as nucleation sites and promoted the growth of nanostructures, especially on the [111] planes exposed by the grooves or ledges created by the defects due to their lowest surface energies. This resulted in higher amount of SiC nanowires with average diameter of 30 nm and length of tens of μm being found in the scratched regions as opposed to the unscratched regions (Liao et al., 2011).

Placement of Si substrate in the experimental setup is another important factor in the synthesis of Si-based nanostructures using direct growth method. It was found that SiC nanostructures were found only if the Si substrate was placed downstream from the carbon source in order for the carbon species to be deposited onto the Si substrate (Al-Ruqeishi et al., 2010, Baek et al., 2006). The distance between the carbon source and the Si source also affected the morphologies of the nanostructures formed. Al-Ruqeishi et al. (2010) reported the growth of β-SiC nanowires by exposing the silicon substrate to graphite powder that was placed upstream of the tube furnace. Different Si substrates were placed at certain distances from graphite source and its effects were studied. High yield of β-SiC nanowires formed at locations near the graphite source with the maximum yield at a distance of 2 cm and 4 cm. The yield started to decrease with increasing distance. At the location far from the graphite source (10 cm), SiC nanowires were only found at the edges of the Si substrates where defects such as grooves and ledges existed. The nanowires on the Si substrate at locations near the graphite source were also reported to have larger diameters with the diameter range of 40 nm to 500 nm. The reason for the higher yield and larger diameters at locations close to the graphite powder was because of the higher reactant species available at these regions that allowed continuous growth of nanowires.

2.3.1.2 Carbon Source

Different forms of carbon source had been reported in the growth of SiC nanostructures using direct growth on Si substrate. The Si substrate was either exposed to solid carbon that were placed upstream of the Si substrate such as carbon powder (Baek et al., 2006, Niu and Wang, 2007b, Ryu et al., 2004, Wang et al., 2007), graphite (Al-Ruqeishi et al., 2010, Li et al., 2002), detonation soot powders (Yang et al., 2009) and charcoal powders (Du et al., 2007) or gaseous form of carbon such as ethanol (Kim et al., 2009, Yang et al., 2008a), methane (Liao et al., 2011, Lopez-Camacho et al., 2008, Panda and Jacob, 2009), ferrocene (Niu and Wang, 2007a), carbon monoxide (CO) (Attolini et al., 2008) and hexamethyldisilane (HMDS) (Panda et al., 2010). The gaseous carbon source was found to require lower growth temperatures of 1000°C – 1100°C as compared to the solid carbon source with growth temperatures ranging from 1200°C – 1500°C (Kim et al., 2009, Lopez-Camacho et al., 2008). Growth using solid carbon might require a higher growth temperature due to the need to decompose the solid carbon first in order to form gaseous carbon species.

The concentration of the carbon source was found to play an important role as well in determining the final structures of the products. Different products from SiC/SiO_2 core-shell nanowires to SiC/C core-shell nanowires or carbon nanotubes were reported when the methane concentration was increased. Liao et al. (2011) reported the growth using catalyst-assisted chemical vapour reaction by exposing the Si substrate to ferrocene and methane under H_2 flow at 1100°C for 10 min. The ferrocene acted as the catalyst, producing Fe particles that deposited onto the Si substrate surface. At methane concentrations less than 5%, only SiC/SiO_2 core-shell nanowires were formed as opposed to carbon nanotubes that were formed at methane concentrations more than 5%. The reason for different products formed was related to the different catalyst particles formed. When heated at high temperature, decomposition of ferrocene and methane occurred. If methane concentration was low, the Fe particles would deposit on the Si substrate and diffused into the SiO_2 layer to the interface between SiO_2 and Si in order to form iron silicide (FeSi) that would later induced the growth of SiC/SiO_2 core-shell nanowires. When the methane concentration was more than 5%, the carbon species would also deposit onto the Si substrate surface and diffused through the SiO_2 layer to the interface between SiO_2 and Si. Instead of FeSi, iron carbide was formed and induced the growth of carbon nanotubes.

There was also another on the effect of methane concentration (Lopez-Camacho et al., 2009b). In their chemical vapour deposition (CVD) method, they exposed the Ni-coated substrates to methane under H_2 at 950°C for 10 min. They found that SiC/SiO_2 core-shell nanowires were formed when the methane concentration was between 12% and 45% but when the methane concentration was further increased to concentrations between 59% and 75%, SiC/a-C core-shell nanowires was formed instead, whereby the SiC nanowires were encapsulated by an amorphous carbon layer. The evolution of the nanostructures from SiC/SiO_2 to SiC/a-C when methane concentration was increased had been reported to be a result of the change in the growth mechanism from vapour-liquid-solid (VLS) to solid-liquid-solid (SLS). When carbon concentration was increased further, a layer of carbon would be deposited onto the Si substrate and this C layer would hinder the VLS mechanism between SiO, C and Ni nuclei. The Si source would have to diffuse through the solid surface into the Ni and reacted with the C layer. Since the nuclei was surrounded by the C layer, SiO_2 shell could not be formed when the SiC nanowires precipitated out from the nuclei but instead be encapsulated by the amorphous C layer.

2.3.2 Effect of Growth Temperature

The growth temperature is another important parameter in the synthesis of Si-based nanostructures. It was found to be highly dependent on the source materials, ambient and incorporation of catalyst, which will be described in their respective sections. The normal growth temperature using direct growth method in synthesizing Si-based nanostructures ranged from 1100°C – 1550°C. The growth temperature was also found to affect the morphologies and yield. An increase in growth temperature from 1050°C to 1100°C led to a change of structure from nanowires with diameters less than 80 nm to rods with diameters of 2 µm (Attolini et al., 2008). An increase in the growth temperature from 900°C to 1100°C was also reported to cause a change in the product from carbon nanotubes to SiC/SiO_2 core-shell nanowires when the Si substrate was exposed to methane and ferrocene was used as catalyst source (Liao et al., 2011).

2.3.3 Effect of Catalyst

Addition of catalyst in the system was also found to have an effect on the growth of Si-based nanostructures. Catalysts could be defined as substances that were added into the system to change the rate of reaction by participating in the multiple chemical transformations. It promoted the growth of nanostructures by lowering the free energy of activation through different routes of chemical reactions, enabling the growth of nanostructures to proceed at lower temperatures with higher yield. Growth of Si-based nanostructures had been reported to be possible at lower temperatures of 950°C to 1100°C when catalysts were incorporated into the system (Lopez-Camacho et al., 2009a, Wang et al., 2007) as compared to systems without catalysts with the normal growth temperature range of 1200°C-1550°C (Niu and Wang, 2007a). However, the metal catalysts that remained on the nanostructures were also considered as impurities that limited the applications of these nanostructures (Kang et al., 2011).

Here, various types of catalysts had been used such as $Ni(NO_3)_2$ (Al-Ruqeishi et al., 2010, Attolini et al., 2008, Kim et al., 2009, Ryu et al., 2004), Cr (Li et al., 2002), Ni (Lopez-Camacho et al., 2008), Fe from ferrocene (Liao et al., 2011, Niu and Wang, 2007a), Fe_3O_4 (Wang et al., 2007), WO_3 (Baek et al., 2006, Ryu et al., 2004) and ZnS (Niu and Wang, 2009). The catalysts were introduced into the system by dipping the Si substrate into an ethanol solution containing the catalysts (Al-Ruqeishi et al., 2010, Attolini et al., 2008), placing the catalyst powder upstream from the Si substrate (Liao et al., 2011, Niu and Wang, 2007a) or by sputtering a layer of catalyst on the Si substrate surface (Lopez-Camacho et al., 2008).

When using catalysts in the growth of Si-based nanostructures, the mechanism had always been correlated to the VLS mechanism, whereby the metal catalyst particles formed metal silicide and acted as nuclei which absorbed the reactant species from surrounding gases. Upon supersaturation, the nanostructures would precipitate out (Al-Ruqeishi et al., 2010, Attolini et al., 2008, Kim et al., 2009, Lopez-Camacho et al., 2008, Ryu et al., 2004). Nanostructures grown using catalysts under VLS mechanism had also been noted with metallic droplets on the tips of the nanostructures though in some cases, the metallic droplets were found at the base of the nanostructures and this growth mechanism was named as base-growth mechanism (Li et al., 2002, Liao et al., 2011, Niu and Wang, 2007a).

In some cases, the catalyst particles only initiated the decomposition process of silicon and carbon source so as to enhance the reaction rate such as ZnS (Niu and Wang, 2009) and WO_3 (Baek et al., 2006, Ryu et al., 2004). Upon completion of process, the catalyst particles would have been evaporated without having any effects on the nanostructures formed. Niu and Wang (2009) evaporated ZnS powder on Si substrate. The use of sulfide was very important in the growth of nanowires. The Si vapor evaporated from Si substrate reacted with vapor phase of S or SO_2 from ZnS forming SiS vapor. Si then precipitated out from SiS and formed nucleus for the growth of nanostructures. In the case of WO_3, it was used to provide CO source through carbothermal reduction of WO_3.

2.3.4 Effect of Furnace Atmosphere

The atmosphere inside the furnace during the synthesis process was also found to affect the growth kinetics of the nanostructures. The atmosphere inside the furnace was introduced for several reasons, either to provide an inert atmosphere to remove unwanted species, to provide a reductive atmosphere for carbothermal reduction or to act as carrier gas for the reactant species. The functions of different atmospheres would be described in the following parts.

A low partial pressure of oxygen (O_2) in the furnace atmosphere was found to be beneficial in the growth of SiC nanostructures but if the partial pressure of O_2 was too high, it would inhibit SiC growth and favored the growth of SiO_2 nanostructures (Du et al., 2007). The growth of nanostructures under O_2 was related to the oxide-assisted growth (OAG) mechanism (Zhang et al., 2003), whereby the O_2 played an important role in the formation of SiO_2 or SiC. O_2 would react with Si, forming SiO species that later transformed into SiC or SiO_2 species depending on the partial pressure.

Argon (Ar) was commonly used in the synthesis process as a carrier gas for the reactant species (Li et al., 2002). It was also used to provide an inert atmosphere in the furnace chamber (Li et al., 2002, Yang et al., 2008a). Ar was introduced into the furnace in order to remove unwanted species and stabilize the Ni catalysts deposited on the Si substrate surfaces, preventing the oxidation of the catalyst particles that would hinder the functions of catalysts (Lopez-Camacho et al., 2008, Lopez-Camacho et al., 2009a). However, it was reported that Ar had lower efficiency in removing O_2. Residual O_2

still existed in the furnace chamber and would lead to preferential growth of SiO_2 nanowires (Lopez-Camacho et al., 2008). The flow rate of the Ar gas must also be controlled in growing the nanostructures. When synthesizing SiC nanostructures, the carbon source had to dissociate into CO species in order for SiC formation reactions to take place. If the Ar flow was too high, it would either remove the carbon source from the reaction zone or transfer the carbon source to the reaction zone without being oxidized into CO and this would lead to the deposition of carbon nanoparticles on the nanowires, as observed in the nanowires formed by Kim et al. (2009).

Hydrogen (H_2) was normally used to provide a reductive atmosphere in the furnace chamber and it was found to have a higher efficiency in removing residual O_2 in the furnace chamber as compared to Ar to produce an O_2 deficient zone for the growth of SiC nanostructures (Lopez-Camacho et al., 2008). However, it was also reported that the presence of H_2 prevented the growth of SiC nanostructures on SiO_2-coated Si substrates (Park et al., 2007). When heated at high temperature, H_2 dissociated into H species that preferentially adsorbed onto the SiO_2 surface and bonded with the Si dangling bonds whereas the carbon species preferentially adsorbed onto the bare Si substrate and reacted with the Si dangling bonds. The H species on the SiO_2 surface prevented incoming carbon species to react with Si and thus resulted in no SiC nanostructures being formed on the SiO_2 surface while SiC/SiO_2 core-shell nanowires were found on the bare Si substrate. This enabled selective patterning of SiC nanostructures on Si substrate by using a thick layer of SiO_2 and exposing the substrate to H_2 atmosphere. Although the growth of SiC/SiO_2 nanowires was reported to be possible under H_2 atmosphere, the pressure had to be controlled within a narrow range of 375 Torr to 600 Torr (Lopez-Camacho et al., 2008). A pressure of 375 Torr showed the optimum results in terms of high yield and considerable length. As the pressure was increased to 600 Torr, SiC/SiO_2 core-shell nanowires were still formed but with the presence of another side product of SiO_2 nanowires. The lengths of the nanowires were also visibly shorter as compared to that of 375 Torr. This is because the high pressure would suppress the catalytically activated decomposition reaction of methane and decrease the amount of C species available for SiC growth, thus slowing down the growth rate of SiC. The remaining oxide species would then favored the growth of SiO_2 nanowires.

Nitrogen (N_2) atmosphere had also been used in the synthesis of SiC nanowires under direct growth method (Niu and Wang, 2007a). N_2 was only used as a carrier gas and to provide an inert atmosphere for the thermal evaporation of ferrocene on Si substrate. Nitridation did not occur as commonly reported when using N_2 atmosphere due to the high stability of the SiC formed.

2.3.5 Effect of Cooling Rate

Furthermore, the control of the cooling rate is found to be important in determining the yield and morphology of SiC product formed. It was reported that only a small amount of pure SiC nanowires with lengths less than 3 μm were produced when the substrate was rapidly cooled down by taking out the substrate from furnace and exposed to ambient. Whereas large amount of SiC/SiO_2 core-shell nanowires with lengths up to few mm were formed when the substrate was slowly cooled down in furnace at a rate of 10°C/min to room temperature under H_2 protection (Du et al., 2007).

The reason for the different products formed under different cooling rates had been reported to be a result of different reaction kinetics during holding and cooling stages.

During the holding stage, the reaction between SiO and CO took place via Equation 2.1.

$$SiO\ (g) + 3CO\ (g) \rightarrow SiC\ (s) + 2CO_2\ (g) \qquad (2.1)$$

During the cooling stage, the following reaction between SiO and CO had been reported to predominate at temperatures less than 900°C.

$$3SiO\ (g) + CO\ (g) \rightarrow SiC\ (s) + 2SiO_2\ (s) \qquad (2.2)$$

From the above reactions, it could be observed that only SiC was formed during holding stage and thus, pure SiC nanowires were obtained when the substrate was rapidly cooled. For the case of slow cooling, SiC and SiO_2 were formed simultaneously. In addition, since SiC had higher melting point as compared to SiO_2, SiC would solidify first and the SiO_2 would encapsulate SiC, forming the SiC/SiO_2 core-shell nanowires (Silva and Figueiredo, 2001, Luo et al., 2009, Zhang et al., 2009a).

CHAPTER 3

MATERIALS AND METHODOLOGY

3.1 Introduction

This chapter is comprised of two parts. The first part details the synthesis route of chemical vapour growth (CVG) on silicon (Si) wafer. CVG route began with wafer preparation, thermal oxidation of Si wafers and finally the Si-based nanostructure growth process. The second part outlines the characterization techniques that were involved in analysing the samples, which include field-emission scanning electron microscope (FESEM, LEO GEMINI) equipped with an energy dispersive X-ray spectrometer (EDS, ZEISS SUPRA^{TM} 35VP), an energy-filtered transmission electron microscope (EFTEM, ZEISS LIBRA 120) equipped with an electron spectroscopic imaging (ESI), high-resolution transmission electron microscope (HRTEM, Philips Tecnai 20) and X-ray diffraction (XRD, Bruker D8).

3.2 Chemical Vapor Growth (CVG) on Si Wafers

In this section, the chemicals used and the methodology involved in the CVG method are described and summarised in the flow chart in Figure 3.1.

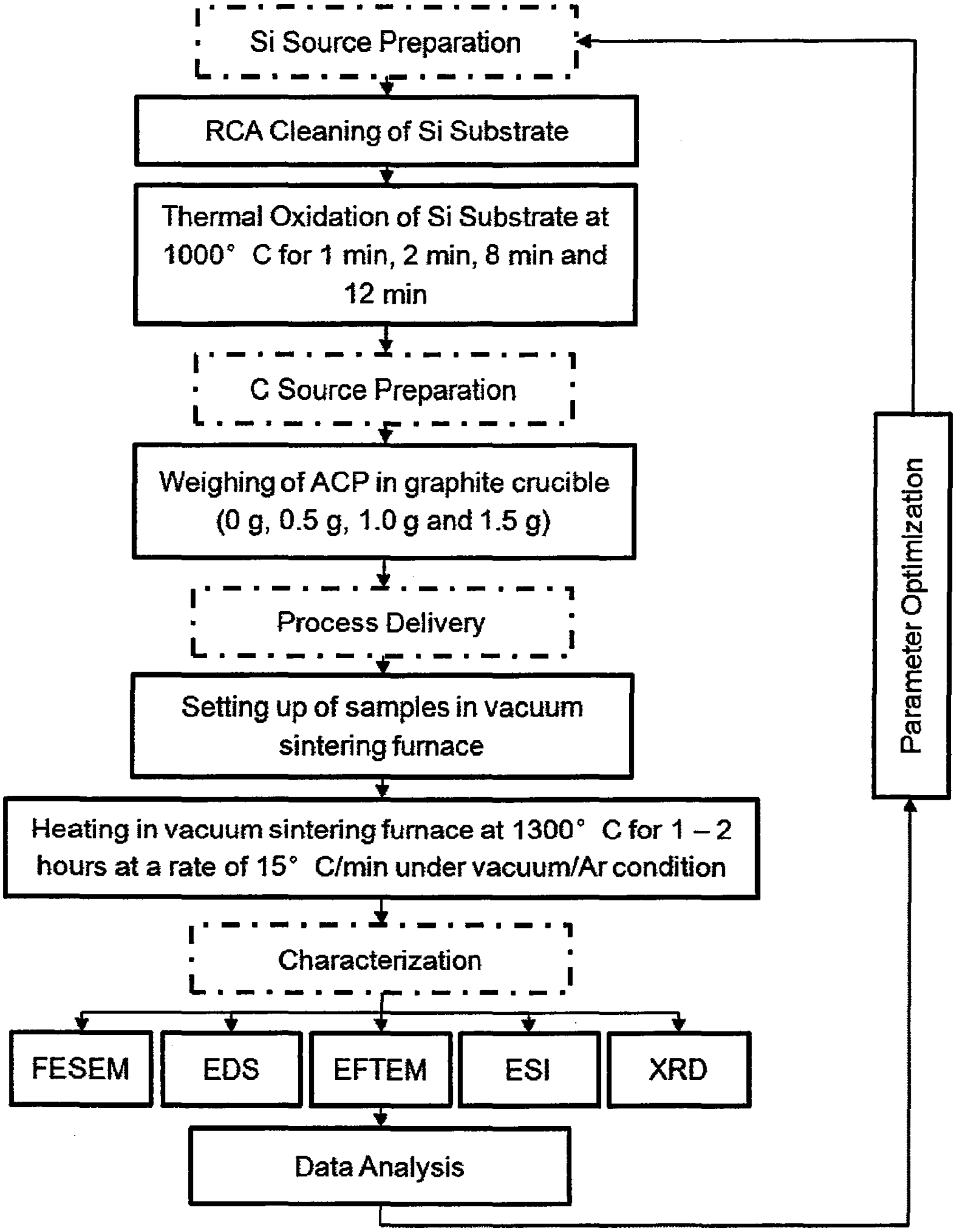

Figure 3.1: Flow chart of the experimental methodologies in CVG.

3.2.1 Chemicals and Reagents

Table 3.1 lists all the chemicals and reagents used in the experiment, detailing their specifications.

Table 3.1: Specifications of the chemicals and reagents used in CVG on Si wafers.

No.	Chemical Name	Chemical Formula	Form	Manufacturer	Specifications
1.	Hydrogen peroxide	H_2O_2	Liquid	J. T. Baker, Germany	CMOS grade
2.	Ammonium hydroxide	NH_4OH	Liquid	J. T. Baker, Germany	CMOS grade
3.	Hydrofluoric acid	HF	Liquid	J. T. Baker, Germany	CMOS grade
4.	Hydrochloric acid	HCl	Liquid	J. T. Baker, Germany	CMOS grade
5.	Activated carbon powder	C	Solid	DARCO®	100 mesh (149 μm) mean particle size

3.2.2 Wafer Preparation

A commercial n-type <100> oriented 2 inch diameter silicon wafer with resistivity of 1-20 Ω-cm and thickness of 525 ± 25 μm was used as a substrate and silicon source for the growth of Si-based nanostructures.

Prior to growth, the 2 inch diameter silicon wafer was cut into half using a diamond cutter and cleaned using a three-step wet chemical cleaning process, known as RCA cleaning, whereby all of the chemicals used were of CMOS grade. The silicon wafer was first immersed in deionized water before the cleaning process.

The first solution was known as RCA 1 solution that needed to be prepared in a glass beaker. It consisted of deionized water, ammonium hydroxide (NH_4OH) and hydrogen peroxide (H_2O_2) in the ratio of 5:1:1 to remove organic contaminants on the wafer surface. The solution was then heated on a hotplate to temperatures between 80-85°C and maintained for 10-15 min. Precautions were taken to ensure that the temperature of the solution did not exceed 85°C because higher temperatures would cause degradation of the cleaning solution and reduce the cleaning efficiency. The wafer was then removed from solution, rinsed with deionized water and immersed in deionized water to protect the wafers from dust particles in the ambient before subsequent processes.

The second solution consisted of a solution of hydrofluoric acid (HF) that should be prepared in a plastic beaker in a ratio of $HF:H_2O$ of 1:50 to remove the native SiO_2 layer on the wafers. The silicon wafer surface also became hydrogen terminated and hydrophobic. The wafer was dipped in the diluted HF solution for about 15 seconds before being removed from the solution and rinsed with deionized water. Lastly, the wafer was immersed in deionized water while preparing the third solution.

The third and final solution was RCA 2 solution prepared in a glass beaker. It consisted of deionized water, hydrochloric acid (HCl) and hydrogen peroxide (H_2O_2) in the ratio of 6:1:1 to remove residual inorganic metal contaminants. The solution was heated to temperatures of 80-85°C and maintained for 10-15 min. The temperature should not exceed 85°C to avoid degradation of the solution that would lead to reduction in the cleaning efficiency. After the heating process, the removed wafer was rinsed with deionized water and immersed in deionized water to ensure complete removal of the cleaning solution.

The cleaned wafer was then ultrasonically cleaned for 15 minutes and finally, the wafer dried using air gun before being stored for subsequent processes.

3.2.3 Thermal Oxidation of Silicon Wafer

The cleaned silicon wafer was subjected to thermal oxidation under different oxidation times (1 min, 2 min, 8 min and 12 min). In this experiment, the wafer was thermally oxidized using dry oxidation. Dry oxidation was chosen here because the oxidation rate was low, making it easier to control the oxide thickness accurately. The chemical reaction that was involved in the oxidation is shown as follow.

$$Si(s) + O_2(g) \rightarrow SiO_2(s) \tag{3.1}$$

The oxidation process involved the heating of Si wafer while being exposed to O_2 atmosphere in a horizontal tube furnace. Before oxidation, the quartz tube was first cleaned using a HF solution of 180 ml deionized water and 20 ml HF. During oxidation, the cleaned wafer was inserted into the center of the quartz tube. Next, the tube was heated according to the heating profile as shown in Figure 3.2, at a rate of 5°C/min to 1000°C and soaked for the pre-determined time of 1 min, 2 min, 8 min and 12 min before cooling down at a rate of 5°C/min to room temperature. Oxygen (O_2) was only introduced during the soaking time while argon (Ar, 99.99%) was supplied during the heating and cooling stages to provide an inert atmosphere.

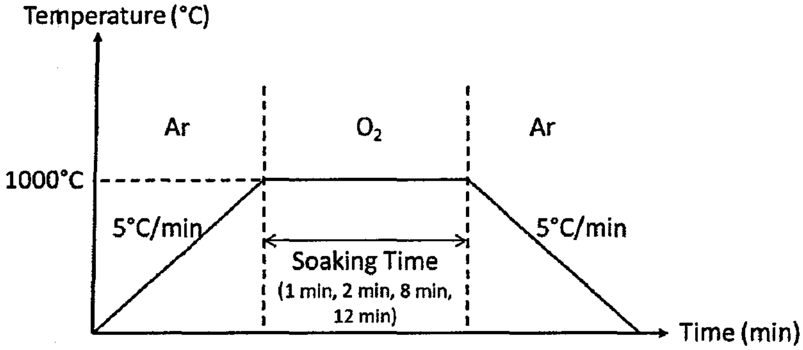

Figure 3.2: Heating profile for thermal oxidation.

3.2.4 Growth of Nanostructures in Vacuum Sintering Furnace

The oxidized Si wafer was placed on the graphite crucible with polished surface facing the crucible and held in place by a graphite block in the centre of a vacuum sintering furnace (Korea Furnace Development Co. LTD). The graphite crucible had a height of 4.5 cm. Prior to that, activated carbon powder (ACP) of mean particle size 149 μm was added into the crucible at a pre-determined amount (0 g, 0.5 g, 1.0 g and 1.5 g) as carbon source to produce SiC nanostructures. The product specifications of the activated carbon powder used is shown in Appendix A. The samples were designated as 0ACP, 0.5ACP, 1.0ACP and 1.5ACP according to the amount of ACP being used. The experimental setup is shown in Figure 3.3.

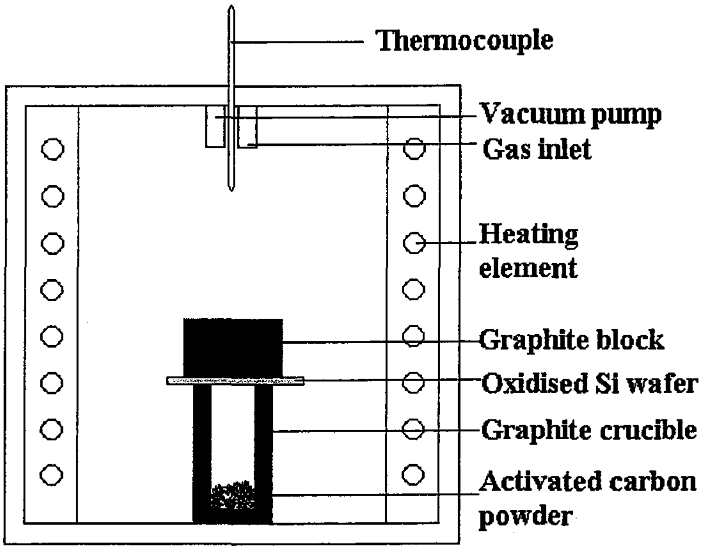

Figure 3.3: Experimental setup in the vacuum sintering furnace.

The furnace was then pre-evacuated to 10^{-3} mTorr using a mechanical pump and later the vacuum was released while Ar gas was introduced at a rate of 15 sccm. The furnace was then heated up at a rate of 15°C/min to 1300°C and maintained for different soaking times (1 hour and 2 hours). The parameters used in the experiment are shown in Table 3.2.

Table 3.2: Experimental parameters used in CVG on Si wafers.

Oxidation Time (min)	**1 Hour Soaking Time**				**2 Hour Soaking Time**			
	0ACP	**0.5ACP**	**1.0ACP**	**1.5ACP**	**0ACP**	**0.5ACP**	**1.0ACP**	**1.5ACP**
1		√						
2		√			√	√	√	√
8		√						
12		√						

Next, the sample was left to cool in furnace at a rate of 15 °C/min to room temperature before it was removed from furnace. The common heating profile used for all samples is shown below in Figure 3.4.

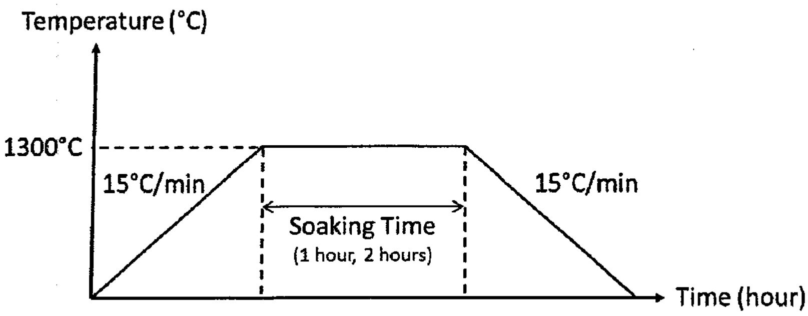

Figure 3.4: Heating profile in vacuum sintering furnace.

3.3 Characterization

The raw materials and the products were subjected to characterization by the following testing of a field-emission scanning electron microscope (FESEM, LEO GEMINI) equipped with an energy dispersive X-ray spectrometer (EDS, ZEISS SUPRA^{TM} 35VP), an energy-filtered transmission electron microscope (EFTEM, ZEISS LIBRA 120) equipped with an electron spectroscopic imaging (ESI), high-resolution transmission electron microscope (HRTEM, Philips Tecnai 20) and X-ray diffraction (XRD, Bruker D8). These characterization techniques will be described briefly in terms of their purposes, principles and sample preparation in the following sections.

3.4.1 Field-Emission Scanning Electron Microscope (FESEM)

Field-emission scanning electron microscopy (FESEM) was conducted using the model LEO GEMINI to observe the surface topography and the morphology of the nanostructures. The FESEM was also equipped with energy-dispersive X-ray spectrometer (EDS) with model of ZEISS SUPRA^{TM} 35VP to identify the elements present at the test location. This testing was based on the interactions of the electron beam with the sample surface. When high energy electrons were focused into a fine beam by electromagnetic lens and scanned the specimen surface in vacuum, the interactions between the energy beam and the specimen produced a variety of signals which include secondary electrons, back-scattered electrons, characteristics X-rays, cathodoluminescence and transmitted electrons that would be collected by the detectors. Secondary electron detectors were common detectors in SEM. The secondary electrons were a result of the interaction of electron beam and atoms at or near the surface, thereby creating high resolution images of the sample surface. Back-scattered electrons were also common in analytical SEM. Since the intensity of back-scattered electrons was strongly related to the atomic number of specimen, they could provide information on the distribution of elements in sample. Characteristic X-rays were emitted when the electron beam removed an inner shell electron from its orbital, causing a higher energy electron to fill the shell and released energy. These characteristic X-rays constituted EDS in identifying and measuring the mass fractions of the elements in the sample.

FESEM was performed on the Si wafers and the OP samples after pyrolysis. The Si wafer samples were placed on the sample holders and held in place by carbon tape. For the OP samples, the samples were dispersed onto the carbon tape stuck to the sample holders. The samples were then observed at several magnifications.

3.4.2 Energy-Filtered Transmission Electron Microscope (EFTEM)

Energy-filtered transmission electron microscopy (EFTEM) was conducted using model ZEISS LIBRA 120 to determine the morphology and crystallographic information. EFTEM was also equipped with electron spectroscopic imaging (ESI) to determine the compositional information of specimen. TEM was based on the principle of the interaction between the electron beam and the atoms in the sample. When a beam of high energy electrons was focused onto a thin specimen, most electrons would be transmitted through the sample, but some interacted with the sample and resulted in elastic and inelastic scattering. The electrons were collected and used to form an image on the detector. EFTEM was one of the techniques of TEM, in which only electrons of particular kinetic energies, filtered through adjustable slits, were used to form the image or diffraction pattern. The ability to control the electrons within certain kinetic energies prevented inelastic scattering from contributing to the image and hence produced enhanced contrast image. By comparing a few images of electrons that had lost a specific amount of energy, quantitative analysis could provide an elemental map that constituted ESI.

The TEM samples were prepared using ultrasonic method. The nanostructures from the Si wafers were scrapped from the surface and dispersed in absolute ethanol. As for the OP samples, the nanostructures after HF treatment were directly dispersed in absolute ethanol. The mixture then was sonicated to create suspensions. The suspensions were then dripped onto holey carbon films on Cu grids and left to air-dry.

3.4.3 High-Resolution Transmission Electron Microscope (HRTEM)

This test was performed using Philips Tecnai 20, 200kV using LaB_6 gun. High-resolution transmission electron microscopy (HRTEM) is an imaging mode of the transmission electron microscope (TEM) that allows the imaging of the crystallographic structure of a sample at an atomic scale. The working principle of HRTEM is similar to that of TEM. However, its high resolution makes it preferable in observing the nanoscale properties of crystalline materials. The HRTEM system is also equipped with Selected Area Electron Diffraction (SAED) and Energy dispersive X-ray spectroscopy (EDS), similar to that of attached to FESEM. SAED is a crystallographic experimental technique whereby the wave-like electrons are diffracted by the atoms. The diffraction is due to the slightly large spacing between the atoms in a solid and the electron beam causing the atoms to act as diffraction grating. Some of the electrons will be scattered to particular angles, determined by the crystal structure of the sample, while others pass through without deflection. As a result, the image on TEM screen consists of a series of spots where each spot corresponds to a satisfied diffraction condition of the sample's crystal structure.

The sample preparation method for HRTEM is the same as that of TEM. The sample was prepared using ultrasonic method. The nanowires were dispersed in ethanol after being scrapped off the surface and sonicated in ultrasonic bath for 30 minutes. A drop of the suspension was then dripped onto the carbon holey film on the Cu grid and left to dry in air before being placed in the sample holder for TEM investigation.

3.4.4 X-ray Diffraction (XRD)

X-ray diffraction (XRD) was performed using Bruker D8 model in determining the phase composition. XRD was based on measurement of the angles and intensities of the diffracted beams when a X-ray beam struck the sample and caused the beam to be diffracted into many specific directions that were characteristics of the phases present in a material.

The Si wafer were submitted for testing without further preparation but for the samples from pyrolysis of OP, the powder was ground and pressed into pellet form for testing.

CHAPTER 4

RESULTS AND DISCUSSION

4.1 Introduction

This chapter details the results obtained from different characterization techniques, which include optical microscope, scanning electron microscope (SEM), energy-dispersive X-ray spectroscopy (EDX) and transmission electron microscope (TEM). The results will be presented and discussed according to the synthesis methods and the parameters studied.

For the method of chemical vapour growth on Si substrate, results on the effects of growth temperature and soaking time under constant oxidation time of 24 min, oxidation time, soaking time and activated carbon powder amount will be presented and discussed. From the analysis, the growth mechanisms for the nanostructures formed will also be proposed.

4.2 Chemical Vapour Growth (CVG) on Si Substrates

4.2.1 Effect of growth temperature with constant soaking time

When the growth temperature was increased from 1100 to 1300 °C, nanowires only began to form at the temperature of 1200 °C. No nanowires were obtained at 1100 °C [Figure 4.1(a)] while aligned nanowires had been formed at 1200 °C [Figure 4.1(b)] at regions surrounded by activated carbon powder particles. As the temperature was further increased to 1300 °C, it could be observed that the nanowires increased in length [Figure 4.1(c)] but became randomly distributed. The lattice image of the nanowires obtained from high-resolution transmission-electron microscopy (HRTEM) at 1200 °C showed that the nanowires are amorphous [Figure 4.2(a)] which was confirmed by the selected area diffraction (SAED) image in the upper inset of Figure 4.2(a). The lower inset showed a TEM image of a single-layer nanowire. Based on energy dispersive x-ray (EDX) result of an individual nanowire, the nanowire consisted of Si (40.32 at%) and O (59.68 at%) elements only, with the Si:O ratio approximately 1:2.6, which is the typical value for all the nanowires. The nanowires formed by our method had higher oxygen content that those obtained in other reports (Hu et al., 2003, Liang et al., 2000b).

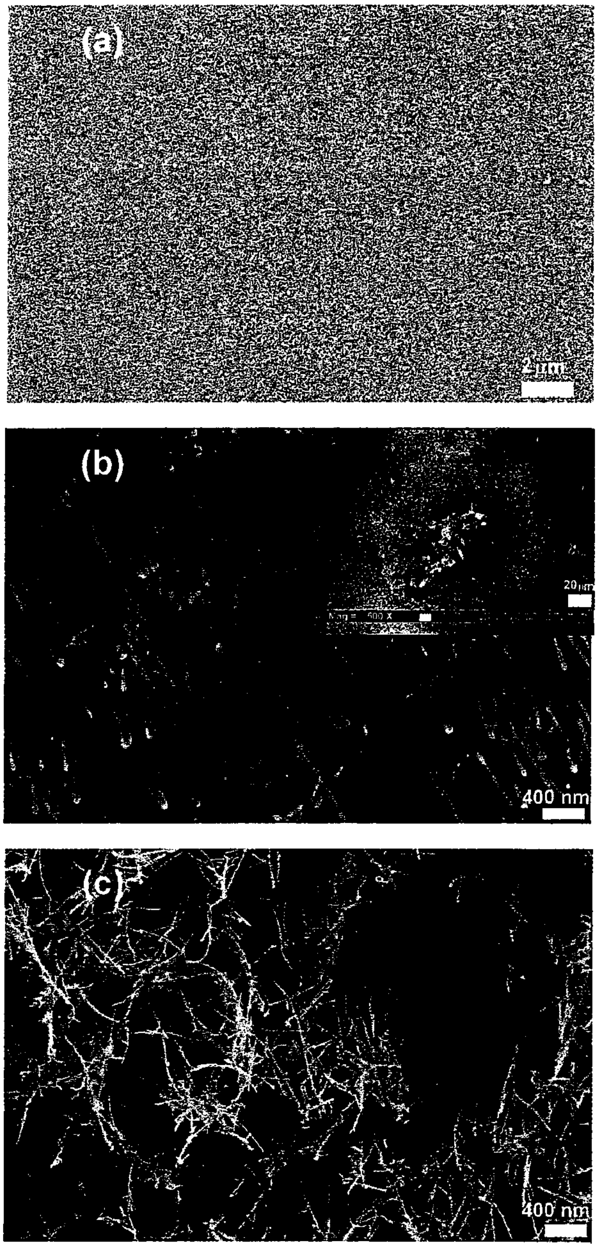

Figure 4.1: (a) A FESEM image showing that no nanowires were formed on the silicon wafer at a growth temperature of 1100 °C. (b) A FESEM image of the aligned SiO_z nanowires formed on silicon wafer at a growth temperature of 1200 °C. (Inset) A FESEM image of the nanowires formed surrounding the activated carbon powder particles on the wafer surface. (c) A FESEM image of nanowires with length up to several micrometers long on the wafer surface at a growth temperature of 1300 °C.

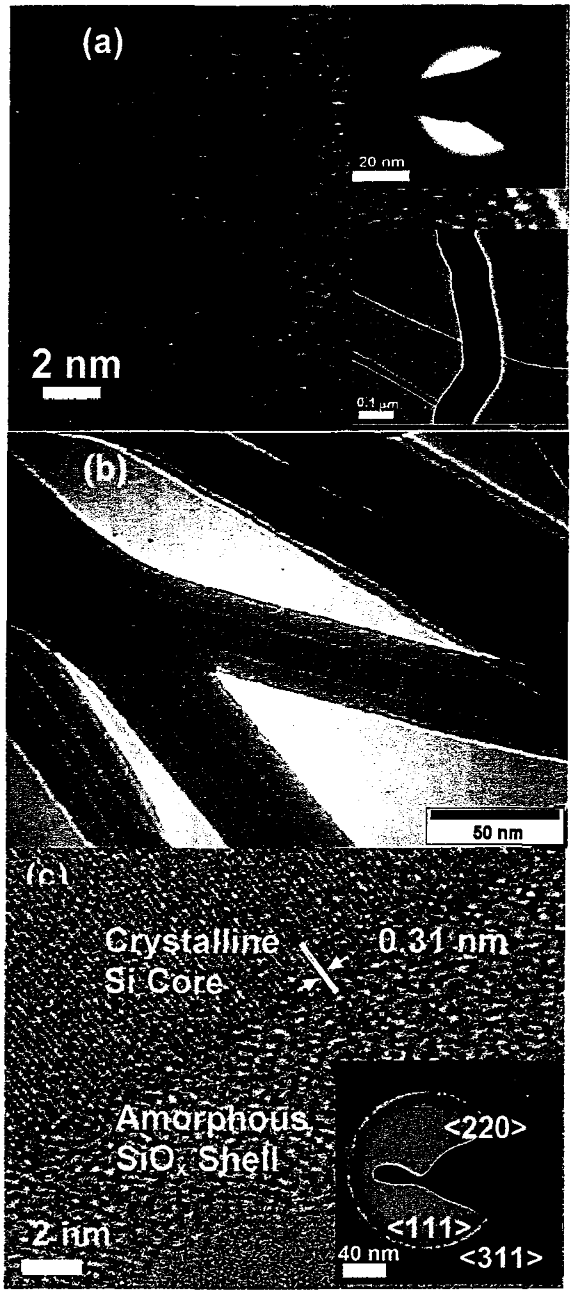

Figure 4.2: (a) A lattice image from HRTEM of the amorphous SiO$_x$ nanowires formed at 1200 °C. (Upper inset) SAED pattern of a SiO$_x$ nanowire showing amorphous nature. (Lower inset) A typical TEM image of the single-layer SiO$_x$ nanowires. (b) A typical TEM image of the Si/SiO$_x$ core-shell nanowires formed at 1300 °C. (c) A lattice image from HRTEM of a Si/SiO$_x$ core-shell nanowire. (Inset) SAED pattern of a Si/SiO$_x$ nanowire.

Nanowires formed at 1300 °C were core-shell structures [Figure 4.2(b)]. EDX results showed that Si and O were present in the ratio of 1.47:1. A higher amount of Si indicated that the core might be consisted of crystalline Si and the shell SiO_x. Atomic arrangements of Si/SiO_x nanowires had been inspected by HRTEM [Figure 4.2(c)]. The results clearly showed that core of the nanowires had (111) atomic planes with a separation of 0.31 nm perpendicular to the nanowire axis and an atomically sharp interface with the amorphous shell. Based on SAED pattern [inset of Figure 4.1(c)], it indicated that the core of nanowires were polycrystalline and the lattice planes existing in the core were found to be (111), (220) and (311) planes.

4.2.2 Effect of soaking time with constant growth temperature

When the soaking time in the vacuum sintering furnace was increased from 1 h to 2 h and finally to 4 h, while maintaining the soaking temperature at 1300 °C, Si/SiO_x core-shell nanowires were formed on the wafer surface as wool-like nano-materials in increasing amount and length (Figure 4.3). It could also be observed that as the soaking time increased to 4 hours, node-like cores began to form as indicated by the red circles in Figure 4.3(c).

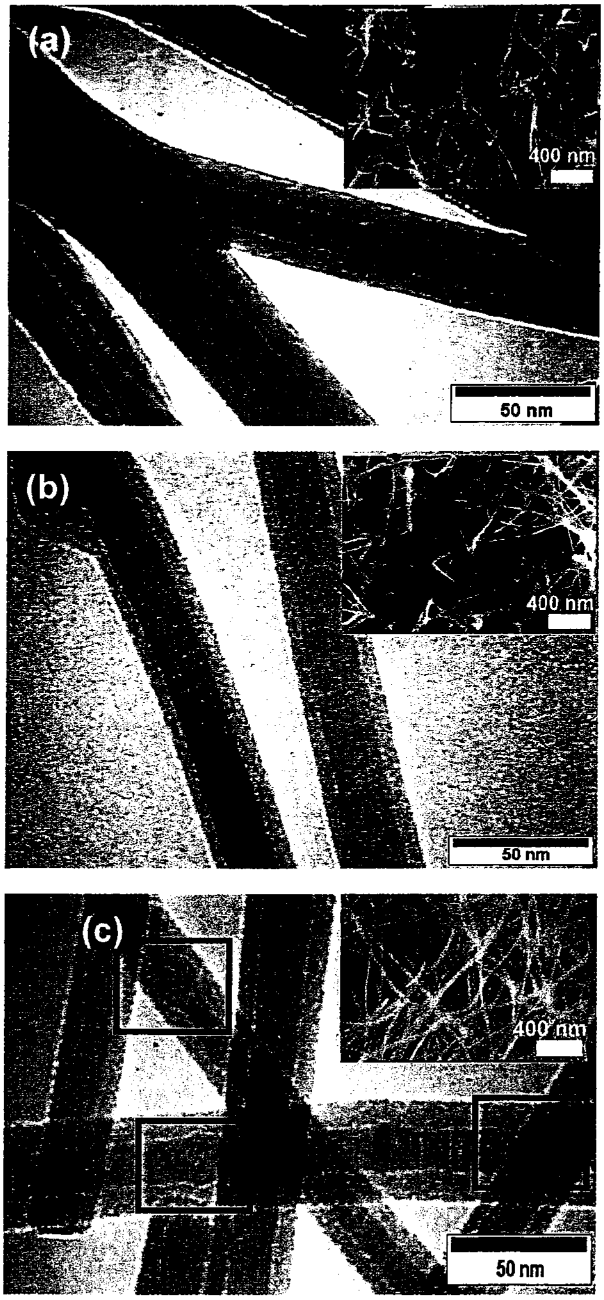

Figure 4.3: TEM images of the core-shell nanowires formed at growth temperature of 1300 °C for soaking time of (a) 1 h, (b) 2 h and (c) 4 h. Inset showing the SEM images of the nanowires at the respective soaking time.

The diameters of these nanowires fluctuated along the length of the nanowires, causing some areas to have larger diameters that led to the formation of the node-like structure. The thickness of crystalline core and diameter of the nanowire inclusive of the core and shell were measured. The values were then plotted and linearly regressed as shown in Figure 4.4, with the r^2 values for the three different soaking times (1 h, 2 h and 4 h) between 0.52 and 0.66. Although the r^2 values did not reached unity, it could be suggested that the diameters of nanowires and cores had slightly linear relationships and thus it could also be suggested that both the Si core and SiO_x shell grew from the same mechanism through the disproportionation reaction of SiO (Chen and Ruoff, 2007). In addition, the plots revealed that both diameters of the core and the nanowire only increased slightly when the soaking time was prolonged. This is because lateral growth of the nanowires had been limited by the oxide shell surrounding the nanowires. The diameters of nanowires ranged from 20 to 40 nm with the core diameter between 5 to 20 nm, which was smaller than the reported diameter (Gundiah et al., 2003).

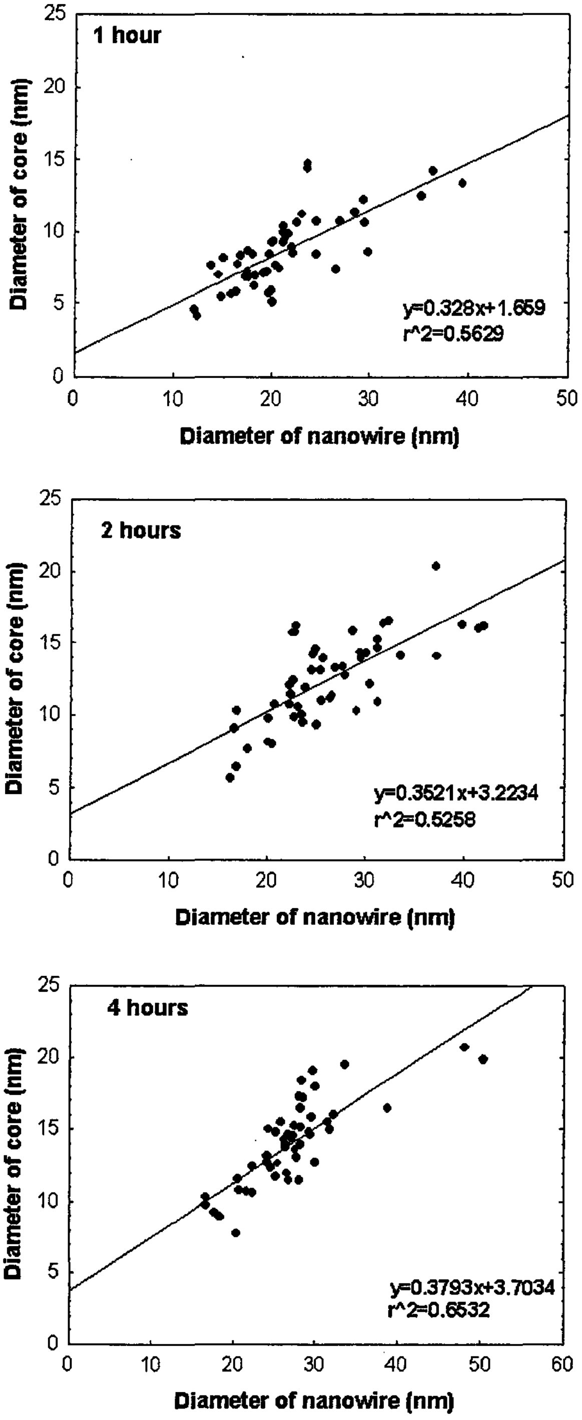

Figure 4.4: Correlation of the diameter of core to the diameter of the nanowire (inclusive of the core and shell) at growth temperature of 1300 °C at different soaking times of 1 h, 2 h and 4 h.

4.2.3 Effect of Oxidation Time

Different oxidation times had been used to investigate the effect of oxidation time on the growth of nanostructures. The oxidation time was varied from 1 min, 2 min, 8 min and 12 min during the thermal oxidation process at 1000°C. The oxidized substrate were then heated in vacuum sintering furnace at 1300°C for 1 hour while exposed to 0.5 g activated carbon powder. The results obtained are presented as follow.

Two different types of nanostructures, namely nanorods and nanocolumns, were observed on the silicon wafer at different regions regardless of the change in the oxidation time (or SiO_2 thickness), as shown in the FESEM images for different oxidation times in Figure 4.5 at the centre and at the sides of the wafer. Nanostructures at both regions were identified to consist of mainly Si and C that existed in almost equal ratio with some small amounts of O and Fe using EDS, as shown in Figure 4.6 and 4.7 for the nanostructures at the centre and at the side, respectively. At the centre of the silicon wafer that was exposed to activated carbon powder in the crucible, nanorods or nanoneedles with diameters ranging from 60 to 90 nm and average length of 200 nm could be observed. Whereas at the side of the wafer, which was in contact with the graphite crucible, nanocolumns in polygonal shapes with diameters ranging from 200 nm to 450 nm could be observed. An EFTEM image of the nanostructures formed is shown in Figure 4.8, showing a rod-like shape.

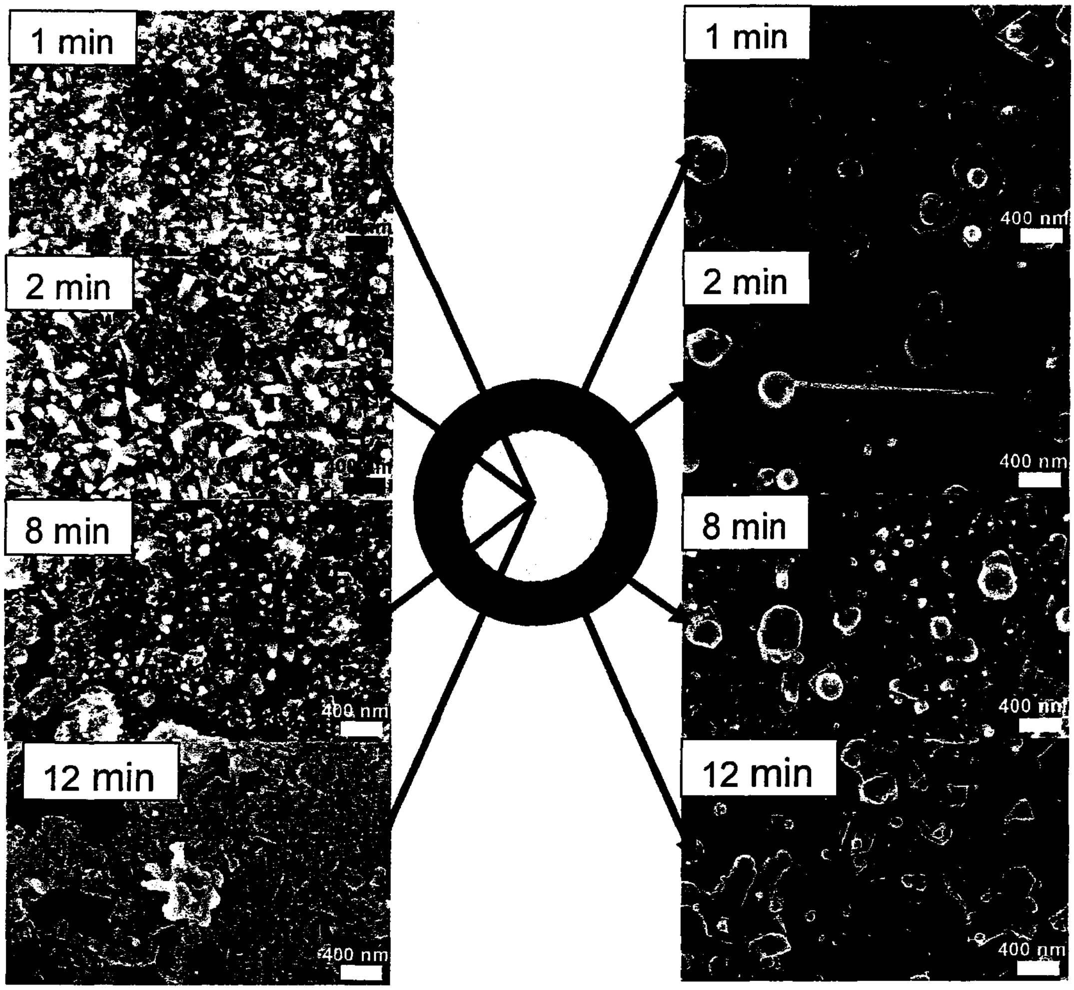

Figure 4.5: FESEM images of the nanorods and nanocolumns formed at the centre and the sides of silicon substrate when heated at 1300°C for 1 hour under different oxidation time of 1 min, 2 min, 8 min and 12 min.

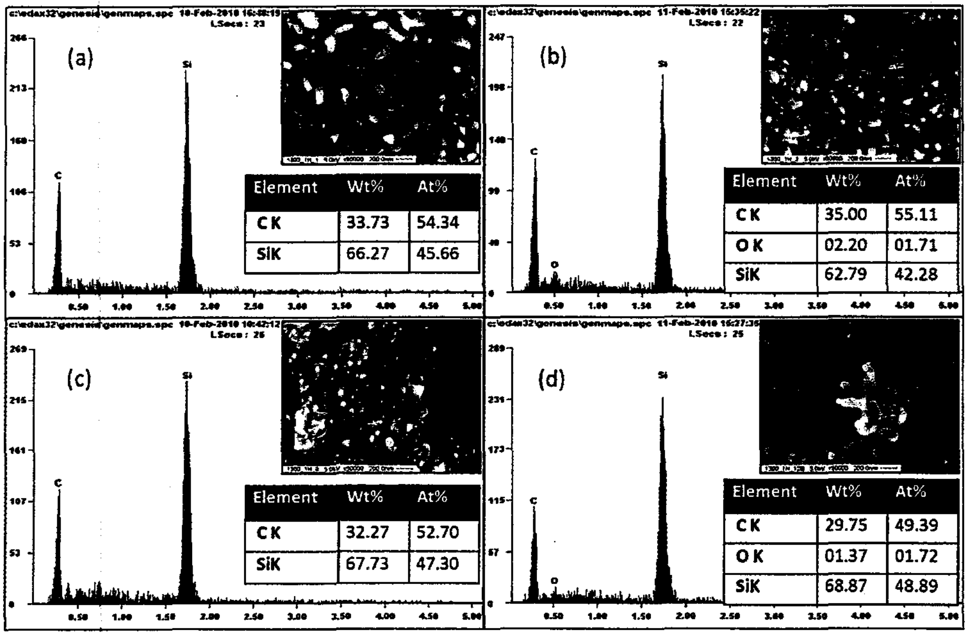

Element	Wt%	At%
C K	33.73	54.34
SiK	66.27	45.66

Element	Wt%	At%
C K	35.00	55.11
O K	02.20	01.71
SiK	62.79	42.28

Element	Wt%	At%
C K	32.27	52.70
SiK	67.73	47.30

Element	Wt%	At%
C K	29.75	49.39
O K	01.37	01.72
SiK	68.87	48.89

Figure 4.6: EDS results of the nanorods at the centre of silicon wafer under different oxidation times of (a) 1 min, (b) 2 min, (c) 8 min and (d) 12 min.

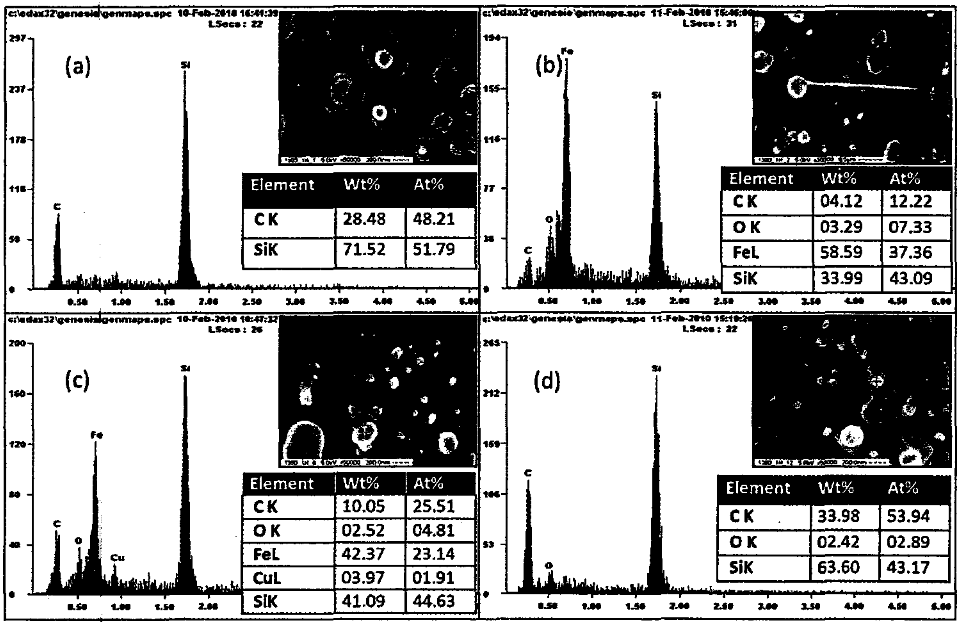

Element	Wt%	At%
C K	28.48	48.21
SiK	71.52	51.79

Element	Wt%	At%
C K	04.12	12.22
O K	03.29	07.33
FeL	58.59	37.36
SiK	33.99	43.09

Element	Wt%	At%
C K	10.05	25.51
O K	02.52	04.81
FeL	42.37	23.14
CuL	03.97	01.91
SiK	41.09	44.63

Element	Wt%	At%
C K	33.98	53.94
O K	02.42	02.89
SiK	63.60	43.17

Figure 4.7: EDS results of the nanorods at the side of silicon wafer under different oxidation times of (a) 1 min, (b) 2 min, (c) 8 min and (d) 12 min.

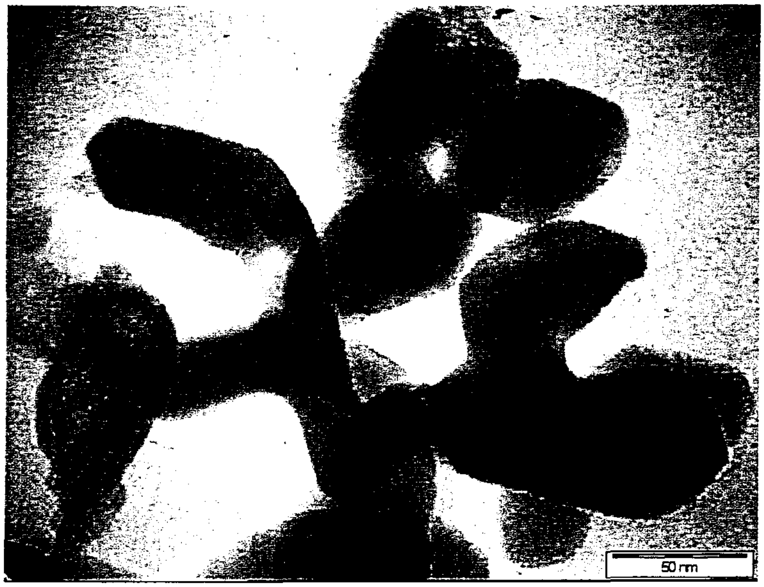

Figure 4.8: An EFTEM image of the nanostructures formed on a silicon wafer at the oxidation time of 2 min.

From the FESEM images at the centre of silicon wafer, it could be noticed that the nanorods or nanoneedles increased in diameter but reduced in amount while at the sides of the wafer, both the diameters and the amount of nanocolumns decreased as the oxidation time increased. When the oxidation time was increased, the SiO_2 layer became thicker and contributed to more SiO and O_2 species being released when heated. The higher partial pressure of SiO species increased the reaction rate for SiC formation, leading to more SiC being deposited onto Si wafer. Therefore, significantly higher amount of nanorods and nanocolumns could be observed as oxidation time was increased. However, when the oxidation time was increased to 8 min and 12 min, the nanocolumns started to agglomerate, forming SiC clusters again and SiC nanorods with smaller diameter could be observed on the clusters. This observation concurred with reports by others detailing that a thin layer of SiO would promote the growth of Si-based nanostructures (Jeong et al., 2008, Park et al., 2007) but if it was too thick, it would inhibit the growth of nanostructures instead (Park et al., 2007).

To summarise, short oxidation times of 1 min and 2 min were preferable for the growth of SiC nanorods and nanocolumns. When the oxidation time was prolonged to 8 min and 12 min, the nanorods started to agglomerate and formed SiC clusters. Furthermore, the sample thermally oxidized for 2 min showed the onset of the nanowire growth. Thus, oxidation time of 2 min would be used for subsequent studies.

4.2.4 Effect of Soaking Time in Vacuum Sintering Furnace

Different soaking time in the vacuum sintering furnace was investigated on their effects on the growth of nanostructures. The Si substrate was first thermally oxidized for 2 min. The oxidized Si substrate was then heated at 1300°C while exposed to 0.5 g of activated carbon powder. Two soaking times (1 hour and 2 hours) were studied. The results reporting the effects of soaking time are shown as follow.

When the soaking time was increased from 1 hour to 2hours, there was a transition of nanostructures, as shown in Figure 4.9. At the centre of Si substrate, SiC nanorods were observed under the soaking time of 1 hour, as discussed in previous section. However, when the soaking time was increased to 2 hours, no nanorods were found. Only grains consisting of higher amount of Si and C as well as a small amount of O were detected using EDS (Figure 4.10). The higher content of Si and C suggested that the grains might have consisted of SiC and the O originated from the oxide layer. The morphological change from nanorods to grains might have been a result of coagulative recrystallization of nanorods due to higher reaction rate with increasing soaking time.

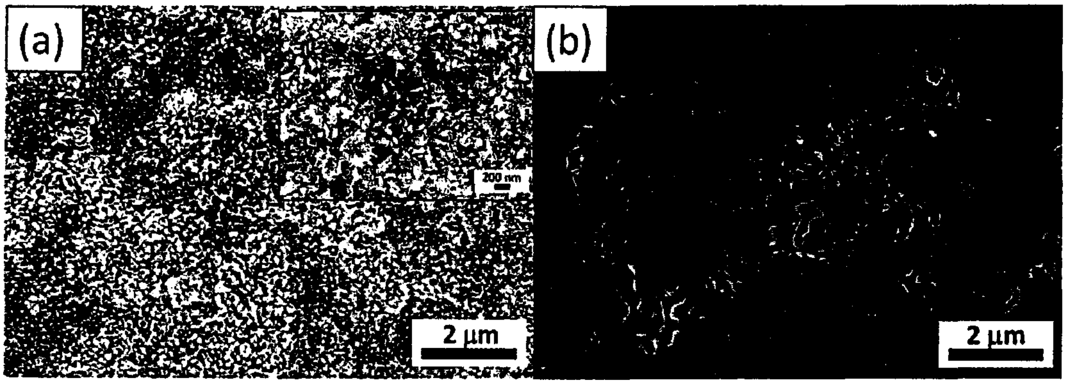

Figure 4.9: FESEM micrographs of nanostructures formed at the centre of Si substrate under different soaking time of (a) 1 hour (Inset showing higher magnification micrograph of the nanostructures) and (b) 2 hours.

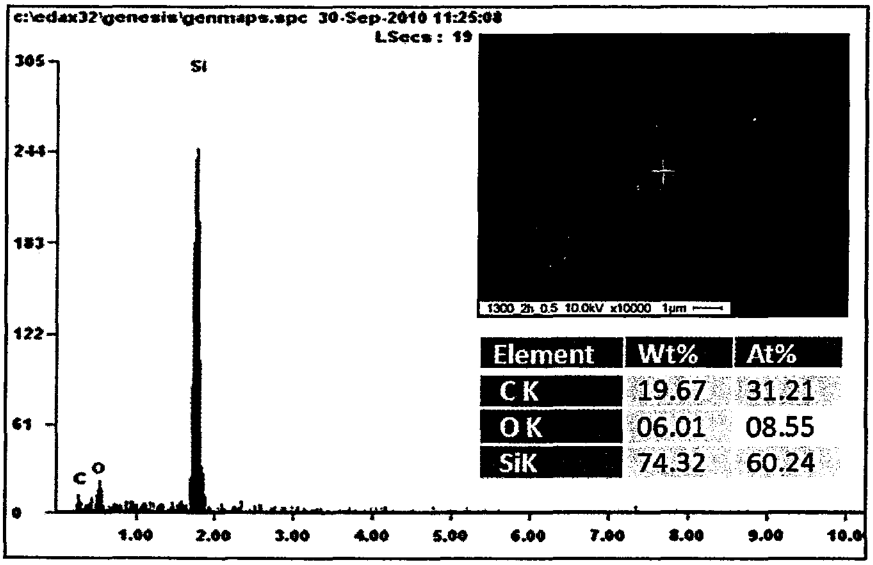

Element	Wt%	At%
C K	19.67	31.21
O K	06.01	08.55
SiK	74.32	60.24

Figure 4.10: EDS results of the grains formed at the centre of Si substrate under a soaking time of 2 hours.

At the side of the Si substrate, only SiC nanocolumns were observed under a soaking time of 1 hour, as discussed in previous section, while two different nanostructures which include nanowebs and randomly oriented nanowires were observed when the soaking time was increased to 2 hours. Nanowebs consisted of several intersecting nanowires that bonded together, forming a web-like structure. These nanostructures are shown in Figure 4.11.

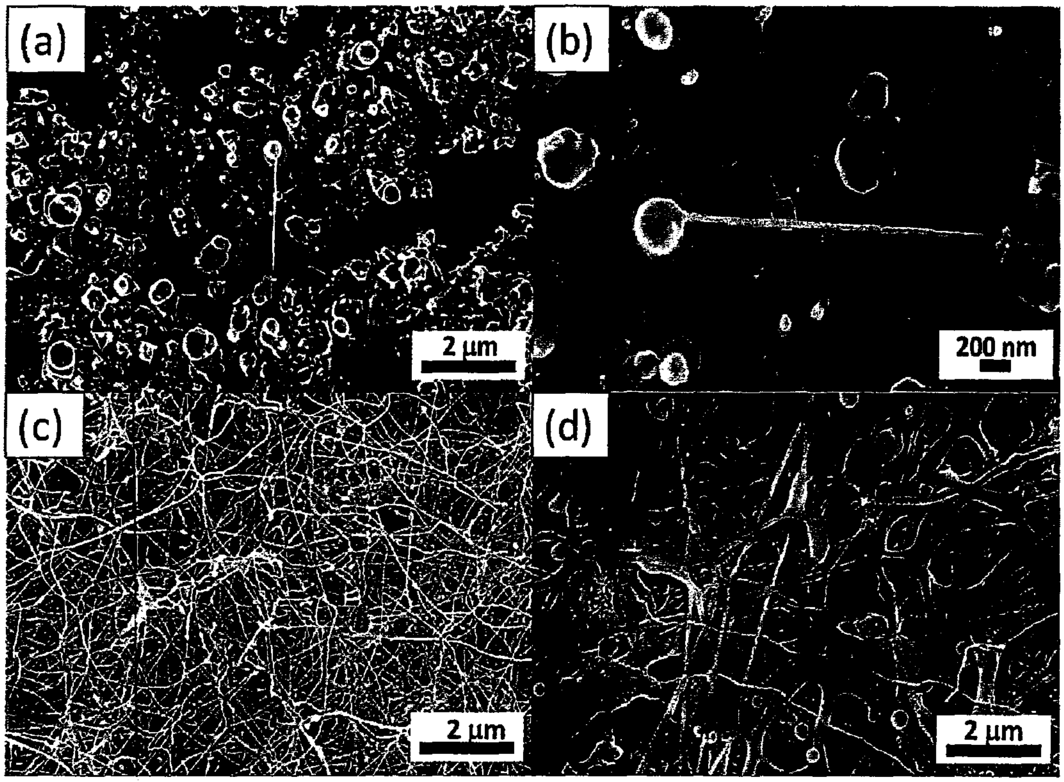

Figure 4.11: (a) and (b) shows the FESEM micrographs of nanocolumns formed at the side of Si substrate under a soaking time of 1 hour while (c) and (d) shows the FESEM micrographs of nanowires and nanowebs formed at the side of substrate under a soaking time of 2 hours.

Figure 4.12 shows the EFTEM images of the nanostructures formed under different soaking times. The nanostructures formed under 1 hour soaking time were only observed with a single layer, suggesting that no oxide layer was formed around the SiC nanorods or nanocolumns. Whereas the nanowires formed under 2 hours soaking time consisted of a core-shell structure. ESI results in Figure 4.13 show a higher concentration of Si and C at the core and a higher concentration of O at the shell, suggesting that the nanowires might be SiC/SiO_2 core-shell nanowires.

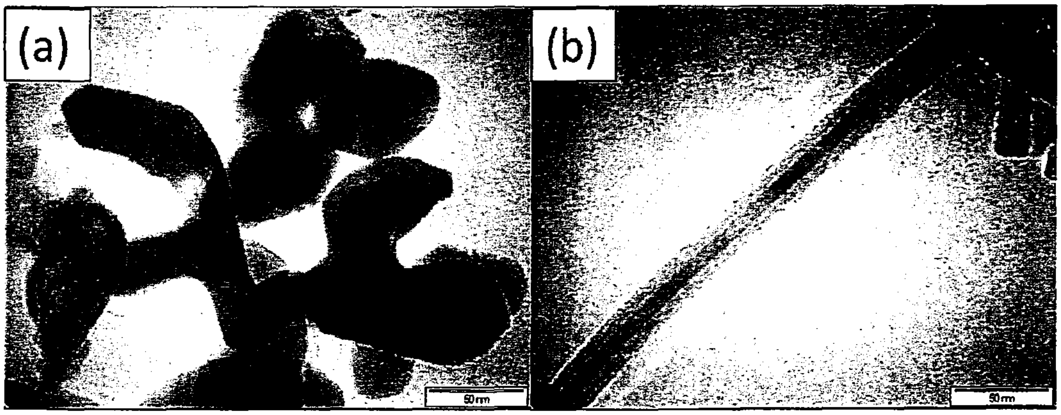

Figure 4.12: EFTEM images of (a) nanorods or nanocolumns formed under soaking time of 1 hour and (b) core-shell nanowires formed under soaking time of 2 hours.

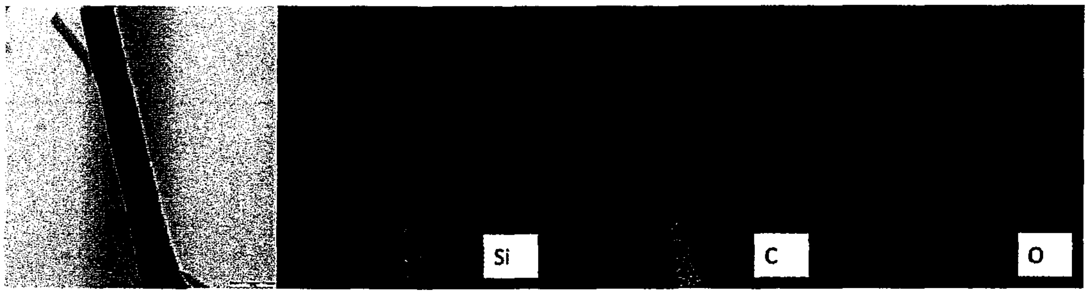

Figure 4.13: ESI results showing composition of nanowires formed under soaking time of 2 hours.

The change of structure from nanocolumns to nanowires when the soaking time was increased might have been a result of the longer reaction time available for reactions to take place. As could be observed frim FESEM images, short nanowires were already observed under soaking time of 1 hour. When the soaking time was increased, more nanowires were nucleated and grew in length, thus forming bundles of nanowires. Since the nanowires were randomly oriented, the chances of the nanowires intersecting one another were high and this led to formation of nanowebs. The detailed growth mechanisms of these nanostructures will be discussed in the section on growth mechanism.

From this study, it could be concluded that a longer soaking time of 2 hours was preferential for the formation of nanowires. Thus, in the following study, a soaking time of 2 hours was used when investigating the effect of activated carbon powder amount.

4.2.5 Effect of Activated Carbon Powder Amount

Different activated carbon powder (ACP) amounts were used to investigate their effects on the growth of nanostructures. The Si substrate was first thermally oxidized for 2 min. Then, the growth of nanostructures proceeded in vacuum sintering furnace by heating at 1300°C for 2 hours with the carbon amount used varied from 0 g, 0.5 g, 1.0 g and 1.5 g. Designation of 0ACP, 0.5ACP, 1.0ACP and 1.5ACP based on the amount of ACP will be used in the figures to differentiate the samples. The results obtained are presented as follow.

Various types of nanostructures were found on the surface of Si substrates, depending on its location, either at the centre, boundary or the side of the substrate (Figure 4.14). The centre is the region where the substrate is exposed directly to activated carbon powder; the boundary is the region in contact with the graphite crucible; and the side is the region outside of the crucible. A summary of the different nanostructures formed depending on the location and amount of ACP is shown in Table 4.1.

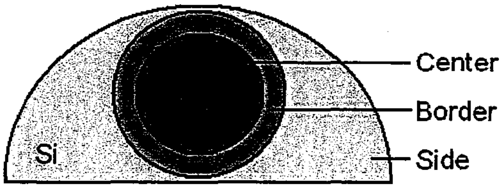

Figure 4.14: Location of nanostructures formed on the SiO_2/Si wafer.

Table 4.3: Summary of nanostructures formed on Si wafer depending on the amount of ACP and the location on Si wafer.

Sample	**Location on Si Wafer**		
	Centre	**Border**	**Side**
0ACP	Si or Si/SiO_x nanowires	SiC/SiO_2 nanowires	Randomly oriented SiC/SiO_2 nanowires
0.5ACP	SiC/SiO_2 nanograins	SiC/SiO_2 nanowebs	Randomly oriented SiC/SiO_2 nanowires
1.0ACP	SiC/SiO_2 nanograins	SiC/SiO_2 nanowebs	Randomly oriented SiC/SiO_2 nanowires
1.5ACP	SiC/SiO_2 nanograins	SiC/SiO_2 nanowebs	SiC/SiO_2 nanowire clusters

At the centre, the surface appeared etched and filled with voids in various shapes with particles found growing in the voids when ACP was added (Figure 4.15). EDS showed that these voids consisted of Si, C and O, with higher amount of Si and C [Figure 4.16(a)] as compared to the surrounding surface which consisted of only Si and O with lower content of C [Figure 4.16(b)]. This indicated that the voids might be grown with SiC nanograins. When no ACP was added, short nanowires consisting of Si only based on EDS results were detected. This suggested that the nanowires might be SiO_x nanowires, which were commonly grown by heating mixture of Si and SiO_2 at temperatures above 1100°C through oxide-assisted growth mechanism (Zhang et al., 2000b, Pan et al., 2001a, Shi et al., 2000a, Zhang et al., 2003).

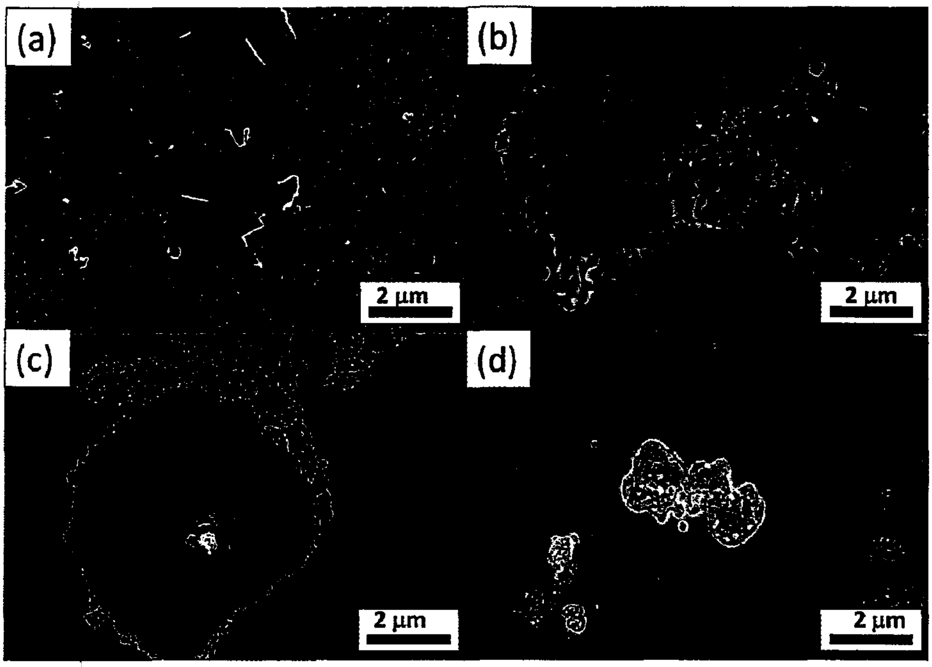

Figure 4.15: FESEM images of nanostructures formed at the centre under different ACP amount of (a) 0 g, (b) 0.5 g, (c) 1.0 g and (d) 1.5 g.

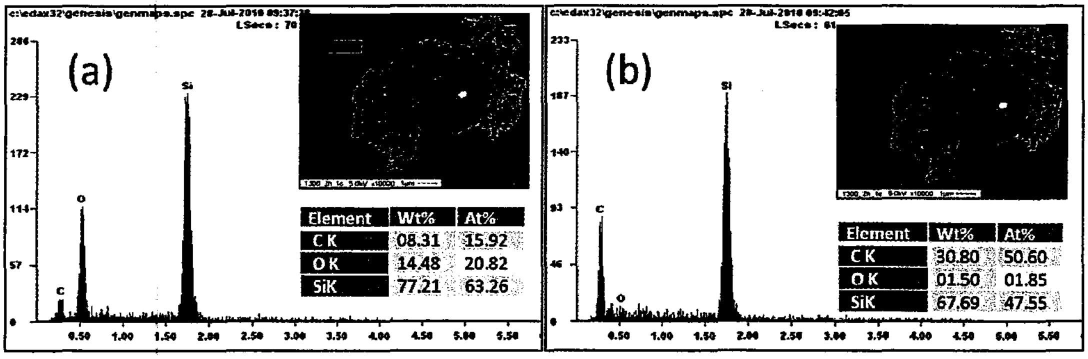

(a)

Element	Wt%	At%
C K	08.31	15.92
O K	14.48	20.82
SiK	77.21	63.26

(b)

Element	Wt%	At%
C K	30.80	50.60
O K	01.50	01.85
SiK	67.69	47.55

Figure 4.16: EDS results of the (a) unetched Si substrate surface and (b) voids formed on Si substrate at the centre.

At the border, the nanostructures changed from randomly oriented nanowires to nanowebs consisting of intersecting nanowires with the presence of small amount of nanoparticles on the surface of Si substrate when ACP was added (Figure 4.17). The randomly oriented nanowires in 0ACP showed significantly smaller diameters as compared to the nanowebs. It could also be noticed that the diameters of these nanowebs increased when the ACP amount was increased from 0.5 g to 1.0 g, with signs of surface roughening of the nanowires, but then the diameter was found to reduce when ACP was further increased to 1.5 g. EDS of these nanowires showed the presence Si and O with some showing the presence of C as well (Figure 4.18). In addition, thin nanowires were observed growing from the nanoparticles, proposing that these nanoparticles acting as nuclei for the growth of the nanowires.

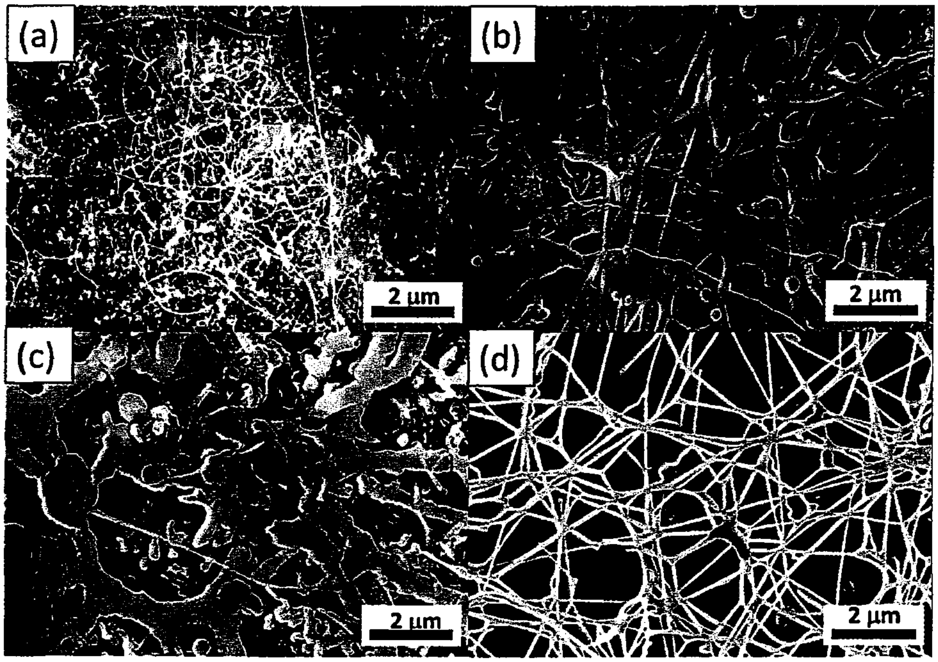

Figure 4.17: FESEM images of nanostructures formed at the border under different ACP amount of (a) 0 g, (b) 0.5 g, (c) 1.0 g and (d) 1.5 g.

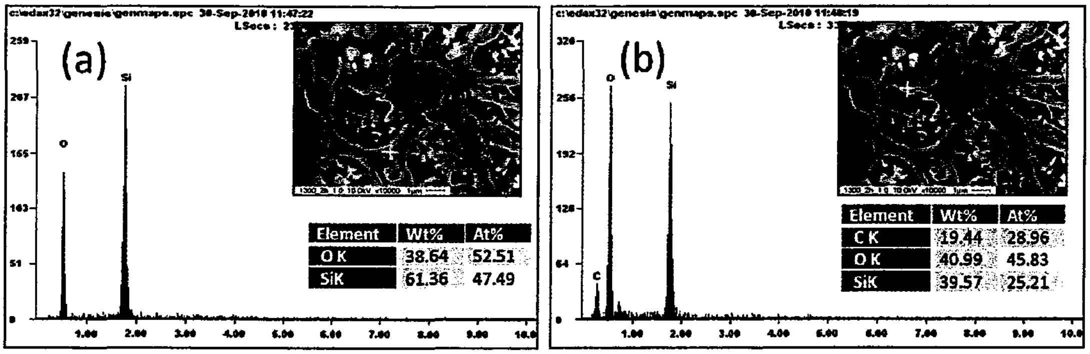

Element	Wt%	At%
O K	38.64	52.51
SiK	61.36	47.49

Element	Wt%	At%
C K	19.44	28.96
O K	40.99	45.83
SiK	39.57	25.21

Figure 4.18: EDS results of the nanowebs at the borders at two different locations showing (a) only Si and O and (b) Si, O and C.

The EFTEM images of the nanowires formed at the border under different ACP amount are shown in Figure 4.19. From the EFTEM images, the nanowebs consisted of core-shell structures, most with a single core and some could be observed with several thin cores located inside the nanowires. The nanowires had diameters ranging from 15 to 70 nm with the cores having diameters of 4 to 15 nm. Similar nanostructure had been reported by Shim et al. (Shim, 2008, Shim and Huang, 2007). The nanostructure with several thin cores within the shell was named nanocable due to their resemblance to power transmission cables. The core-shell nanowires were observed with decreasing diameter of the core when ACP amount increased. Amorphous nanowires were also found growing as branches from the core-shell nanowires [Figure 4.19(d)].

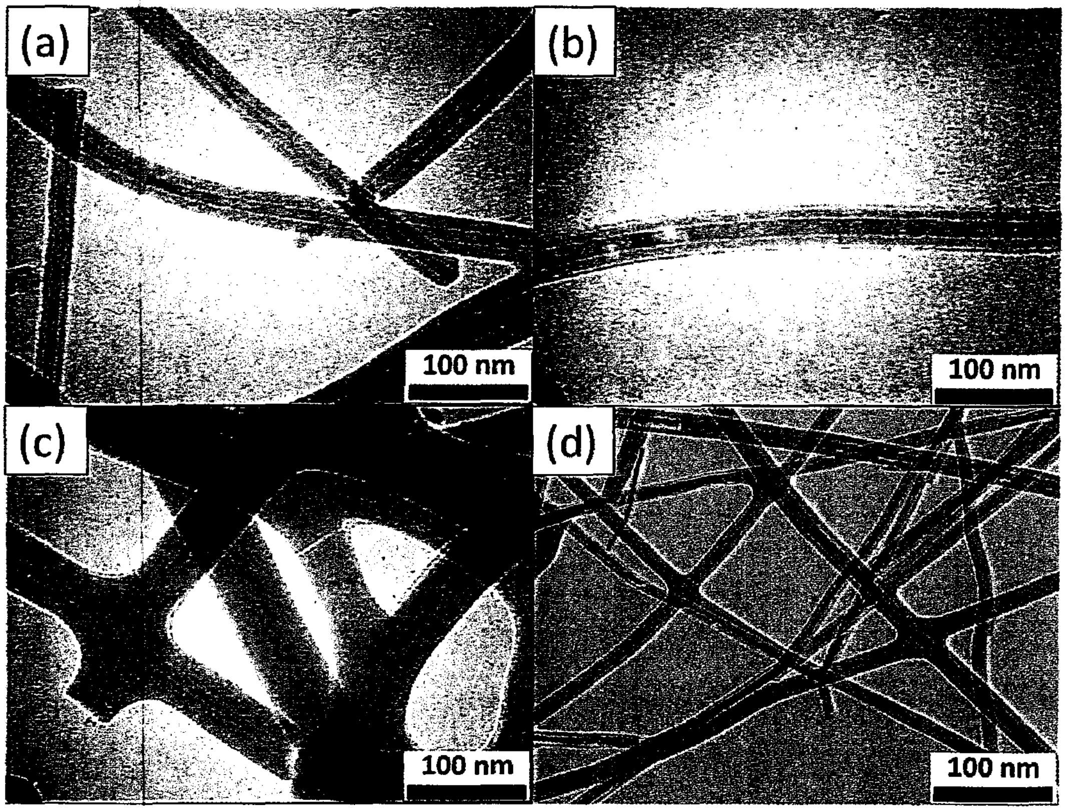

Figure 4.19: EFTEM images of nanostructures formed at the border under different ACP amount of (a) 0 g, (b) 0.5 g, (c) 1.0 g and (d) 1.5 g.

At the side, randomly oriented nanowires were observed in the samples exposed to 0 g, 0.5 g and 1.0g of ACP while thick nanowire clusters were observed in the sample exposed to 1.5 g ACP, as shown in Figure 4.20. The randomly oriented nanowires consisted of Si, C and O [Figure 4.21(a) and (b)] while the thick nanowires in the sample exposed to 1.5 g ACP were found growing from single origin [inset of Figure 4.20(d)] and they were consisted of Si and O based on EDS [Figure 4.21(c) and(d)].

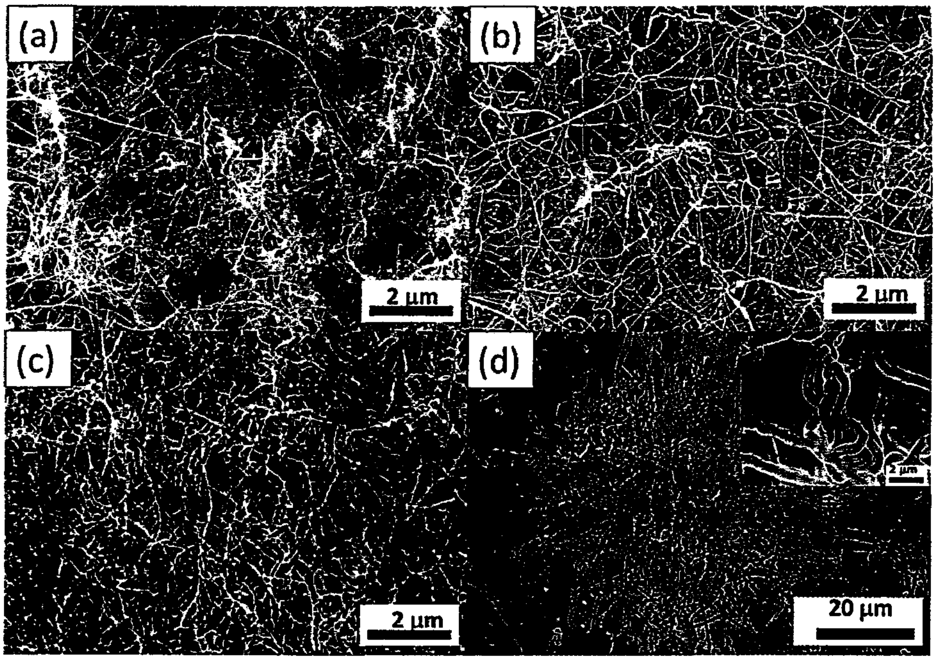

Figure 4.20: FESEM images of nanostructures formed at the side under different ACP amount of (a) 0 g, (b) 0.5 g, (c) 1.0 g and (d) 1.5 g (Inset showing higher magnification of the nanowire cluster formed in 1.5ACP).

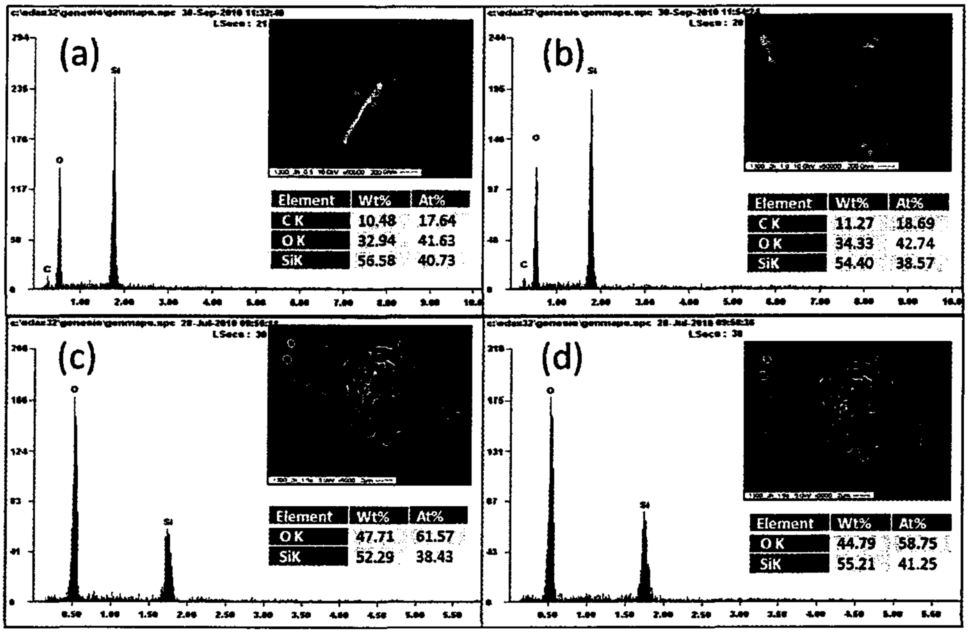

(a)

Element	Wt%	At%
C K	10.48	17.64
O K	32.94	41.63
SiK	56.58	40.73

(b)

Element	Wt%	At%
C K	11.27	18.69
O K	34.33	42.74
SiK	54.40	38.57

(c)

Element	Wt%	At%
O K	47.71	61.57
SiK	52.29	38.43

(d)

Element	Wt%	At%
O K	44.79	58.75
SiK	55.21	41.25

Figure 4.21: EDS results of (a) and (b) randomly oriented nanowires when exposed to 0 g, 0.5 g and 1.0 g ACP as well as (c) and (d) the nanowire clusters formed when exposed to 1.5 g ACP at the sides of Si substrate.

The EFTEM images of the samples are shown in Figure 4.22. From the EFTEM images, amorphous nanowires and core-shell nanowires were observed as well. However, the diameters of the nanowires were smaller (20 – 50 nm) but with thicker cores (7 -20 nm). Branching of the thick crystalline core was also observed [Figure 4.22(c)]. In addition, some of the crystalline cores could be observed with planar defects of stacking faults, as circled in Figure 4.22(d). Stacking faults are common in SiC nanowires due to lower energy contribution during the growth of nanowires (Cai et al., 2008, Shim and Huang, 2007, Zhang et al., 2009a).

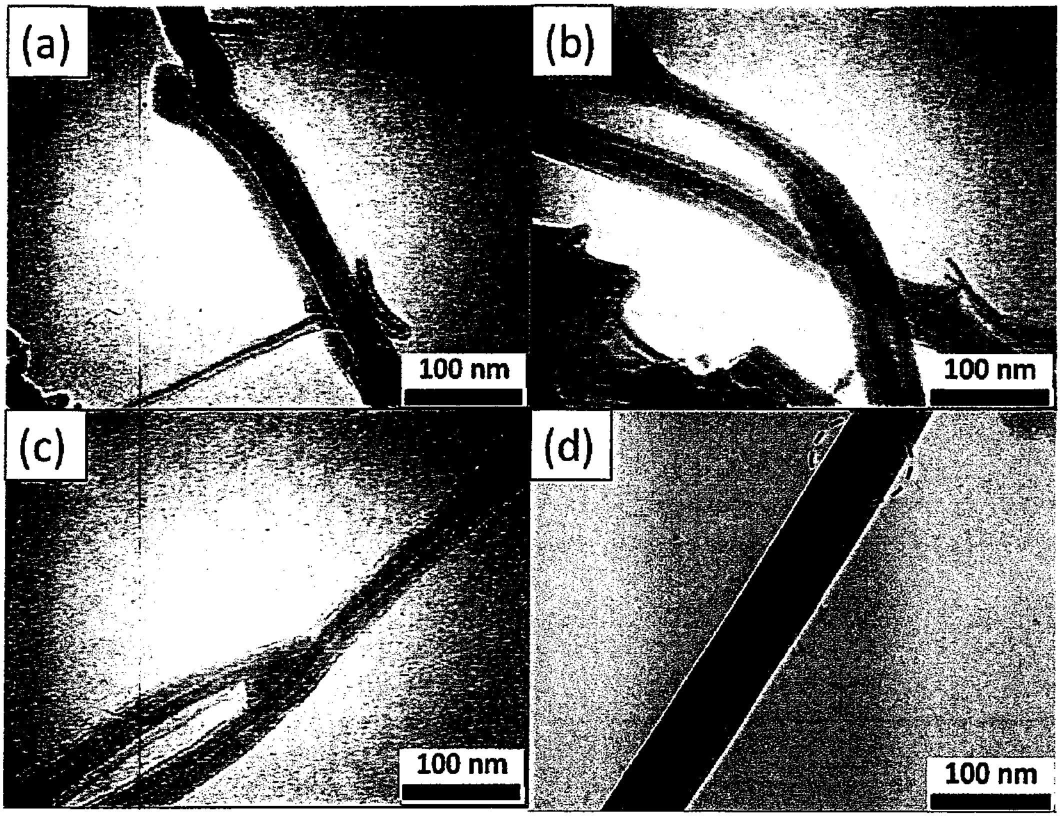

Figure 4.22: EFTEM images of nanostructures formed at the side under different ACP amount of (a) 0 g, (b) 0.5 g, (c) 1.0 g and (d) 1.5 g (Circled shows the presence of stacking faults).

To determine the composition of the core-shell nanowires, ESI and XRD were performed. XRD was performed on the whole Si wafer surface covering the three regions. ESI results showed a higher concentration of Si and C at the core and a higher concentration of O at the shell for both nanostructures at the border and at the side [Figure 4.23(a) and (b)]. XRD spectra of the entire Si wafer surface exposed to different ACP amount are shown in Figure 4.23(c). The XRD patterns showed only diffraction peaks of Moissanite 3H-SiC (ICDD 01-073-1708) as well as SiO_2 in the form of quartz (ICDD 01-086-1562) and cristobalite (ICDD 00-039-1425). The detection of SiC peaks even when no ACP was added indicated that the graphite crucible might have acted as a secondary carbon source for SiC formation aside from

ACP. The high SiO_2 peaks might originate from the SiO_2 thin film on the pre-oxidized Si wafer. Although thermally grown SiO_2 was amorphous in nature, devitrification of SiO_2 into a mixture of cristobalite and quartz had been reported to be possible when heated at temperatures above 1200°C, especially in the presence of hydroxyl (OH) radicals that were bound to the surface of SiO_2 (Zaplatynsky, 1972). From the results above, it could be concluded that the cores were SiC and the amorphous shells were SiO_2.

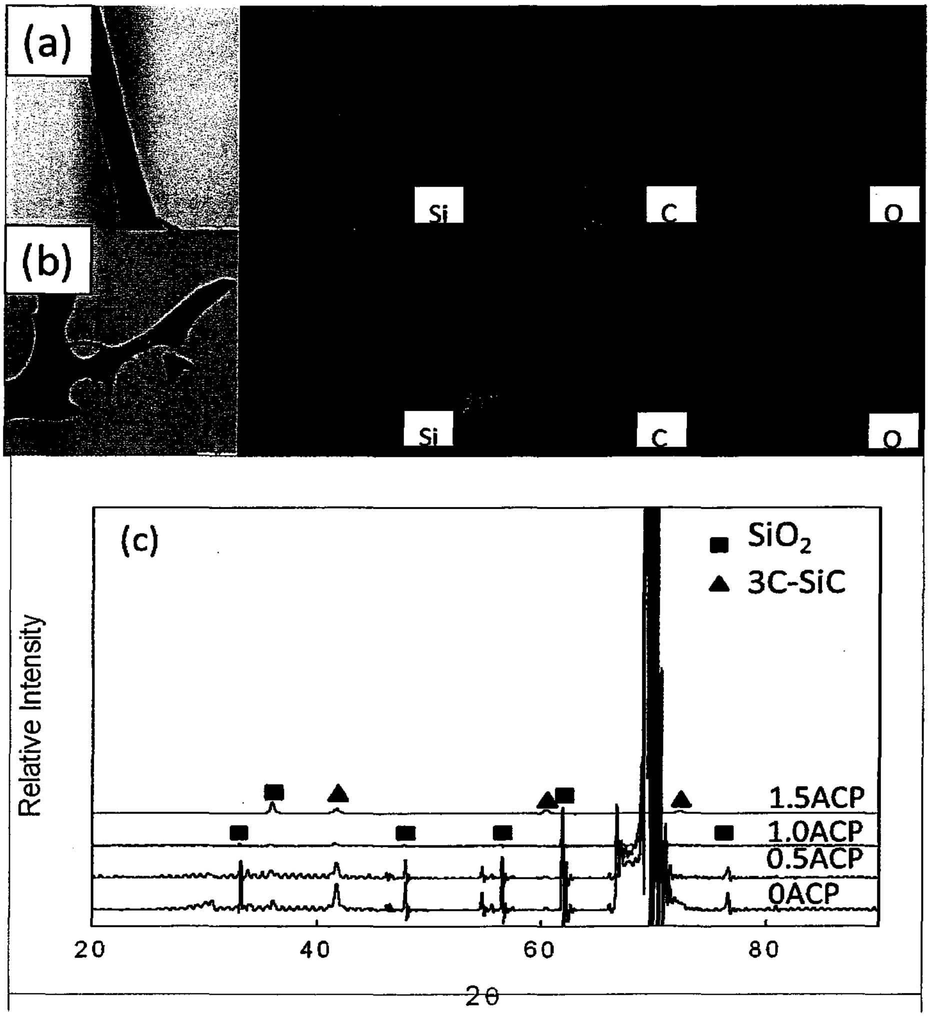

Figure 4.23: (a) ESI results of the core-shell nanowires at the side of wafer, (b) ESI results of the nanowebs at the border and (c) XRD spectrum of the samples.

4.2.6 Growth Mechanism

4.2.6.1 SiO_x and Si/SiO_x Core-shell Nanowires

Based on the results obtained, formation of SiO_x and Si/SiO_x core-shell nanowires in the presence of carbon could be explained using carbon-assisted growth via vapor-solid mechanism (Park and Yong, 2004, Gundiah et al., 2003). In this proposed growth mechanism for our study, CO gases played an important role in the growth of SiO_x nanowires and Si/SiO_x core-shell nanowires. The proposed reactions that might have taken place are as follow:

$$2C(s) + O_2(g) \rightarrow 2CO(g) \tag{4.1}$$

$$CO(g) + SiO_2(s) \rightarrow SiO(g) + CO_2(g) \tag{4.2}$$

$$SiO(g) + O_2(g) \rightarrow SiO_x(s), x > 1 \tag{4.3}$$

$$SiO(g) \rightarrow Si(s) + SiO_2(s) \tag{4.4}$$

$$SiO_2(s) \rightarrow SiO_x(s) + O_2(g), x > 1 \tag{4.5}$$

C atoms from the activated carbon powder were transferred to surface of Si wafer during vacuuming. They then reacted with the limited amount of oxygen that existed in the activated carbon powder to form CO gases (Equation 4.1). The CO gas was then transported to the oxide surface and reacted with the oxide layer to form SiO vapor and CO_2 gases (Equation 4.2). The SiO vapor condensed to form homogeneous amorphous SiO_x on the surface from the excess oxygen from the oxide layer or the oxygen in the activated carbon powder (Equation 4.3). As time passed, more SiO vapor adsorbed onto the surface and condensed to form solid that tended to grow in one dimension, which led to the formation of amorphous SiO_x nanowires (at 1200 °C for 1 h). The nanowires were found to be oriented in the same direction as the orientation of Si wafer.

For the growth of Si/SiO_x core-shell nanowires, it is found that the SiO vapor begins to disproportionate into Si and SiO_2 when it reaches a critical temperature (Hass and Salzberg, 1954). Hass and Sulzberg (1954) found that SiO_x film began to decompose or disproportionate into Si and SiO_2 starting at 700 °C, while Pan et al. (2001a) in their work to produce silicon-based nanostructures, found that the critical temperature was 930 °C. For our case, the critical temperature lies between 1200 °C and 1300 °C. Thus, when the temperature was raised from 1200 °C to 1300 °C, the critical temperature was reached and the disproportionation reaction took place. The large difference in the critical temperature might be attributed to the difference in the pressure maintained during the process. Hass and Sulzberg (1954) stated that a good vacuum condition of less than 1 x 10-5 Torr was required for the disproportionation reaction to proceed. Pan et al. also use a low pressure of 300 Torr throughout the process (Pan et al., 2001b). In our study, the pressure used was higher as compared to the other two. The pressure was maintained at atmospheric pressure (760 Torr) throughout the process.

SiO vapor was obtained from the reduction of SiO_2 by C. It then disproportionated into Si and SiO_2 solid and deposited onto the surface (Equation 4.4). As soaking time increased, more SiO vapor dissociated and condensed onto the surface, leading to an increase in the length of the nanowires. SiO_x shell was obtained instead of SiO_2 because certain percentage of O_2 was lost into gas phase (Equation 4.5). The slightly linear relationship between the diameter of the core and the nanowire could further confirmed the formation of Si/SiO_x through the disproportionation reaction since the reaction [$SiO\ (g) \rightarrow Si\ (s) + SiO_2\ (s)$] should produce Si and SiO_2 in equal amount.

4.2.6.2 Growth Mechanism of SiC Nanostructures

The growth mechanisms of these nanostructures at different locations under different carbon amount will be discussed in the subsequent section.

The growth of SiC/SiO$_x$ nanostructures here is quite similar to the Si-C-O system commonly reported and two reactions [Equations 4.6 and 4.7 as shown below] had been identified as the most likely reactions that occurred in several intermediate processes that included active SiO and CO species (Shim, 2008):

$$SiO_2(s) + 2C(s) \rightarrow SiC(s) + CO_2(g) \tag{4.6}$$

$$SiO_2(s) + 3C(s) \rightarrow SiC(s) + 2CO(g) \tag{4.7}$$

Considering the results, the reactions above and their thermodynamics in terms of free energy, the following mechanism for the growth of SiC/SiO$_2$ nanostructures based on vapour-solid (VS) growth mechanism is proposed. The free energies (G) were calculated at atmospheric pressure and at a temperature (T) of 1300°C using the equation $\Delta G_T = \Delta H_T - T\Delta S_T$, where H and S represent enthalpy and entropy, respectively. The properties were obtained from NIST-JANAF thermochemical tables (Chase, 1998).

First, SiO and CO need to be generated in order for SiC formation to proceed. One of the possibilities of the formation of SiO is according to Equation 4.8. At 1300°C, thermal decomposition of SiO$_2$/Si at the interface could proceed via Equation 4.8. Although the reaction in Equation 4.8 was not favourable in terms of energy calculations, reports had confirmed that this reaction was still possible kinetically at high temperature (> 700°C) when O$_2$ partial pressure was low and oxide layer was thin (≤ 70 nm) (Starodub et al., 1999), as proven in the FESEM images showing etched Si surfaces. The etched surface of the wafer indicated the loss of Si species from the wafer (Wang et al., 2001). Another possible source of SiO species was the active oxidation of Si wafer, as shown in Equation 4.9, which had been reported to occur at high substrate temperature (> 700°C) and low O_2 pressure (Starodub et al., 1999). O_2 could diffuse through the thin oxide layer and react with the Si beneath. The CO species was provided by the reaction between ACP and residual O_2 in the powder according to Equation 4.10.

$$Si(s) + SiO_2(s) \rightarrow 2SiO(g), \Delta G = 164.53\ kJ/mol \tag{4.8}$$

$$2Si(s) + O_2(g) \rightarrow 2SiO(g), \Delta G = -466.633\ kJ/mol \tag{4.9}$$

$$2C(s) + O_2(g) \rightarrow 2CO(g), \Delta G = -499.97\ kJ/mol \tag{4.10}$$

Higher partial pressure of CO gas at the bottom resulted in diffusion of CO gas upwards. As the furnace was heated up to 1300°C, reaction between gaseous SiO and CO was possible for the formation of SiC nuclei through Equation 4.11. Although the thermodynamics calculations that showed the reaction was energetically favourable for temperatures below 927°C (Zhou et al., 2006b), there were few reports that found that this reaction was still possible at higher temperatures if it was under a supersaturated condition of CO vapour in the reaction chamber (Han et al., 1997, Wang et al., 2008).

$$3SiO(g) + CO(g) \rightarrow SiC(s) + 2CO_2(g) \tag{4.11}$$

Furthermore, the reaction between the active species of SiO and CO could also proceed near the Si wafer via Equation 4.12, which had been reported to occur under supersaturation condition of SiO (Wang et al., 2008). From the reaction, SiC and SiO_2 were formed simultaneously. However, since SiC had a higher melting point than SiO_2, SiC would solidify first and the amorphous viscous SiO_2 would encapsulate the crystalline SiC, forming the core-shell structures (Silva and Figueiredo, 2001, Luo et al., 2009, Zhang et al., 2009a).

$$SiO(g) + CO(g) \rightarrow SiC(s) + 2SiO_2(s), \Delta G = -1273.44\ kJ/mol \qquad (4.12)$$

According to the results, SiC nanowires were also found at the border when no ACP was added. This suggested that SiO could also react with graphite directly through Equation 4.13 and 4.14 to form SiC.

$$2SiO(g) + 3C(s) \rightarrow 2SiC(s) + CO_2(g), \Delta G = -51.7714\ kJ/mol \qquad (4.13)$$

$$SiO(g) + 2C(s) \rightarrow SiC(s) + CO(g), \Delta G = -77.7097\ kJ/mol \qquad (4.14)$$

To maintain the SiC formation, there must be sufficient source of CO, which could be replenished through Equation 4.15.

$$CO_2(g) + C(s) \rightarrow 2CO(g), \Delta G = -103.648\ kJ/mol \qquad (4.15)$$

After the nucleation process, SiC species formed were preferentially adsorbed onto the nuclei and further reactions led to the growth of different shapes and sizes of nanostructures depending on their locations. The nanoparticles formed could also act as nucleation sites for further growth of SiC nanowires. The formation of different nanostructures would be discussed in the following section.

When the furnace was cooled down, SiC formation ceased, which in turn resulted in excess SiO species. In the presence of excess SiO species, the following reaction in Equation 4.16 would predominate, thereby producing the SiO_x nanowires, as proposed in oxide-assisted growth of Si nanowires (Zhang et al., 2000b, Pan et al., 2001a, Shi et al., 2000a, Zhang et al., 2003).

$$SiO\ (g) + O_2\ (g) \rightarrow SiO_x\ (s),\ 1 < x \leq 2 \qquad (4.16)$$

Furthermore, the SiO_x species formed through reoxidation process in Equation 4.16 could be adsorbed onto the nanowire surfaces due to larger surface energy of the nanowires. Gradual absorption of the oxide species caused the growth of oxide shell. Some of SiO droplets on the nanowires would also induce the growth of amorphous SiO_x branches from the core-shell nanowires since they were energetically favoured sites for absorption of SiO vapour (Lin et al., 2009).

(a) Formation of SiC/SiOx core-shell clusters, nanowires, nanowebs and nanocables

The different nanostructures formed at different locations on the Si wafer could be attributed to aerodynamic effects. A small gap existed between Si substrate and crucible, creating a narrow path for gas flow towards the outside environment. The existence of this narrow gap resulted in a change of the diffusion path of gases, with more reactants attracted to the side, trying to diffuse through the gap towards the outside environment which had a lower pressure. As a result, there were lower concentrations of reactants at the centre of substrate. The lower concentration of reactants limited the reaction and thus only small amount of SiC could be produced in the form of clusters and in the case of the sample without the ACP source, only small amount of SiO_x nanowires were produced. With increasing amount of ACP, more CO gas was produced. Since CO was the reaction-limiting species in Equations 4.11 and 4.12 because SiO gas had a never-ending supply from Si wafer, this meant that an increase in the amount of ACP might increase the chances of CO gas reaching the centre of Si wafer and enhanced the reaction rate, which ultimately led to more SiC clusters being formed.

At the border where the Si wafer was in contact with the crucible, the small gap between them posed as a constriction to the flow of reactant gas. When gases tried to pass through the gap, the gases had to flow from a high volume region inside the crucible to a low volume region in the gap. The sudden change in volume caused an increase in the speed of gas flow and corresponding reduction in pressure based on Venturi effect (Lamb, 1953). The increase in gas flow rate reduced the reaction rate as a consequence of high removal rate of reactant species along the gap during the 2-hours soaking period. Therefore, the SiC cores had smaller diameters as compared to nanowires formed at the side of the substrate. Although the SiC cores had smaller diameters, they were observed with thick oxide shells. This could be due to the slow heat dissipation of the graphite crucible. Graphite, which had higher heat capacity, dissipated heat slower as compared to the surrounding environment and thus a longer cooling period allowed the SiO adsorption to continue to take place and resulted in a thicker oxide shell.

Due to the close proximity of nanowires and the strong van der Waals forces between the nanowires, the nanowires were attracted to each other and formed an aligned bundle or intersection of junctions. Further oxide growth and self-organization through surface diffusion might cause the oxide shells to merge with one another in order to reduce the surface energy, creating the nanocables and nanojunctions in the nanoweb (Lin et al., 2009, Shim, 2008, Shim and Huang, 2007). Amorphous SiO_x nanowires found as branches might have grown from smaller droplets of SiO adsorbed onto the shell (Lin et al., 2009). These amorphous nanowires then grew in length and bridged the separated nanowires and nanocables. The joining of nanowires through "welding" could be proven by the lack of lattice matching of the crystalline cores of the junctions in the EFTEM images and the two nanowires appeared to be overlapped through welding by SiO_2.

The different diameters of the samples at the border could be explained by the increase in local pressure in the gap. Higher amount of ACP produced more CO species. Since gas flow rate remained constant throughout the length of the gap, higher amount of CO species would increase the local pressure in the gap. A slight increase in pressure had been reported to increase the growth rate and the diameter of nanowires but a large increase would significantly reduce the yield (Zhao et al., 2008, Weng et al., 2010, Fan et al., 2001). For the sample without ACP, the lack of CO species and reduced pressure from higher gas flow rate promoted the growth of large amount of randomly oriented nanowires with smaller diameters. When ACP was increased from 0.5 g to 1.0 g, increased vapour pressure at that region increased the growth rate due to higher reactant concentration and thus, larger diameters of nanowires could be observed. However, for the sample exposed to 1.5 g ACP, the high vapour pressure of CO in that region increased the local pressure and suppressed the evaporation of SiO species. The limited SiO species controlled the growth of the nanowebs and thus only thin nanowebs could be observed.

At the side, the growth of SiC/SiO_x randomly oriented nanowires could be explained as follow. When reactant species exited the gap, gas flow rate decreased due to an increase in volume based on Venturi effect. The sudden speed reduction caused the reactant species to be accumulated near the crucible and increased the chances for SiC formation to take place at that particular reaction site. Thus, thicker cores were observed as compared to the border. The flow of Ar gas limited the diameter of oxide shell because of the constant gas flow that might remove excess SiO species during the cooling process. As for the nanowire clusters formed in sample exposed to 1.5 g ACP, the nanowires were found originating from a single spot, which is quite similar to the nanostructures formed according to vapour-liquid-solid (VLS) mechanism where a single metallic catalyst droplet could induce the growth of several nanowires (Wagner and Ellis, 1964). Here, no metallic elements were detected along the nanowire clusters, as shown in Figure 4.17(c) and (d). Thus, this suggested the nanowires were self-catalytic, as reported by Zhang et al. (Zhang et al., 2009b) but it differed from the normal VLS mechanism since no Si-rich droplets were found at the tips of nanowires.

(b) Formation of SiC Nanorods and SiC Nanocolumns

The growth of SiC nanorods and nanocolumns on the same substrate could also be explained by the aerodynamics effect. However, since the soaking time was only 1 hour, the aerodynamics effect was not that significant and the reaction time was shorter as compared to that in the case of 2-hours soaking time. This resulted in the growth of only SiC nanorods and nanocolumns.

Similar to the mechanisms proposed for the growth of SiC/SiO_2 clusters, nanowires and nanowebs, the SiO and CO species were attracted to the side of Si substrate due to the pressure difference in the crucible and the outside environment. This led to lower concentrations of reactant species at the centre and higher concentrations of reactant species at the sides of the silicon wafer.

At the centre of the silicon wafer, the reaction between SiO and CO in Equation 4.11 predominated, forming SiC and CO_2. This observation could be proven by the lack of oxide layer on the SiC nanorods, as shown in the EFTEM image in Figure 4.8. The SiC species formed were then deposited onto the Si substrate and formed SiC nuclei. Due to lower concentrations of reactant species, limited SiC was deposited onto these nuclei and thus straight nanorods with smaller diameter were formed.

While at the side of the silicon wafer that was in contact with crucible, the higher concentration of reactant species caused an increase in SiC formation rate based on the reactions between SiO and CO in Equation 4.11 as well as the reactions between SiO and C in Equations 4.13 and 4.14. This resulted in the agglomeration of the SiC clusters formed from the deposition of SiC onto the existing nuclei, creating a thick faceted and spherical SiC layer. The presence of SiC layer on top of the oxidized silicon wafer might reduce the dissociation of the SiO_2 layer, thereby limiting the reaction between SiO and CO. However, nanocolumns could still be observed, this meant that the mechanism involved in the growth of these nanocolumns differed from the mechanism proposed for the growth of nanorods or the nanowires. Further reactions were involved in the growth of nanocolumns.

The growth mechanism of the SiC nanocolumns were similar to that reported by (Cheong and Lockman, 2009a, Mohd Halil and Cheong, 2008, Cheong and Lockman, 2009b). CO gas had to diffuse deeper through the SiC layer into the SiO_2 layer or Si wafer below and reacted with them. CO gas then reacted with SiO_2, forming more SiO species (Equation 4.17) for further reaction with CO to form SiC (Equation 4.11) or it might have reacted with solid Si to form SiC directly (Equation 4.18).

$$SiO_2\,(s) + CO\,(g) \rightarrow SiO\,(g) + CO_2\,(g) \qquad (4.17)$$

$$Si\,(s) + CO\,(g) \rightarrow SiC\,(s) + O(g) \qquad (4.18)$$

The difference in molecular size of SiC and atomic size of Si or SiO_2 caused a redistribution of the atoms and molecules in the lattice laterally and/or vertically, so that the induced strain could be relaxed. The spherical and faceted SiC layer structures were then transformed into pyramid-like structures with stacked SiC layers, forming polygonal SiC nanocolumns.

CHAPTER 5

CONCLUSION

In this chapter, conclusions were drawn and recommendations were suggested for future works.

5.1 Conclusion

The objectives of this research were achieved and final remarks based on the objectives are shown as follow:

1. Different Si-based nanostructures, namely Si/SiO$_x$ core-shell nanowires, SiO$_x$ nanowires, SiC nanorods, SiC nanocolumns, SiC/SiO$_2$ core-shell nanowires, SiC/SiO$_2$ core-shell nanocables and nanowebs, were successfully synthesized using direct growth on Si substrates depending on the oxidation time, amount of activated carbon powder and growth locations on the Si substrates.
2. SiO$_x$ and Si/SiO$_x$ core-shell nanowires were formed when the oxidation time was fixed at 24 min while exposed to 0.5 g activated carbon powder. SiO$_x$ nanowires were formed at the growth temperatures of 1200 °C whereas Si/SiO$_x$ core-shell nanowires were formed at growth temperatures of 1300 °C. As the soaking time increased from 1 h to 4 h, the Si/SiO$_x$ core-shell nanowires increased in amount and length, though the change in the diameters of the nanowires was not significant due to constraints by the oxide layer.
3. SiC nanorods and nanocolumns were successfully synthesized at 1300°C and at a soaking time of 1 hour while exposed to 0.5 g activated carbon powder. As the oxidation time was increased, an increase in the amount of nanorods and

nanocolumns could be observed but ultimately led to agglomeration of these nanostructures into SiC clusters or SiC layers. SiC nanowires were also found only at an oxidation time of 2 min.

4. When the soaking time was increased from 1 hour to 2 hours while the experiment was fixed at an oxidation time of 2 min, a growth temperature of 1300°C and an activated carbon powder amount of 0.5 g, the products changed from SiC nanorods and nanocolumns to SiC/SiO_2 core-shell nanostructures in the form of clusters, nanowires, nanocables and nanowebs.
5. SiC/SiO_2 core-shell nanostructures in the form of clusters, nanowires, nanowebs and nanocables were formed along with side products of Si/SiO_x or Si nanowires and SiC nanoparticles. When ACP was increased to 1.0 g ACP, the diameter of nanowires increased but then started to decrease with further increase to 1.5 g ACP. The fluctuation of the diameters with increasing ACP amount was due to the increasing vapor pressure of CO produced. Addition of ACP also resulted in the formation of nanowebs and nanocables.
6. The growth of all these Si-based nanostructures was correlated to vapor-solid mechanism though the reaction kinetics differed for each product formed. The difference in nanostructures formed at different growth locations was a result of the aerodynamic effects created by pressure difference between the inner crucible chamber and the outside environment, and increased reactant gas flow rate in the gap.

5.2 Recommendations for Future Work

Several suggestions for future works in order to understand further the growth of Si-based nanostructures and to improve the synthesis method are listed as below:

1. Up scaling production of Si-based nanostructures using direct growth method.
2. A study on the properties of the Si-based nanostructures produced in terms of electronic properties and photoluminescence properties.
3. Development of applications for the Si-based nanostructures such as nanoelectronic devices or optical sensors.

Choi, H. J., Seong, H. K., Lee, J. C. & Sung, Y. M. (2004) Growth and modulation of silicon carbide nanowires. *Journal of Crystal Growth,* 269, 472-478.

Colli, A., Hoffmann, S., Fasoli, A., Ferrari, A. C., Ducati, C., Dunin-Borkowski, R. E. & Robertson, J. (2006) Synthesis and optical properties of silicon nanowires grown by different methods. *Applied Physics A: Materials Science and Processing,* 85, 247-253.

Du, X. W., Zhao, X., Jia, S. L., Lu, Y. W., Li, J. J. & Zhao, N. Q. (2007) Direct synthesis of SiC nanowires by multiple reaction VS growth. *Materials Science and Engineering B: Solid-State Materials for Advanced Technology,* 136, 72-77.

Fan, J. Y., L., W. X. & Chu, P. K. (2006a) Low-dimensional SiC nanostructures: Fabrication, luminescence, and electrical properties *Progress in Materials Science,* 51, 983-1031.

Fan, J. Y., Wu, X. L. & Chu, P. K. (2006b) Low dimensional SiC nanostructures: Fabrication, luminescence, and electrical properties. *Progress in Materials Science,* 51, 983-1031.

Fan, X. H., Xu, L., Li, C. P., Zheng, Y. F., Lee, C. S. & Lee, S. T. (2001) Effect of ambient pressure on silicon nanowire growth. *Chemical Physics Letters,* 334, 229-232.

Gundiah, G., Deepak, F. L., Govindaraj, A. & Rao, C. N. R. (2003) Carbon-assisted synthesis of silicon nanowires. *Chemical Physics Letters,* 381, 579-583.

Han, W., Fan, S., Li, Q., Liang, W., Gu, B. & Yu, D. (1997) Continuous synthesis and characterization of silicon carbide nanorods. *Chemical Physics Letters,* 265, 374-378.

Hass, G. & Salzberg, C. D. (1954) Optical properties of silicon monoxide in the wavelength region from 0.24 to 14.0 microns. *Journal of the Optical Society of America,* 44, 181.

Hu, J. Q., Jiang, Y., Meng, X. M., Lee, C. S. & Lee, S. T. (2003) A simple large-scale synthesis of very long aligned silica nanowires. *Chemical Physics Letters,* 367, 339-343.

Jeong, H., Seong, H. K. & Choi, H. J. (2008) Self growth of silica nanowires on a Si/SiO_2 substrate. *Journal of the Korean Ceramic Society,* 45, 142-145.

Jin, L., Wang, J., Cao, G. & Choy, W. C. H. (2008) Fabrication and characterization of amorphous silica nanostructures. *Physics Letters A,* 372, 4622-4626.

Kang, P., Zhang, B., Wu, G., Su, J. & Gou, H. (2011) Synthesis of SiO_2 covered SiC nanowires with milled Si,C nanopowders. *Materials Letters,* 65, 3461-3464.

Kim, R., Qin, W., Wei, G., Wang, G., Wang, L., Zhng, D., Zheng, K. & Liu, N. (2009) Synthesis of large-scale SiC-SiO_2 nanowires decorated with amorphous carbon nanoparticles and Raman and PL properties. *Chemical Physics Letters,* 475, 86-90.

Lai, Y. S., Wang, J. L., Liou, S. C. & Tu, C. H. (2008) Tailoring of amorphous SiO_x nanowires grown by rapid thermal annealing. *Chemical Physics Letters,* 453, 97-100.

Lamb, H. (1953) *Hydrodynamics,* Cambridge, Cambridge Univ. Press.

Law, M., Goldberger, J. & Yang, P. D. (2004) Semiconductor nanowires and nanotubes. *Annual Review of Materials Research,* 34, 83-122.

Li, H. J., Li, Z. J., Meng, A. L., Li, K. Z., Zhang, X. N. & Xu, Y. P. (2003) SiC nanowire networks. *Journal of Alloys and Compounds,* 352, 279-282.

Li, J. C., Lee, C. S. & Lee, S. T. (2002) Direct growth of β-SiC nanowires from SiO_x thin films deposited on Si (100) substrate. *Chemical Physics Letters,* 355, 147-150.

Li, Y., Qian, F., Xiang, J. & Lieber, C. M. (2006) Nanowires electronic and optoelectronic devices. *Materials Today,* 9, 18-27.

Liang, C. H., Meng, G. W., Zhang, L. D., Wu, Y. C. & Cui, Z. (2000a) Large-scale synthesis of β-SiC nanowires by using mesoporous silica embedded with Fe nanoparticles. *Chemical Physics Letters,* 329, 323-328.

Liang, C. H., Zhang, L. D., Meng, G. W., Wang, Y. W. & Chu, Z. Q. (2000b) Preparation and characterization of amorphous SiO_x nanowires. *Journal of Non-Crystalline Solids,* 277, 63-67.

Liao, K.-H., Wu, W.-Y., Yang, B.-W. & Ting, J.-M. (2011) Growth and Properties of Core-Shelled SiC–SiO_2 Nanowires Using Chemical Vapor Deposition. *International Journal of Applied Ceramic Technology,* no-no.

Lin, L. W., Tang, Y. H. & Chen, C. S. (2009) Self-assembled silicon oxide nanojunctions. *Nanotechnology,* 20, 175601.

Lopez-Camacho, E., Fernaįndez, M. & Gomez-Aleixandre, C. (2008) The key role of hydrogen in the growth of SiC/SiO_2 nanocables. *Nanotechnology,* 19, 305602.

Lopez-Camacho, E., Fernandez, M. & Gomez-Aleixandre, C. (2009a) Influence of the Atmosphere on the Growth by CVD of Silicon Based Nanostructures. *Journal of Nanoscience and Nanotechnology,* 9, 4187-4193.

Lopez-Camacho, E., Fernandez, M. & Gomez-Aleixandre, C. (2009b) Tailormade SiC-based nanocables by the control of the methane concentration. *Journal of Physics D: Applied Physics,* 42, 045302.

Luo, X., Ma, W., Zhou, Y., Liu, D., Yang, B. & Dai, Y. (2009) Synthesis and Photoluminescence Property of Silicon Carbide Nanowires Via Carbothermic Reduction of Silica. *Nanoscale Research Letters,* 5, 252 - 256.

Mamails, A. G., Vogtlander, L. O. G. & Markopoulos, A. (2004a) Nanotechnology and nanostructured materials: Trends in carbon nanotubes. *Precis Engineering,* 28, 16-30.

Mamails, A. G., Vogtlander, L. O. G. & Markopoulos, A. (2004b) Nanotechnology and nanostructured materials: Trends in carbon nanotubes. *Precision Engineering,* 28, 16-30.

Meng, G. W., Cui, Z., Zhang, L. D. & Phillipp, F. (2000) Growth and characterization of nanostructured β-SiC via carbothermal reduction of SiO_2 xerogels containing carbon nanoparticles. *Journal of Crystal Growth,* 209, 801-806.

Mohd Halil, M. H. & Cheong, K. Y. (2008) Synthesis of silicon carbide (SiC) nanopillar via a catalyst-free vertical chemical vapor growth (CVG) route. *Malaysian Journal of Microscopy (Electron Microscopy Society of Malaysia),* 4, 89 - 93.

Nagarajan, V., Stanishevsky, A. & Ramesh, R. (2006) Ferroelectric nanostructures via a modified focused ion beam technique. *Nanotechnology,* 17, 338-243.

Narciso-Romero, F. J. & Rodriguez-Reinoso, F. (1996) Synthesis of SiC from rice husks catalysed by iron, cobalt or nickel. *Journal of Materials Science,* 31, 779-784.

Ni, H., Li, X. & Gao, H. (2006) Elastic modulus of amorphous SiO_x nanowires. *Applied Physics Letters,* 88, 1-3.

Niu, J. J. & Wang, J. N. (2007a) An approach to the synthesis of silicon carbide nanowires by simple thermal evaporation of ferrocene onto silicon wafers. *European Journal of Inorganic Chemistry,* 4006-4010.

Niu, J. J. & Wang, J. N. (2007b) A simple route to synthesize scales of aligned single-crystalline SiC nanowires arrays with very small diameter and optical properties. *Journal of Physical Chemistry B,* 111, 4368-4373.

Niu, J. J. & Wang, J. N. (2009) Growth mechanism of scales of SiC nanowires with/without ZnS powders at varying temperatures. *Applied Physics A: Materials Science and Processing,* 94, 613-618.

Pan, Z. W., Dai, Z. R., Xu, L., Lee, S. T. & Wang, Z. L. (2001a) Temperature-controlled growth of silicon-based nanostructures by thermal evaporation of SiO powders. *Journal of Physical Chemistry B,* 105, 2507-2514.

Pan, Z. W., Dai, Z. R., Xu, L., Lee, S. T. & Wang, Z. L. (2001b) Temperature-controlled growth of silicon-based nanostructures by thermal evaporation of SiO powders. *Journal of Physical Chemistry B,* 105, 2507-2514.

Panda, S. K. & Jacob, C. (2009) Patterned silicon wafer for selective Î²-SiC nanowire growth. *Advanced Materials Research,* 67, 77-82.

Panda, S. K., Sengupta, J. & Jacob, C. (2010) Synthesis of β-SiC/SiO_2 Core-Sheath Nanowires by CVD Technique Using Ni as Catalyst. *Journal of Nanoscience and Nanotechnology,* 10, 3046-3052.

Pang, C. L., Cui, H. & Wang, C. X. (2011) Synthesis and photoluminescence of ultralong amorphous SiO_2 nanowires catalysed by germanium. *CrystEngComm,* 13, 4082-4085.

Park, B. T. & Yong, K. J. (2004) Controlled growth of core-shell Si-SiO_x and amorphous SiO_2 nanowires directly from NiO/Si. *Nanotechnology,* 15, S365-S370.

Park, J. H., Kim, W.-J., Kim, D. J., Ryu, W.-S. & Park, J. Y. (2007) Selective growth of β-SiC whisker on a patterned Si (111) substrate for a field emission device. *Thin Solid Films,* 515, 5519-5523.

Powell, A. R. & Rowland, L. B. (2002) SiC Materials - Progress, Status and Potential Roadblocks. *IEEE Proceedings,* 90, 942-955.

Ryu, Y., Park, B., Song, Y. & Yong, K. (2004) Carbon-coated SiC nanowires: direct synthesis from Si and field emission characteristics. *Journal of Crystal Growth,* 271, 99-104.

Ryu, Y., Tak, Y. & Yong, K. (2005) Direct growth of core-shell SiC-SiO_2 nanowires and field emission characteristics. *Nanotechnology,* 16, S370-S374.

Seeger, T., Redlich, P. K. & Ruhle, M. (2000) Synthesis of nanometer-sized SiC whiskers in the arc-discharge. *Advanced Materials,* 12, 279-282.

Sekhar, P. K., Ramjir, N. S., Joshi, R. K. & Bhansali, S. (2006) Selective growth of silica nanowires using Au catalyst for optical recognition of interleukin-10. *Nanotechnology,* 19, 245502.

Shen, G. Z., Bando, Y., Ve, C. H., Liu, B. & Goldberg, D. (2006) Synthesis, characterization, and field-emission properties of bamboo-like β-SiC nanowires *Nanotechnology,* 17, 3468-3472.

Shen, G. Z., Chen, D., Tang, K. B., Qian, Y. T. & Zhang, S. Y. (2003) Silicon carbide nanospheres, nanowires, and coaxial nanowires. *Chemical Physics Letters,* 375, 177-184.

Shi, W. S., Peng, H. Y., Zhang, Y. F., Wang, N., Shang, N. G., Pan, Z. W., Lee, C. S. & Lee, S. T. (2000a) Synthesis of large areas of highly oriented, very long silicon nanowires. *Advanced Materials,* 12, 1343-1345.

Shi, W. S., Zheng, Y. F., Peng, H. Y., Wang, N., Lee, C. S. & Lee, S. T. (2000b) Laser ablation synthesis and optical characterization of silicon carbide nanowires. *Journal of American Ceramics Society,* 83, 3228-3230.

Shim, H. W. (2008) Fabrication and Properties of Silicon Carbide Nanowires. *Mechanical Engineering, Faculty of Rensselaer Polytechnic Institute.* Troy, New York, Rensselaer Polytechnic Institute.

Shim, H. W. & Huang, H. (2007) Nanowebs and nanocables of silicon carbide. *Nanotechnology,* 18, 335607.

Silva, P. C. & Figueiredo, J. L. (2001) Production of SiC and Si_3N_4 whiskers in C+SiO_2 solid mixtures. *Materials Chemistry and Physics,* 72, 326-331.

Spanier, J. E. (2006) One-dimensional semiconductors and oxide nanostructures. IN GOGOTSI, Y. (Ed.) *Nanomaterials Handbook.* 1st edition ed. USA, CRS Press, Taylor & Francis Group.

Starodub, D., Gusev, E. P., Garfunkel, E. & Gustafsson, T. (1999) Silicon oxide decomposition and desorption during the thermal oxidation of silicon. *Surface Review and Letters,* 6, 45-52.

Sudarshan, T. (2006) SiC Power Materials Devices and Applications. IN FENG, Z. C. (Ed. *Materials Science.* New York, Springer.

Vaseastha, A. (2005) Nanostructured Materials based Next Generation Devices and Sensor. IN VASEASTHA, A., MALINOVSKA, D. D. & MARSHALL, J. M. (Eds.) *Nanostructured and Advanced Materials.* 1st Edition ed., IOS Press, Amsterdam and Springer, Netherland.

Wagner, R. S. & Ellis, W. C. (1964) Vapor-liquid-solid mechanism of single crystal growth. *Applied Physics Letters,* 4, 89.

Wang, F. L., Zhang, L. Y. & Zhang, Y. F. (2008) SiC nanowires synthesized by rapidly heating a mixture of SiO and arc-discharge plasma pretreated carbon black. *Nanoscale Research Letters,* 4, 153-156.

Wang, J., Lu, C., Wang, Q., Xiao, P., Ke, F., Bai, Y., Shen, Y., Liao, X. & Gao, H. (2012) Influence of microstructures on mechanical behaviours of SiC nanowires: a molecular dynamic study. *Nanotechnology,* 23, 025703.

Wang, S. J., K.Ong, C., Xu, S. Y., Chen, P., Chai, J. W., Tjiu, W. C., Pan, J. S., Huan, A. C. H., Feng, W., Lim, J. S., Yoo, W. J. & Choi, W. K. (2001) RHEED and XPS studies of the decomposition of silicon dioxide by the bombardment of metal ions. *Surface Review and Letters,* 8, 521-526.

Wang, X. J., Tian, J. F., Bao, L. H., Hui, C., Yang, T. Z., Shen, C. M., Gao, H. J., Liu, F. & Xu, N. S. (2007) Large scale SiC/SiO_x nanocables: Synthesis, photoluminescence, and field emission properties. *Journal of Applied Physics,* 102, 014309.

Weaver, S. C., Nixdorf, Richard D. (1989) Method for the preparation of silicon carbide whiskers. United States, American Matrix, Inc. (Knoxville, TN).

Wei, B. Q., Ward, J. W., Vajtai, R., Ajayan, P. M., Ma, R. & Ramanath, G. (2002) Simultaneous growth of silicon carbide nanorods and carbon nanotubes by chemical vapor deposition. *Chemical Physics Letters,* 354, 264-268.

Wei, Q., Meng, G. W., An, X. H., Hao, Y. F. & Zhang, L. D. (2006) Synthesis and photoluminescence of aligned straight silica nanowires on silicon substrate. *Solid State Communications,* 138, 325-330.

Weng, X., Burke, R. A., Dickey, E. C. & Redwing, J. M. (2010) Effect of reactor pressure on catalyst composition and growth of GaSb nanowires. *Journal of Crystal Growth,* 312, 514-519.

Wong, E. W., Sheehan, P. E. & Lieber, C. M. (1997) Nanobeam mechanics: Elasticity, strength, and toughness of nanorods and naotubes. *Science,* 26, 5334.

Wu, X. C., Song, W. H., Wang, K. Y., Hu, T., Zhao, B., Sun, Y. P. & Du, J. J. (2001) Preparation and photoluminescence properties of amorphous silica nanowires. *Chemical Physics Letters,* 336, 53-56.

Xia, Y. N., Yang, P. D., Sun, Y. G., Wu, Y. Y., Mayers, B., Gates, B., Yin, Y. D., Kim, F. & Yan, H. Q. (2003) One-dimensional nanostructures: synthesis, characterization and applications. *Advanced Materials,* 15.

Xu, W. J., Xu, Y., Sun, X. Y., Liu, Y. Q., Wu, D. & Sun, Y. H. (2006) Fabrication of tower like β-like by sol-gel and carbothermal reduction processing. *New Carbon Materials,* 21, 167-170.

Yan, B., Zhou, G., Duan, W., Wu, J. & Gu, B. L. (2006) Uniaxial-stress effect on electronic properties of silicon carbide nanowires. *Applied Physics Letters,* 89, 023104.

Yang, G. Z., Cui, H., Sun, Y., Gong, L., Chen, J., Jiang, D. & Wang, C. X. (2009) Simple catalyst-free method to the synthesis of Î²-SiC nanowires and their field emission properties. *Journal of Physical Chemistry C,* 113, 15969-15973.

Yang, W., Araki, H., Hu, Q. L., Ishikawa, N., Suzuki, S. & Noda, T. (2004) In situ growth of SiC nanowires on RS-SiC substrates. *Journal of Crystal Growth,* 264, 278-283.

Yang, W., Araki, H., Thaveethavorn, S., Suzuki, H. & Nada, T. (2005) In situ synthesis and characterization of pure SiC nanowires on silicon wafer. *Applied Surface Science,* 241, 236-240.

Yang, Y., Meng, G., Liu, X., Zhang, L., Hu, Z., He, C. & Hu, Y. (2008a) Aligned SiC porous nanowire arrays with excellent field emission properties converted from Si nanowires on silicon wafer. *Journal of Physical Chemistry C,* 112, 20126-20130.

Yang, Z., Yu, Z., Chen, H., Jiao, Z., Jin, Y., He, Y., Gong, M. & Sun, X. (2008b) Growth of amorphous SiO_2 nano-wires on pre-oxidized silicon substrate via chemical vapor deposition. *Journal of Non-Crystalline Solids,* 354, 1731-1735.

Yao, Y., Li, F. H. & Lee, S. T. (2005) Oriented silicon nanowires on silicon substrates from oxide-assisted growth and gold catalysts. *Chemical Physics Letters,* 406, 381-385.

Ying, Y. C., Gu, Y., Li, Z. F., Gu, H. Z., Cheng, L. Y. & Qia, Y. T. (2004) A simple route to nanocrystalline silicon carbide. *Journal of Solid State Chemistry,* 177, 4163-4166.

Yu, D. P., Hang, Q. L., Ding, Y., Zhang, H. Z., Bai, Z. G., Wang, J. J., Zou, Y. H., Qian, W., Xiong, G. C. & Feng, S. Q. (1998) Amorphous silica nanowires: Intensive blue light emitter. *Applied Physics Letter,* 73, 3076.

Zaplatynsky, I. (1972) Devitrification and shrinkage behavior of silica fibers. *NASA Technical Note,* D-6891.

Zhang, E., Tang, Y., Zhang, Y. & Guo, C. (2009a) Synthesis and photoluminescence property of silicon carbon nanowires synthesized by the thermal evaporation method. *Physica E: Low-dimensional Systems and Nanostructures,* 41, 655-659.

Zhang, J., Wang, Q., Wang, F., Chen, X., Lei, W., Cui, Q. & Zou, G. (2009b) Plasma-assisted self-catalytic vapour-liquid-solid growth of β-SiC nanowires. *Journal of Physics D: Applied Physics,* 42, 035108.

Zhang, J., Xu, B. L., Yang, Y. D., Jiang, F. H., Li, J. P., Wang, X. C. & Wang, S. M. (2006) Catalyzed-assisted growth of well-aligned silicon oxide nanowires. *Journal of Non-Crystalline Solids,* 352, 2859-2862.

Zhang, R. Q., Lifshitz, Y. & Lee, S. T. (2003) Oxide-Assisted Growth of Semiconducting Nanowires. *Advanced Materials,* 15, 635-640.

Zhang, Y. F., Tang, Y. H., Lam, C., Wang, N., Lee, C. S., Bello, I. & Lee, S. T. (2000a) Bulk-quantity Si nanowires synthesized by SiO sublimation. *Journal of Crystal Growth,* 212, 115-118.

Zhang, Y. F., Tang, Y. H., Lam, C., Wang, N., Lee, C. S., Bello, I. & Lee, S. T. (2000b) Bulk-quantity Si nanowires synthesized by SiO sublimation. *Journal of Crystal Growth,* 212, 115-118.

Zhang, Y. J., Wang, N. L., He, R. R., Chen, X. H. & Zhu, J. (2001) Synthesis of SiC nanorods using floating catalyst. *Solid State Communications,* 118, 595-598.

Zhao, H. Z., Zhou, S., Hasanali, Z. & Wang, D. W. (2008) Influence of pressure on silicon nanowire growth kinetics. *Journal of Physical Chemistry C,* 112, 5695-5698.

Zhou, W. M., Fang, F., Y., H. Z., Yan, L. J. & Zhang, Y. F. (2006a) Field-effect transistor based on β-SiC nanowires. *IEEE Electron Device Letters,* 27, 463-465.

Zhou, W. M., Yang, Z. X., Zhu, F. & Zhang, Y. F. (2006b) SiC/SiO$_2$ nanocables and nanosprings synthesized by catalyst-free method. *Physica E: Low-dimensional Systems and Nanostructures,* 31, 9-12.

Zhou, W. M., Zhang, Y. F., Niu, X. M. & Min, G. Q. (2008) One-dimensional SiC nanostructures: synthesis and properties. *One-Dimensional Nanostructures, Lecture Notes in Nanoscale Science and Technology.* Springer New York.

Zhou, X. T., Wang, N., Lai, H. L., Peng, Y., Bello, I. & Lee, S. T. (1999a) β-SiC nanorods synthesized by hot filament chemical vapor deposition *Applied Physics Letter,* 74, 3942-3944.

Zhou, X. T., Wang, N., Lai, H. L., Peng, Y., Bello, I. & Lee, S. T. (1999b) β-SiC nanorods synthesized by hot filament chemical vapor deposition. *Applied Physics Letters,* 74, 3942-3944.

Zimmermann, U. About Silicon Carbide.[Online], [Accessed 15 October 2010]. Available from World Wide Web: http://www.ele.kth.se/SiCEP/english/index.html